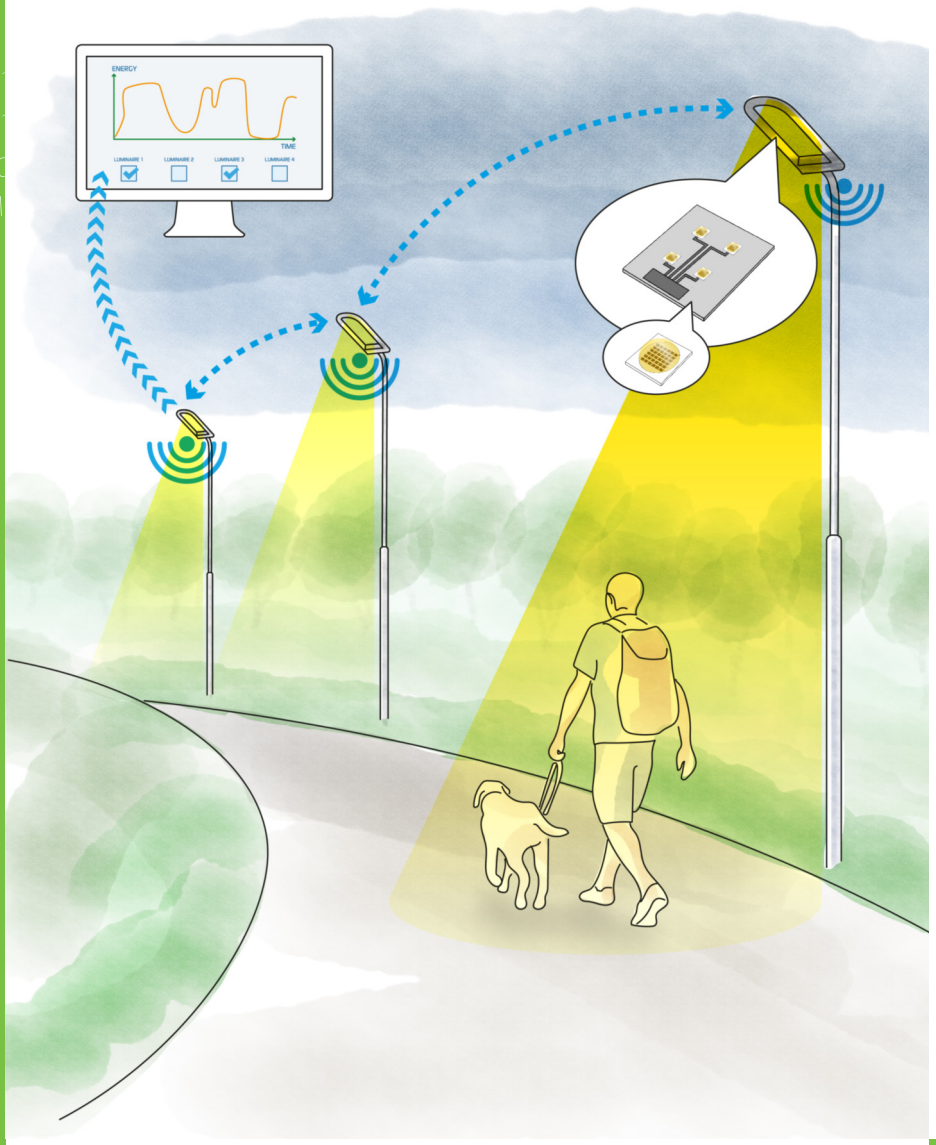

VISIONS • SCIENCE • TECHNOLOGY • RESEARCH HIGHLIGHTS

Dissertation
64

From LED die to a lighting system

Performance improvement in LED lighting by means of thermal management and smart control

Eveliina Juntunen

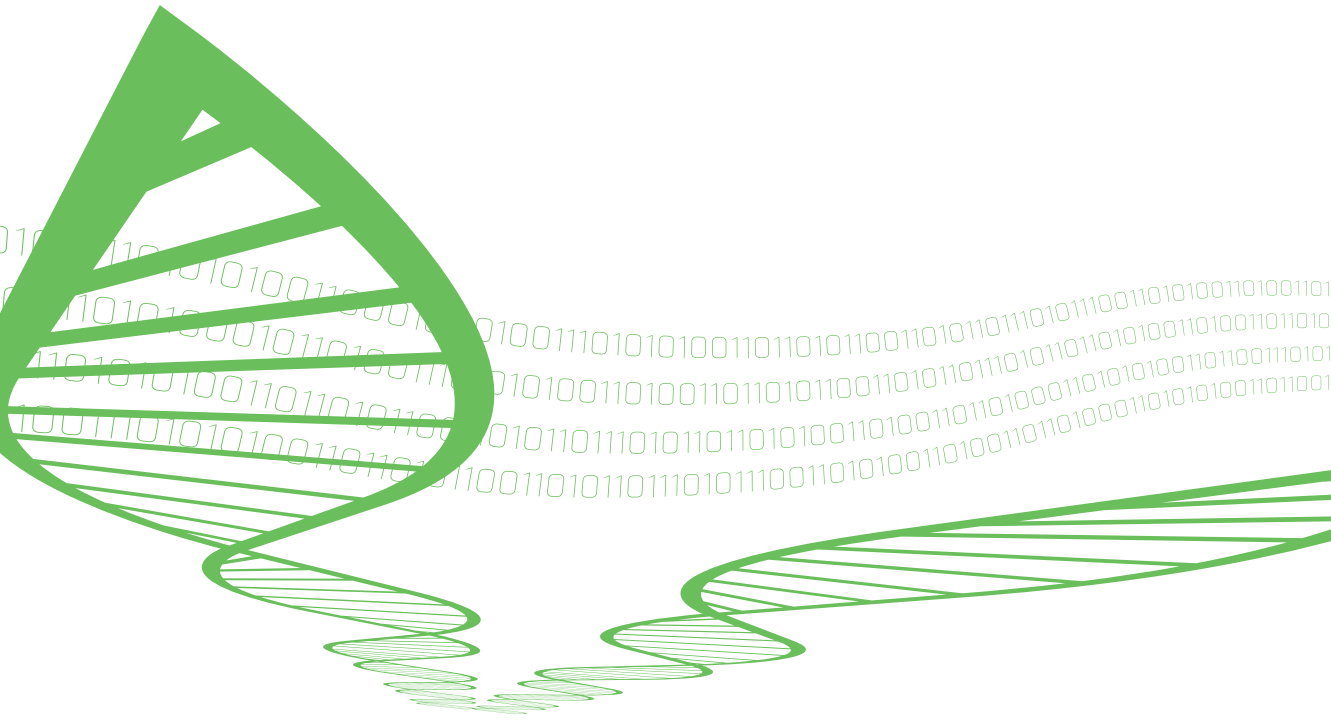

VTT SCIENCE 64

From LED die to a lighting system

Performance improvement in LED lighting by means of thermal management and smart control

Eveliina Juntunen

Thesis for the degree of Doctor of Technology to be presented with due permission for public examination and criticism in Auditorium IT115, Linnanmaa, at the University of Oulu, on the 24th of October at 12 o'clock noon.

ISBN 978-951-38-8152-8 (Soft back ed.)
ISBN 978-951-38-8153-5 (URL: http://www.vtt.fi/publications/index.jsp)

VTT Science 64

ISSN-L 2242-119X
ISSN 2242-119X (Print)
ISSN 2242-1203 (Online)

JULKAISIJA – UTGIVARE – PUBLISHER

VTT
PL 1000 (Tekniikantie 4 A, Espoo)
02044 VTT
Puh. 020 722 111, faksi 020 722 7001

VTT
PB 1000 (Teknikvägen 4 A, Esbo)
FI-02044 VTT
Tfn +358 20 722 111, telefax +358 20 722 7001

VTT Technical Research Centre of Finland
P.O. Box 1000 (Tekniikantie 4 A, Espoo)
FI-02044 VTT, Finland
Tel. +358 20 722 111, fax +358 20 722 7001

Grano Oy, Kuopio 2014

Preface

The work covered in this thesis has been carried out at VTT Technical Research Centre of Finland during the years 2010–2013. The major part of the research was performed in the research projects Tesle, Produla and AthLEDics, funded mainly by Tekes – the Finnish Funding Agency for Innovation and VTT. The thesis work was also supported in part by the Infotech Oulu Doctoral Program.

I wish to thank my supervisor, Prof. Heli Jantunen (University of Oulu), for her guidance and support during the course of this research. Prof. Georges Zissis (University Toulouse 3 – Paul Sabatier) and Dr. Rafael Jordan (Fraunhofer IZM) are greatly acknowledged for comprehensive peer-reviewing of the thesis manuscript. I wish also to thank Prof. Pentti Karioja (VTT) for encouragement to complete my post-graduate studies and his efforts to generate research projects.

I am most grateful to the co-authors and all colleagues in the Tesle, Produla and AthLEDics projects for their expertise. I specially wish to emphasise the contributions of Dr. Veli Heikkinen (VTT), Olli Tapaninen (VTT), and Aila Sitomaniemi (VTT). I also thank Dr. Eino Tetri (Aalto University) and Markku Jämsä (Aspocomp) for their contribution. Furthermore, I would like to thank my sister Essi for the pictures she drew for this thesis and all my co-workers and friends for supporting me in this dissertation process.

I would like to acknowledge the financial support for the thesis from Tauno Tönning Foundation, The Finnish Society of Electronics Engineers, Tekniikan edistämissäätiö, and Ulla Tuominen Foundation.

Finally, I wish to thank Lasse for his great patience and encouragement.

With gratitude, I wish to dedicate this thesis to my beloved mummu.

Oulu, September 2014
Eveliina Juntunen

Academic dissertation

Supervisor	Professor Heli Jantunen Microelectronics and Materials Physics Laboratories University of Oulu
Reviewers	Professor Georges Zissis Laboratory of Plasma and Conversion of Energy (LAPLACE) University Toulouse 3 – Paul Sabatier
	Doctor Rafael Jordan Fraunhofer IZM, Berlin
Opponent	Professor Mircea Guina Optoelectronics Research Centre Tampere University of Technology
	Professor Georges Zissis Laboratory of Plasma and Conversion of Energy (LAPLACE) University Toulouse 3 – Paul Sabatier

List of publications

This thesis is based on the following original publications, which are referred to in the text as Papers I–IV. The publications are reproduced with kind permission from the publishers.

I **Copper-Core MCPCB with Thermal Vias for High-Power COB LED Modules**, E. Juntunen, O. Tapaninen, A. Sitomaniemi, M. Jämsä, V. Heikkinen, M. Karppinen and P. Karioja. *IEEE Transactions on Power Electronics,* March 2014, Vol. 29, No. 3: 1410–1417.

II **Effect of Phosphor Encapsulant on the Thermal Resistance of a High-Power COB LED Module**, E. Juntunen, O. Tapaninen, A. Sitomaniemi and V. Heikkinen. *IEEE Transactions on Components, Packaging and Manufacturing Technology,* July 2013, Vol. 3, No. 7: 1148–1154.

III **Thermal Performance Comparison of Thick-Film Insulated Aluminum Substrates With Metal Core PCBs for High-Power LED Modules**, E. Juntunen, A. Sitomaniemi, O. Tapaninen, R. Persons, M. Challingsworth and V. Heikkinen. *IEEE Transactions on Components, Packaging and Manufacturing Technology*, Dec. 2012, Vol. 2, No. 12: 1957–1964.

IV **A smart LED luminaire for energy savings in pedestrian road lighting**, E. Juntunen, E. Tetri, O. Tapaninen, S. Yrjänä, V. Kondratyev, A. Sitomaniemi, H. Siirtola, E. M. Sarjanoja, J. Aikio and V. Heikkinen. *Lighting Research and Technology*, published online 7 November 2013. Doi: 10.1177/1477153513510015

Author’s contributions

The results presented in this thesis have been achieved in co-operation in the research group and with the co-authors.

For publications I and II, the author was responsible for the LED component packaging task in the photonics production platform project. She participated in the test structure design, realization and analysing of the results. Especially, the component concepts to be tested were defined by the author. The manuscripts were prepared by the author with the help of the co-authors.

For publication III, the author was responsible for the thermal substrate development project. She participated in the module design, realization, testing and analysing of the results. Especially, the author originated the idea of thermal via on the IAMS substrate under the LED heat source. The manuscript was prepared by the author with the help of the co-authors.

For publication IV, the author was responsible for the smart LED luminaire project. She participated in the smart luminaire design, realization and analysing of the results. Especially, the author defined the smart luminaire concept to be tested in the research. The luminaire laboratory measurements and the user survey were carried out by Aalto University. The manuscript was prepared by the author with the help of the co-authors.

Contents

List of abbreviations and symbols

1D	one-dimensional
2D	two-dimensional
3D	three-dimensional
ΔT	temperature difference
AlGaInP	aluminium gallium indium phosphide semiconductor material
AlN	aluminium nitride ceramic substrate material
AlSiC	aluminium silicon carbide metal matrix composite substrate material
$A_{substrate}$	substrate area
BeO	beryllium oxide ceramic substrate material
CCT	correlated colour temperature
CO_2	carbon dioxide gas
COB	chip-on-board
CRI	colour rendering index
CTE	coefficient of thermal expansion
DBC	direct bonded copper
Ethernet	standard communications protocol for local area networks
FloTherm	simulation software (Mentor Graphics Corp.)
FR	flame retardant
GPRS	general packet radio service
GPS	Global Positioning System
H20E	die attach material (epoxy technology)
HPS	high pressure sodium

IAMS	insulated aluminium material system
I_{blue}	drive current of the blue LED chip
$I_{component}$	drive current of the LED component
I_{red}	drive current of the red LED chip
IMS	insulated metal substrate with an inorganic insulation layer
InGaN	indium gallium nitride semiconductor material
k	thermal conductivity
K	thermal calibration factor
LED	light-emitting diode
LTCC	low-temperature co-fired ceramic
MCPCB	metal core printed circuit board with an organic insulation layer
MH	metal halide
$P_{average}$	average power
PC	personal computer
PCB	printed circuit board
P_{heat}	heating power
PIR	passive infrared
P_{rad}	radiant power
RF	radio frequency
RGB	red, green, blue
Rth	thermal resistance
SMS	short message service
SnAgCu	tin silver copper solder alloy
SRH	Shockley, Read, Hall
T3Ster	thermal transient tester (Mentor Graphics Corp.)
$T_{junction}$	junction temperature of the LED
UV	ultraviolet
UV-A	a type of ultraviolet radiation
YAG:Ce	cerium-doped yttrium aluminium garnet, crystalline phosphor material
ZigBee	specification for small, low-power digital radio

1. Introduction

1.1 Background and motivation

Since the discovery of the light-emitting diode (LED) by Holonyak and Bevacqua in 1962 [1] and the achievements of Nakamura in growing blue and green LEDs on a GaN substrate in the early 1990s [2, 3], LEDs have made remarkable progress from simple indicators to revolutionary lighting technology. Like the famous Moore's Law for semiconductors, for more than 30 years, the evolution of LED technology has followed Haitz's Law, which predicts that every decade the amount of light per LED package will increase by a factor of 20 while the cost per lumen will fall by a factor of 10 [4]. Since the emergence of high-power white LEDs in the 21st century, the lumen output development has even surpassed Haitz's prediction [5].

Currently, driven by rising energy costs and concerns over carbon emissions, LEDs have taken over major lighting segments from displays to general lighting [4, 6, 7]. Besides the environmental benefits of energy efficiency, long lifetime and lack of mercury content, features like small size, easy control also at low temperatures, and low UV radiation level are appreciated among the lighting industry [4]. The first wave of LED replacements over the traditional lighting technologies will gradually give way to a more sophisticated second wave of smart lighting systems with built-in intuitive controls, greater energy saving capability and added functionality. Future lighting systems will improve the lighting experience with the ability to adjust spectral content and light distribution, transmit digital information and interface with other energy management systems in power distribution grids and building controls. These are not new concepts in lighting, but the current revolution of LEDs is making the realization of such functions more practical than ever before. [4, 7, 8, 9]

The performance requirements of next-generation LED lighting will not be fulfilled with current technology. Besides the need for high-performance and energy efficiency, lighting designed to benefit the user is requested to achieve economic success [4, 8]. There is good business potential, as the global lighting market is expected to grow from 73 billion euros in 2011 to over 100 billion euros in 2020 despite the economic growth, especially in Europe, having declined [10]. In addition, the emphasis on smart lighting provides potential for new features and applications prospective for future research and development of the industry. Beyond illumination, lighting will be increasingly integrated with communication, sensor

and actuator technologies. These trends are just starting to emerge in the market, and they will enable a wide range of novel LED-based solution for enhanced illumination in the future. While LED lighting is rapidly developing and extending to new products, applications and even whole new industries, it is prone to increase energy consumption. This is a true counteraction against the current green targets of society, and research efforts, like the ones introduced in this thesis, are needed to compensate for the increasing energy consumption with enhanced energy efficiency and performance. [8, 9, 11]

1.2 Scope and objectives of the thesis

The scope of this work is to improve the performance of high-power LED lighting. The research concentrates on thermal management because it is one of the main factors for reliable and efficient operation of LED devices [5, 7, 9]. The research objective is to reduce the thermal resistance of the LED lighting structure. General lighting calls for high luminosity. Besides the elevated power levels, the reach for high luminous flux also increases power density in applications such as spot lights and automotive head lamps, as more and more LEDs are packaged into a small space. The extreme requirements for thermal performance also come with low cost and high reliability expectations. This poses a major challenge for the thermal management of LED devices, which would benefit from a lower junction temperature with increased efficacy, lifetime and light quality [6, 7, 9].

Smart control for performance improvement in high-power LED lighting is another topic considered in this thesis. The research objective is to achieve energy savings with added intelligence in LED lighting. This topic is especially important for environmental reasons since it is estimated that lighting consumes 6.5% of world primary energy [8]. However, performance cannot only be evaluated by technical values because lighting is essentially a service for people. For this reason, the aim of the research was to improve energy efficiency while also considering end-user comfort.

1.3 Contribution of the thesis

The main thesis of this work is that

- *Thermal resistance can be reduced with thermal vias in the LED substrate, and*
- *Energy savings can be achieved by controlling the lighting according to lighting environment and person presence.*

This topic is addressed at four different levels, as illustrated in Figure 1. The thesis is based on the articles also shown in Figure 1. The LED component is a structure with bare LED dies bonded and encapsulated on a board (Papers I and II), while the LED module consists of packaged LED components solder-joined on a substrate (Paper III). The luminaire utilizes LED modules (Paper IV). Finally, the sys-

tem is a combination of luminaires and integrated sensors (Paper IV). The research concentrates on reducing thermal resistance and energy consumption in LED lighting devices. Besides the technical performance, the user experience aspect and the manufacturing cost consideration are included in the discussion of the achieved results. The reliability issues are excluded from the thesis. Thus, reliability testing and the analysis of the effect of reduced thermal resistance on reliability are left for future studies.

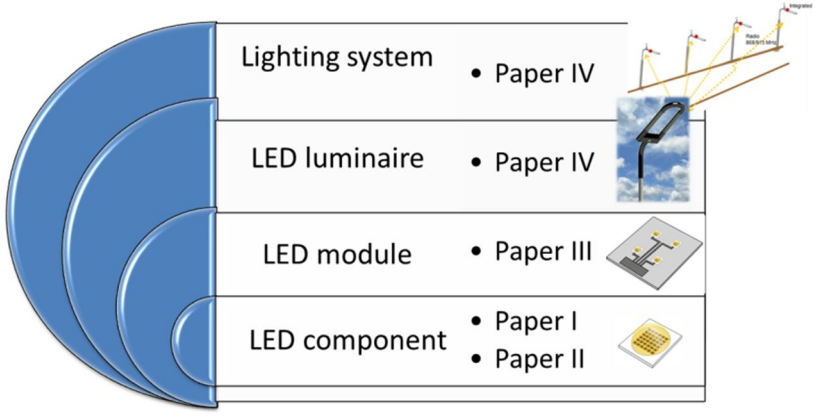

Figure 1. Relations between articles at different levels of LED lighting addressed in the thesis.

To start at component level, a high-power chip-on-board (COB) LED module with enhanced thermal performance is introduced. The improvement in thermal resistance is achieved with copper-filled microvias on a copper metal core printed circuit board (MCPCB) (Paper I). As the Cu MCPCB was processed in standard printed circuit board (PCB) manufacturing, and low-cost material, Flame Retardant-4 (FR4), was utilized for the electrical insulation, the solution is cost-effective despite the higher cost of copper compared with aluminium, that is, the most commonly used MCPCB core material. Phosphor packaging is also discussed. The phosphor that is used to convert light from blue to white can be applied directly on the LED chips or used remotely on some other object. The effect of phosphor encapsulant on the thermal resistance of a high-power COB LED component is analysed in this thesis (Paper II).

At module level, novel substrates based on insulated aluminium material system (IAMS) technology are introduced and their thermal resistance is compared with traditional MCPCBs (Paper III). IAMS technology inherently allows the use of thermal vias under the LED components. As the technology enables purely inorganic substrates, there is also great potential for reliable packaging of LEDs as well as other high-power devices in the future.

A smart LED luminaire with integrated sensors and wireless communication is described. The optical, thermal and electrical design of the luminaire contributes to good technical functionality. The performance of the luminaire is validated compared with commercial lamp and LED-based lighting technology. End-user comfort issues, such as glare and light appearance, are also discussed. (Paper IV)

Finally, at system level, the developed smart LED luminaire is tested in a pilot installation for energy savings in pedestrian street lighting. With wireless communication, the luminaires form a system that can react to the lighting environment and pedestrian presence. The energy-saving potential of such a street lighting system is discussed in the thesis. (Paper IV)

2. High-power LED devices

Aiming for performance improvements in general lighting, this thesis concentrates on LED devices operating in high electrical power (> 10 W) conditions. The heart of the high-power LED device is the LED chip – a semiconductor die that emits light when the correct electrical power is applied. The generation of light in LED chips is discussed briefly in Section 2.1 with the emphasis on thermal issues and white light generation relevant to this thesis. With current technology, the common light emission efficiency is about 20–30% of the electrical power [6]. The remaining 70–80% of the power is turned into heat. In general lighting, this can easily mean tens to hundreds of watts of cooling demand. Unlike traditional light sources, LEDs typically do not emit infrared radiation. Consequently, the heat has to be conducted away along the following structure [5]. Such a heat load is a challenge and is addressed in this thesis by introducing LED component and module substrates with improved thermal performance. To ground the research, a review of the available substrate technologies is given in Section 2.2.

2.1 Light-emitting diodes

An LED is a forward-biased p-n junction with the ability to produce light. Light production is based on the recombination of an electron-hole pair and simultaneous emission of a photon in the direct band gap semiconductors. In indirect gap semiconductors, the light emission efficiency is quite poor and the recombination is more likely to generate heat than light. [12]

For devices with high radiative recombination efficiency, the maximization of light extracting from the LED chip is the key challenge. The emitted photons can be reabsorbed in the semiconductor, creating an electron-hole pair. Some photons will also reflect back due to the semiconductor surface interface, metal contacts and total internal reflection. To maximize the light extraction chip shape, the construction and surface structure can be altered with great effect. [6,12]

The photon energy and, consequently, the desired emission wavelength of an LED can be tailored by choosing a semiconductor material with the appropriate energy band gap. Today, the InGaN LEDs exhibit good external quantum efficiency in the violet and blue range from UV-A (~365 nm) to deep green (~550 nm) while

the AlGaInP-based LEDs have shown impressive performance in the red region (~650 nm). The challenge is the 'green-yellow gap' between these two material systems, which is attracting significant research attention worldwide. [6, 7, 9]

2.1.1 LEDs and temperature

Common LED types used in high-power devices are shown in Figure 2 [6]. Sapphire substrate isolates the electrical contacts in the horizontal LED, that enables the use of chip bottom contact for cooling. With vertical and flip-chip LEDs, the bottom contact needs to be electrically isolated in the substrate side, because the electrical contacts are in the chip bottom. This restricts the conductive cooling options in the following substrate, as good thermal conductors, such as metals, are typically also electrical conductors.

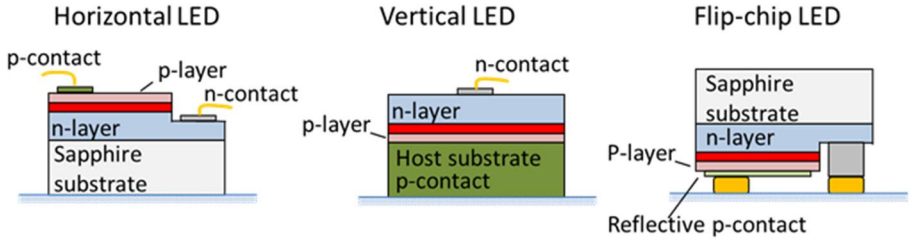

Figure 2. Common LED types used in high-power devices. The light emitting layer is indicated with red colour. [6]

The heat is generated along with the light emission in the red region in Figure 2. Depending on the LED configuration, the heat is generated in different parts of the chip, and size of the die attach contact area varies. The die attach constitutes a large portion of the junction to ambient thermal resistance of LED devices, and the die attach materials should be carefully selected [5]. Metallic joining, such as thermo-compression, eutectic bonding or soldering, enables good thermal contact [6]. Adhesive die attachment is also widely utilized due to the lower thermal load during curing, although thermal performance is not as good as with metallic bonds [9]. Adhesives also enable joining between incompatible metallization of the die and the following substrate. Besides the effective heat dissipation, the materials should present excellent adhesion between the attached surfaces, and good stress relaxation at the interface. Any defects, such as voids or intermetallic compounds, would increase the junction temperature, leading to premature failure of LEDs. [5]

The non-radiative recombination in the LED junction turns into heat. The main causes and consequences of heat in the LED device are summarized in Table 1. Chemical impurities and native defects like vacancies or dislocations can trap free electrons. Such defects can also allow recombination of the electron-hole pair in a non-radiative manner. This is the most common physical mechanism for heat generation in the LED, and it is called Shockley, Read, Hall (SRH) recombination.

The recombination is significant especially at the surfaces of devices, as there can be a high density of defects. [12]

Another important mechanism for heat generation in an LED junction is the Auger process. In the initial state, the process involves three carriers, two electrons and one hole for example. In Auger recombination, they form one 'hot' electron or hole with no emission of a photon. The process is strongly dependent on the carrier density and band gap structure. The process also has strong temperature dependence. Especially in narrow band gap materials, the Auger process can be important source of non-radiative recombination. [12] In phosphor converted white LEDs, the conversion from blue to white light also generates heat [6], This topic is further discussed in Section 2.1.2.

Table 1. Summary of heat generation and thermally induced failures in the LED device.

Heat generation in the LED	Failures caused by the heat
• Non-radiative recombination o SRH recombination o Auger process • White light conversion in phosphor	• Radiative efficiency loss • Phosphor efficiency loss • Colour shift • Material deterioration • Thermo-mechanical stress • Corrosion • Hygro-mechanical stress

In general, heat is one of the main causes of failure in electronic systems [13], and LED devices are no exception. Failure in LEDs occurs gradually as the non-radiative recombination increases at high temperatures, decreasing the optical efficiency [14]. This is mainly caused by a leakage current of injected carriers into the contact areas and the Auger process described above [12]. Heat also induces material deterioration, local stress and delamination, which can degrade reliability and performance of the light source significantly [5]. On top of the light generation issues, thermal deterioration of packaging materials such as corrosion, colour changes of the white packages, phosphor thermal quenching and failures in the package interfaces, lenses, encapsulation and bonding have been reported [5, 9, 14–17].

Besides the negative effect on optical power, the heat also changes the colour of the light. The band gaps of all semiconductors decrease with temperature. Consequently, the peak of the emission spectrum shifts towards longer wavelengths with increasing temperature. [12] In phosphor-converted LEDs, also the excitation spectrum of phosphor will shift with increasing temperature, causing degradation in light output performance [9]. Such reduction in device performance might recover, if temperature is reduced. Instead, lifetime effects related to material deterioration or failure in temperature conditions are permanent.

2.1.2 White light generation

By definition, white light contains all the wavelengths of visible light. With thermal radiators, like incandescent bulbs, this is fairly achievable as the spectrum of the emission is continuous. However, with LEDs, the spectral line width of the emission is narrow, representing a single colour rather than the entire visible spectrum [9, 12]. The usual methods to produce white light with LEDs are illustrated in Figure 3.

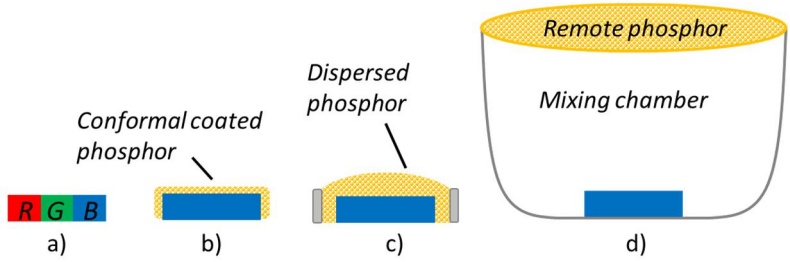

Figure 3. Illustration of a) RGB, b) conformal coated phosphor, c) dispersed phosphor and d) remote phosphor methods to generate white light with an LED.

In principle, there are two ways to produce white light with LEDs. White light can be generated by combining the three primary colours of red (R), green (G) and blue (B) (Figure 3a). In practice, this is achieved by driving LEDs of each colour with adequate intensity for the desired light output. With an RGB light source, basically any colour of light is available [6, 9]. However, this makes the device more complex as there is a need for adequate control of the LEDs for proper light-colour mixing. Also, when pursuing white light, the spiked spectrum is not optimal for good colour rendering. Colour consistency under different conditions is another challenge because different colours represent different LED material and manufacturing processes that age and react to diverse conditions differently. [7, 9]

Another method for generating white light is to use fluorescent material in front of the LED to spread the spectrum (Figure 3b, c, d). The concept of wavelength conversion is old and commonly used in cathode ray tubes and discharge lamps [6]. For the LEDs, cerium-doped yttrium aluminium garnet (YAG:Ce) phosphor with a GaN-based blue LED is commonly used. The excitation spectrum of the phosphor matches blue emission well, producing light that is generally perceived as white. The solution is sufficient for most lighting applications and is very widely used in the lighting industry. [5, 6, 14] The lack of red in the spectrum is a problem occasionally encountered. To overcome this, different solutions, such as adding some red LED chips (Paper I, II) or a multi-phosphor approach [5, 6], have been developed. In the market, additional red chips with narrow spectrum are often used to manipulate the colour rendering index (CRI) rather than real improvement in light quality.

Conformal coating of phosphor within polymeric matrix on the LED chip (Figure 3b) is commonly used to make white LED components [5], such as the Luxeon Rebels [18] and the Cree XM-Ls [19] used in this thesis. Another method is to mix phosphor with polymer encapsulant, such as silicone, and disperse the mixture on top of the LEDs (Figure 3c) [5, 9]. This is a common practice with COB LED modules like Bridgelux LED arrays [20]. The phosphor encapsulant covers all the LED chips of the module and is held in place with a supporter ring [21, 22].

The remote phosphor concept (Figure 3d) has attracted much attention since it is promoted to deliver up to 60% better efficacy than solutions with phosphor-coated LEDs [23–26]. In remote phosphor designs, the phosphor is moved away from the immediate vicinity of the LED chips and placed on a secondary optic or diffuser. Conversion from blue to white light generates a significant amount of heat [6], and by removing the phosphor from the LED chip this extra heat load is extracted, constituting increased efficacy and lifetime of the LEDs, as described in Section 2.1.1. The efficiency of the phosphor also decreases exponentially with increased temperature. Removing the heat load caused by the LED on the phosphor is therefore another significant benefit. [5, 9, 14, 26]

Remote phosphor solutions are also promoted to eliminate glare, which is a serious concern for LED products. LED lamps and luminaires are prone to glare due to the small size and high brightness of the LED chips [27]. When using phosphor remotely, the illuminating area is large and the user cannot look directly into the LED under any circumstances.

As illustrated in Figure 3d, a typical remote phosphor solution consists of a plate covering a mixing chamber in which the LEDs sit [23, 28]. Another famous remote phosphor example is the award-winning Philips L-price LED lamp, which imitates an incandescent bulb [9]. Common to these examples is that the dimensions of the light engine are relatively large and the small size of the LED components is not utilized. Another drawback is that the material cost of the solution can be high, as rather large surfaces are coated with phosphor [9, 28]. Also, as stated above, significant amount of heat is generated within the phosphor. When used remotely, the phosphor can hardly utilize the effective cooling provided for the LEDs. This can lead to serious thermal problems [29], as also reported in Paper II. Finally, the deep yellow colour of the remote phosphor solution can be considered a disadvantage as it may appear unattractive to end-users.

2.2 Substrates

The main purpose of the substrate is to provide electrical and thermal contacts to the LED chip or component. The substrate also gives mechanical support and can include optical elements such as lenses. Ceramics, metal core printed circuit boards (MCPCB) and insulated metal substrates (IMS) are typically used as high-power LED substrates [5, 21, 30]. In addition, silicon is used as submount between the LED chip and following structure, because the materials have similar coefficient of thermal expansion (CTE) and silicon can integrate a wide variety

electronics [5]. In literature, the meanings of MCPCB and IMS cross. In this thesis MCPCB is used to define a metal core structure with organic dielectric layer composition, while the IMS refers to a metal substrate with an inorganic insulation layer. Standard PCBs would be cheaper [31] but are rarely utilized due to insufficient thermal performance. Figure 4 displays five LED substrates with advanced thermal performance known in literature.

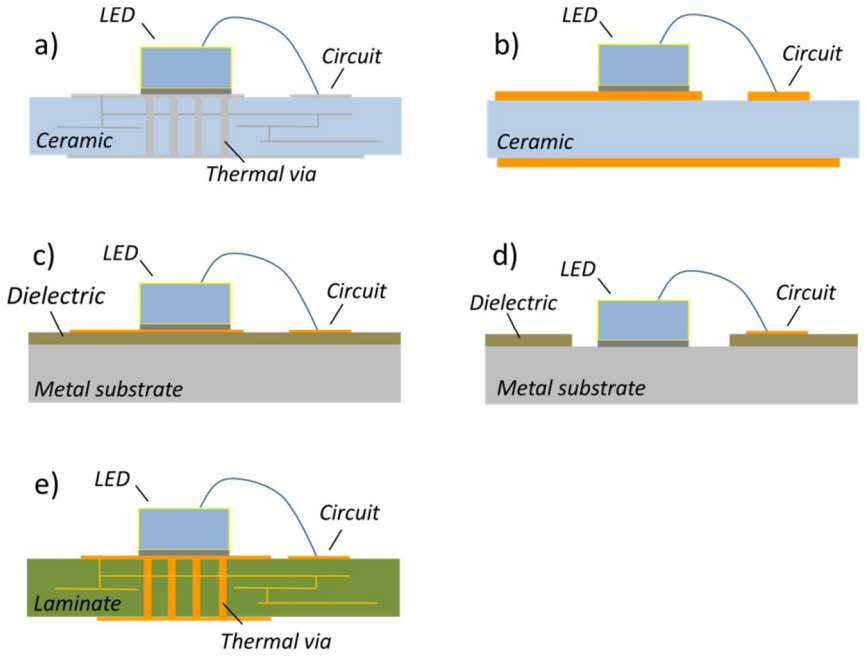

Figure 4. Methods for enhanced thermal performance of LED packaging: a) ceramic substrate with thermal vias, b) direct bonded copper (DBC), c) MCPCB / IMS, d) IMS with patterned dielectrics, e) PCB with thermal vias.

Ceramics (Figure 4a) can tolerate hazardous circumstances and enable multilayer structures and hermetic packaging. Consequently, ceramics are traditionally preferred in demanding applications such as automotive or space [32–34]. Unfortunately, the thermal conductivity of common ceramics like alumina and low-temperature cofired ceramics (LTCC) is low (k = 3 … 30 W/mK). AlN conducts heat well (k = 200 W/mK), but is not common in LED modulesdue to high cost [5, 35]. BeO is also good heat conductor, but toxic and, as such, an environmental and health risk [35]. For these reasons, MCPCB and IMS technologies have overtaken ceramics as common substrates at LED module level. However, due to the environmental stability and better CTE match of ceramics with semiconductors compared with metals, ceramics (alumina, LTCC, AlN) are widely used in LED components, especially in high-reliability applications [5, 36, 37]. In the future, the devel-

opment of novel composite materials, such as AlSiC, and advanced heat management structures, such as metal slugs, on multi-layer ceramic substrates are anticipated for improved LED packaging [5].

Direct bonded copper (DBC), shown in Figure 4b, is a process in which rather thick (~0.3 mm) copper foil is directly bonded to a ceramic substrate at a high temperature in an inert atmosphere. The bonding interface is thermally solid and strong enough to constrain the thermal expansion of copper that lowers the total CTE of the substrate. The disadvantage of DBC is that it cannot fabricate metallized vias through ceramic substrate. DBC substrates also suffer from reliability issues when subjected to extreme temperature cycling during which they have been reported to crack causing a loss of isolation properties. [5, 33, 34, 38]

The MCPCB and IMS technologies illustrated in Figure 4c enable good thermal performance at reasonable costs [5, 38]. The substrate consists of a 1–3 mm thick metal core that serves as a mechanical support and heat spreader, with an electrically insulating layer on the top surface. Typical core metals, copper and aluminium, are good thermal conductors (k = 240 … 390 W/mK). Due to the lower cost and weight as well as easier milling, aluminium boards are more widespread, although copper excels in thermal conductivity. Also, CTE of copper is lower when compared with aluminium, that matches better with semiconductors [5, 38–41]

For the insulation, different materials and techniques are available. Thin (35–125 µm) polymer-based dielectric realized with a lamination process is typical for MCPCB. The electrical circuits are made with deposited copper. [38, 39, 41] Attempts to improve the thermal performance of the MCPCB concentrate on the insulation layer, as the polymer is a poor thermal conductor compared with the base metal [39, 42]. Two basic methods are available – to improve the thermal properties of the insulation material or to develop thinner insulating layers. A common way to enhance thermal conductivity is to charge the polymer resin with ceramic particles. Alumina particles are typically used [39, 40], but more exotic materials like barium titanate [43] and diamond [44] are also proposed. The gained effective thermal conductivity of the dielectric layer depends on the materials used, their relative proportions, the microscopic structure of the particles and the quality of the interface with the metal surface [38, 39, 43].

The challenge of thin insulation layers is to gain low thermal resistance with sufficient electrical isolation because the voltage level on LED devices can be high. With very thin insulation layers, the layer quality can be an issue, as up to 35% variation in overall dielectric thickness has been reported [41], which easily causes problems with missing electric strength [41, 45, 46]. All these enhancements tend to increase the cost of the substrate. Another disadvantage of MCPCBs is that they are subject to delamination. Thermal stress and moisture absorption are known to be the primary causes of the delamination in polymer plastic packages due to hygro-mechanical stress and reduced interfacial adhesion strength [15].

Inorganic insulation layers are available with IMS technique enabling potential for reliable, high-power LED packaging. Electrochemical anodization is a traditional IMS technique. An anodic film thickness of about 20 to 40 µm is usually needed to

provide a high impedance insulation layer. To form electrical conductors, various plating, printing and sputtering methods are available. [47, 48]

Thermal vias under the heat source are known to be an effective heat management solution and are widely used with ceramic substrates (Figure 4a) [5, 36, 37, 42] as well as PCBs (Figure 4e) [31, 50]. The main reason for the lack of thermal vias in common MCPCB and IMS boards is the difficulty of via patterning and filling. With MCPCBs, thermal vias are not typically available since the lamination process is too inaccurate to realize the vias on the insulation layer before lamination by piercing. In addition copper-filled thermal vias cannot easily be made on an aluminium core MCPCB for processing reasons.

For IMS, combinations of metal core and patterned ceramic insulation film, such as alumina [5], LTCC [30] and AlN [49], have been introduced. Patterning of the dielectric layer to thermally connect the LED directly to the metal core of the substrate (Figure 4d), can be accomplished with a thick film printing method [30], aerosol deposition method [49] and patterned anodizing method [45]. The direct thermal contact allows efficient heat dissipation [5, 30, 49]. However, reliability and safety issues may be generated if the metal core is used as an electrical contact due to an electrically active metal base. In case of isolating the metal core electrically from the LEDs, the thermal via solution is limited to horizontal LEDs. The CTE mismatch between the chip and the substrate may also induce high thermal stress and a rapid decay in performance [5].

Regarding the via patterning methods, laser drilling is standard procedure in PCB manufacturing that could be applied rather economically. On the Cu-core MCPCB, some laser drilled thermal via solutions are shown [51]. With the Cu-core MCPCB, the difficulty in via filling could be solved by copper plating. (Paper I) Thick film printing is a well know method, capable of patterning IMS with high accuracy. When compared with anodizing and aerosol patterning methods, the printing is more convenient [30], as anodizing and aerosol methods utilize masks to realize the openings in the insulation layer [45, 49]. The challenge with thick film method is that the insulation film needs to be cured at high temperature. This poses problems with thermal expansion and temperature tolerance of the core metals during curing. (Paper III) A benefit of aerosol deposition method is that the insulation layer can be realized in room temperature [49].

3. Smart lighting control

Energy savings in lighting are currently striven via the switch from traditional light sources to more efficient ones such as LEDs [6, 7, 52]. Nonetheless, smart control is required to achieve the green targets set by many countries [9, 52–54]. Smart lighting control can be defined as a technology developed for energy savings and user comfort. The smart system relies on automated controls to adjust lighting according to different use conditions, such as presence or daylight availability. Unfortunately, user acceptance issues related to automated light levels and occupancy switch-off have been encountered [55–57]. Currently, the energy saving reasons are a strong driver of smart lighting technology development, and increasingly sophisticated controls are coming to the market at lower costs [58].

In this thesis, street lighting is used as a demonstrator for energy savings with smart control. It is estimated that in the world, the 220 million street lights use 159 TWh of energy annually, generating 81 megatons of CO_2 emissions [59]. The environmental impact is significant because street lighting is widely deployed, the power level in luminaires is high (18–400 W) and the intelligence level is typically low [54, 60]. A common way of control is based on a clock and/or daylight sensor adjusting the operating time, and the system is not capable of controlling the light levels. Earlier an active control was not feasible due to the difficulty of dimming traditional light sources. [52, 54, 60, 61] With the current LED revolution, smart features have become reality and intelligent software-controlled street lighting systems have started to emerge on the market [54, 61]. Typical state-of-art systems follow a centralized architecture with a central terminal and a number of local branch nodes communicating with the luminaires. The central terminal is responsible for commanding the luminaires and monitoring the status of the system. Local branch nodes act as a link between the central terminal and the smart luminaires. There is typically long distance communication (GPRS, Internet, Ethernet) between the branch node and the server and shorter distance transmission (proprietary RF, ZigBee, power line communication) from the local nodes to the luminaires. [52, 54]

The biggest energy savings would undoubtedly be achieved by not using the lighting at all. This is generally utilized in office type indoor lighting accustomed to turn the lighting on and off according to the presence of people, constituting considerable energy savings of 20–70% depending on the complexity of the system

and the parameters under control [55, 56, 62]. A review of 240 saving estimates from 88 papers and case studies in commercial buildings by Williams *et al.* [63] revealed that the average lighting energy saving potential was 24% for occupancy sensing, 28% for daylight harvesting, 31% for personal control, 36% for centralized control and 38% for multiple approaches. In street lighting, such simple functionality is typically not acceptable for safety and aesthetic reasons [52, 64–66], and more complex controls based on advanced sensing and dimming are required [52, 61, 65–67].

Energy savings with smart control in street lighting have already been demonstrated with traditional lighting technology. An extensive case study of 1350 street lights with a pre-programmed dimming schedule in Heshan City, China, resulted in a 27% energy saving [68]. Currently, with LEDs, the research has concentrated on dynamic control of the lighting at the operating scene. Lau *et al.* [61] introduced an adaptive street lighting algorithm based on traffic sensing to progressively control the brightness level. A remarkable 90% energy saving compared with conventional schemes was simulated [61]. Sun *et al.* [69] proposed a multi-sensor system to detect humans for solar powered street lights resulting in a reduction in the average energy consumption of 40%. Presence detection was also adopted by TU Delft [70] to create dynamic street lighting with savings of up to 80% promoted. Such savings are impressive. However, they are often based on simulations [61] or show cases [70] rather than real life installations, which would be rather complicated to execute. In addition, street lighting levels are often strictly regulated [60]. Consequently, academic reports of energy savings with smart LED street lighting in real use environments hardly exist.

Besides the energy concerns, the growing interest in smart control arises from the fact that the main function of lighting is to serve people and their demands [54, 64–66]. In the future, smart control should be able to save energy while providing suitable lighting for the user. Features beyond lighting, like guiding or information, are also widely anticipated [4, 7–9]. Future lighting systems like the one illustrated in Figure 5 must therefore consider contextual information such as the number and identity of the end-users and their behaviour, which can be obtained via sophisticated sensor data and interaction between the devices [9, 65]. It is foreseen that in the near future the ‘Internet of things’ will combine many individual devices in our everyday life into one communicating network. A significant number of the communicating devices may be related to lighting. Traditional devices, such as mobile phones, will participate by providing user interfaces and sensors for the lighting and other services [58]. Such development is already being introduced by, for example, Müllner and Riener [52], who propose a system utilizing a Global Positioning System (GPS) and smartphone to adjust street lights around the pedestrian, and Viraktamath and Attimarad [71] who propose using text messaging (SMS) via mobile phones to control street lighting on demand.

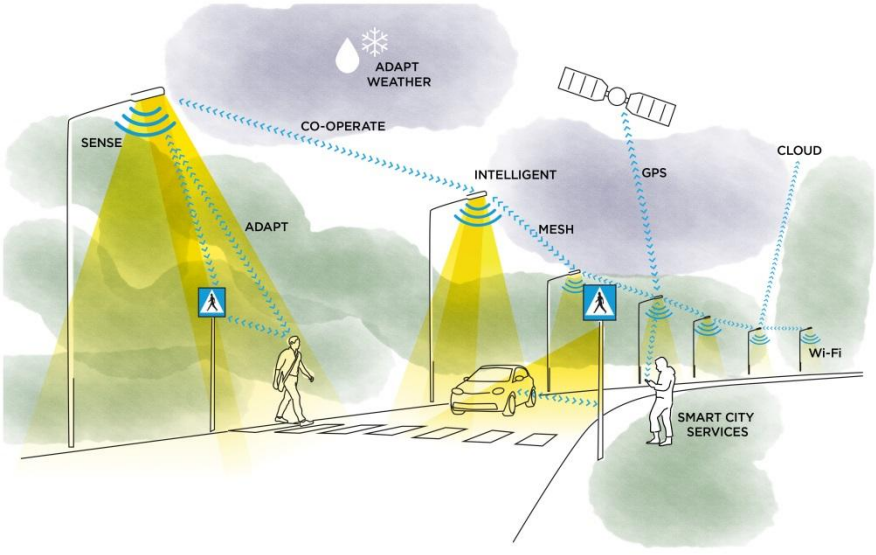

Figure 5. Visio of smart street lighting in the future.

4. Thermal measurements and simulations

A variety of methods exists to measure the temperature of a semiconductor device. A summary of common methods is given in Table 2. Optical methods utilize the temperature variation of some optical property as a thermometer. Infrared radiation is probably the most commonly used optical method for temperature measurements with commercial measurement equipment that are readily available. The method is popular as temperature maps of the surface can easily be made. The concern with infrared temperature measurements is the emissivity of the surface, which can have a major influence on quantitative measurements. Another significant disadvantage is that packaged devices cannot be measured because it is necessary to have optical access to the chip. [72]

Packaged devices can be measured with an electrical method that uses the electrical parameters of the device as the thermometer. No special sample preparation is required if the device is measured as one heat source, as all the necessary electrical connections are already available as they are needed for the normal device operation. The disadvantage is that the method provides an averaging measurement for a device that usually has some temperature distribution. [72]

The temperature measurement can also be performed with a transducer, such as a thermocouple, probe or blanket film, that is placed in physical contact with the semiconductor. Some measurement inaccuracy can be involved due to contact resistance and the heat sink character of such a probe, but an advantage is that a high spatial resolution can be achieved. As with the optical methods, a practical drawback is that the semiconductor chip must be visible. [72]

All these methods were utilized in the framework of this thesis. However, the main results introduced rely on the electrical method using the temperature dependence of the forward voltage of the semiconductor. The thermal measurements performed in this thesis are described in Section 4.1. The inherent inability of the electrical method to show temperature distribution is tackled with thermal simulations, introduced briefly in Section 4.2. Steady-state thermal simulations also served to compare different designs and to validate the results and conclusions.

Table 2. Methods for measuring the temperature of semiconductor devices [72].

Method	Measured quantity	Advantages	Disadvantages
Optical	• Infrared emission • Wavelength shift	+ Temperature map + No contact + Good spatial resolution	– Needs surface view – Surface emissivity issues
Electrical	• Junction voltage • Threshold voltage • Resistance	+ Packaged device + No contact	– Averages – No temperature map
Physical contact	• Scanning nanoprobe • Liquid crystals • Thermographic phosphors	+ Temperature map + Potentially high spatial resolution	– Needs surface view – Contact may disturb temperature

4.1 Thermal resistance and LED junction temperature

In this thesis, thermal resistance is used to characterize developed LED components and modules and compare them with commercial references. By definition, the thermal resistance from the LED junction to the specific environment, R_{th}, is the temperature difference between the junction and the reference ambient, ΔT, divided by the heating power, P_{heat} [13]. For LED components, thermal resistance from the junction to solder point is typically given [18, 19]. The solder point is the thermal contact between the component and the circuit board.

$$R_{th} = \frac{\Delta T}{Pheat} \quad (1)$$

The measured optical power was subtracted from the measured electrical power to calculate the heating power. The measurement set-up utilized in this thesis is illustrated in Figure 6. Optical power was measured simultaneously with the thermal measurement. An integrating sphere with a diameter of 0.5 m (type: UMBB-500, Gigahertz Optik) was used for the measurement. The LED device was placed in the opening of the sphere wall so that the light was guided into the sphere. The calibration coefficient was measured to take into account the non-ideal nature of the sphere surface [73].

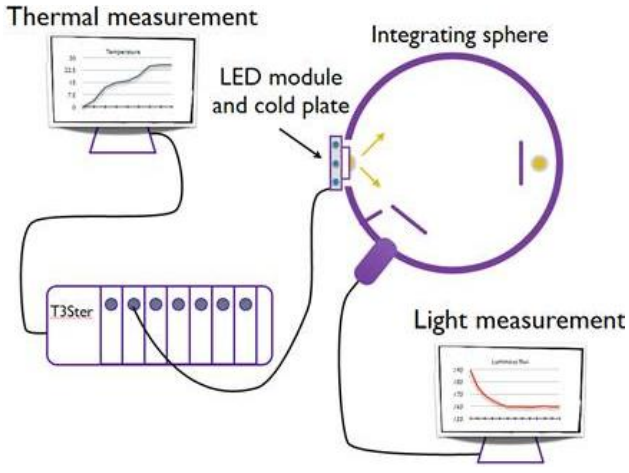

Figure 6. Thermal and optical measurement set-up.

The temperature measurements were performed with the thermal transient tester T3Ster (Mentor Graphics Corp.), commonly employed in LED measurements [15, 30, 40, 44, 50, 74]. T3Ster uses the temperature dependence of the semiconductor forward voltage for thermal characterization of device structures [75]. The measurement system records the junction temperature of the LED as a function of time and calculates the thermal transient response of the structure. From this response, the cumulative structure function describing the thermal resistance is processed [76]. The cumulative structure function is a one-dimensional description of the thermal path from the heat source to the ambient. Characteristic parts in this thermal resistance curve can be used to identify thermal domains of the measured device [9], as illustrated in Figure 7. In many cases the thermal domains are difficult to distinguish because the heat flow path consists of materials with similar thermal conductivity, and the interface quality between the domains is good. The differential structure function is the derivative of the cumulative structure function, bringing out even the small changes as peaks and valleys. The differential structure function is therefore commonly utilized in comparative analysis.

The most complete result would be achieved by measuring each LED chip individually as in Paper III. Unfortunately, in many cases this is not feasible as high-power LED devices typically contain tens or even hundreds of chips. For this reason, a common practice is to consider the entire chip array as a one heat source as in Papers I, II and IV. The result describes the thermal path from the LED array to the ambient, and the temperatures or the thermal resistances of individual chips cannot be distinguished. The measurement procedure follows the JESD51-51 standard [77], which describes the measurement method for individually available single LEDs and any multichip LED array arrangements.

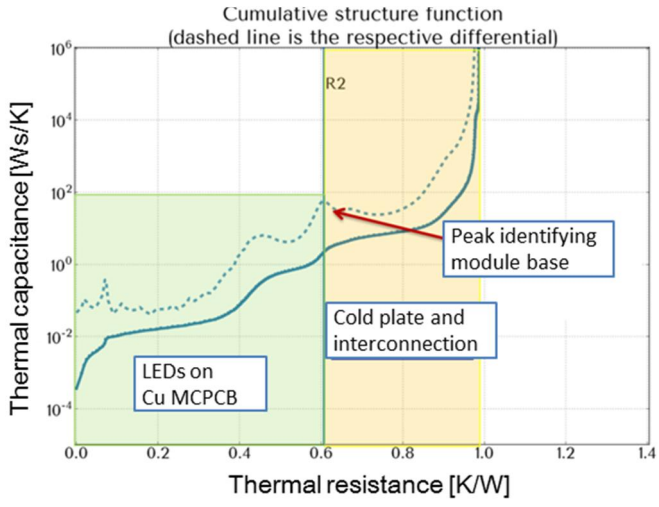

Figure 7. Thermal domains of the chip-on-board LED module with copper core MCPCB substrate. (Paper I)

The measurement procedure has two parts. First, the sensitivity coefficient for the LED heat source is determined in a calibration measurement using a temperature-controlled thermostat chamber, bath or cold plate. The LED device is driven with a small sensor current in order to generate only a negligible amount of heat. For high power devices, that are often composed of several LEDs in an array, sensor currents of 10 to 20 mA are typical. Higher currents would cause self heating with negative impact on the accuracy of the temperature measurement. The voltage over the LED device is recorded at different temperatures, for example, from 20 °C to 80 °C in 10 °C steps. A line is fitted to the measurement points using the least square method. The slope of the line, that is the sensitivity coefficient, describes the dependence between the voltage over the LED and the temperature at the sensor current. This temperature sensitivity of the forward voltage is the reciprocal of the so-called K-factor defined in semiconductor device thermal testing standards [9].

After the calibration, the LED device is subjected to the actual test environment. High-power components and modules are commonly measured with active cooling on a water-cooled cold plate. This way, the environment is well controlled for comparison studies. The measurement time is also relatively short, typically minutes. The method was used in Papers I, II and III, comparing the thermal resistances of different structures. Modules can also be measured with natural convection cooling on a heat sink as in Paper III or in the luminaire chassis as in Paper IV. In this case, the measurement takes hours to complete, but the temperatures and resistances represent the actual use environment. Consequently, the method is typically used when the thermal performance of a particular solution, such as a lamp or luminaire, is recorded.

During the measurement, the LEDs are first driven with the nominal current until the structure is thermally stabilized. With high power devices, currents between 700 mA and 1A are typical. The stabilization time depends on the test environment as described above. In forced cooling it takes minutes, whereas in passive cooling this heating period can take hours. When the structure is thermally stable, the current is suddenly switched to the small sensor current and the voltages over the LEDs are recorded. Commonly, the recording time coincides with the heating time. From the measured voltage values, the corresponding temperatures are calculated according to the sensitivity coefficient determined by the calibration.

Due to the switching procedure, there are effects of electrical interferences during the measurement. The electrical transients result from the measurement circuit response time, the charge storage in the device under test and the parasitic effects due to the device package. The electronic signals settle down after a time delay of microseconds. [72] In this work, this part is neglected when processing the measurement data with the T3Ster measurement software to avoid the electrical interferences affecting the results.

4.1.1 Inaccuracy in thermal measurements

The measured total thermal resistance of the test structure and, consequently, the LED temperature varies significantly with the thermal interface quality to the cooling device. This is particularly critical with components and modules artificially attached to the active cooling device for measurements because the attachment interface is not part of the structure to be measured. This is the case in Papers I, II and III, which use thermal paste and a screw attachment at the active cooling interface. Changes in paste amounts and pressure can cause measurement inaccuracy because the paste is applied and the screws fastened by hand. The high power and small size of the device induces the effect. Consequently, there is some inherent inaccuracy in the LED junction temperature measurement of components and modules on artificial cooling devices. In future, dynamometric key could be used for fastening with equal force.

To eliminate this inaccuracy, the thermal resistance from the LED chips to a characteristic part of the measured structure is used in comparative analysis instead of the total thermal resistance or LED temperature. Typically, the module bottom is used as the measurement point, and the method of making a controlled change is exploited. The method is based on artificially changing some interface resistance of the measured structure to identify this interface in the thermal resistance curve. The location of the change in the structure function coincides with the physical part of the structure that was altered. Thus, by changing the module base – the cold plate interface quality, and by comparing the structure function curves, the peak defining the module base can be identified. This is shown in Figure 8, in which the amount of thermal paste on the module – the cooling plate interface is changed. Occasionally, the module bottom interface is still hard to find, leading to errors in the measurement results. Even so, the procedure is considered more accurate than using the total thermal resistances.

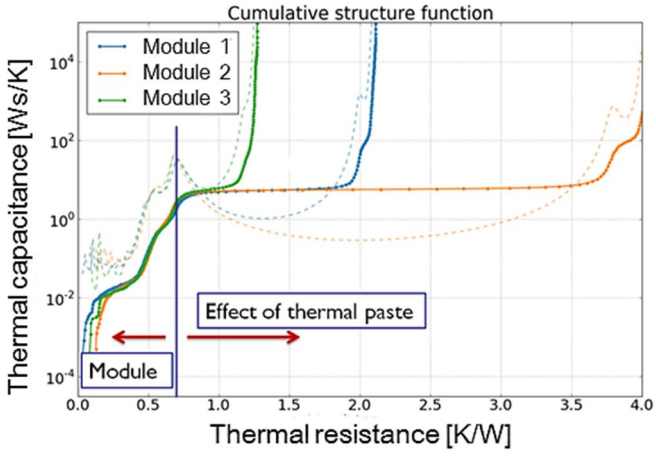

Figure 8. Structure function comparison of similar Cu MCPCB modules 1, 2 and 3 with a different module – cold plate interface quality. (Paper I)

The T3Ster system principle of measurement is based on the assumption of 1D heat flow, although in reality some spreading inside the LED module occurs. This can cause uncertainty of the measurements. However, when the LED heat source occupies a significant portion of the module and the active cooling forces the heat essentially in one direction, this uncertainty can be considered low (Papers I and II). In addition, some sideward spreading, that is a 2D effect, was incorporated into the studies with added phosphor (Paper II) and passive cooling (Papers III and IV), and the resulting effect on the structure function was discussed. Thus, the measured structure function is considered a 1D equivalent circuit representation of the more complex physical system.

Conduction, convection and radiation are all included in the measurements and simulations in this thesis, but neglected in the discussion about results, as the T3Ster measurement system is not capable of differentiating them. Components (Paper I, II) and modules (Paper III) are measured with active cooling and only the conduction heat transfer is considered when analysing the results. Therefore, heat loss due to convection and radiation causes some inaccuracy to the results. However, their effect is negligible due to the small size and low surface temperature of the devices. Based on simulations, the radiation and convection losses at the module substrate only amount to 1% of the total heat dissipation (Paper III). The luminaire is measured when cooled with natural convection and the effect of convection is shown in the structure function (Paper IV).

4.2 Thermal simulations

In this thesis, steady-state thermal simulations are performed with the 3D computational fluid dynamics simulation software FloTherm (Mentor Graphics Corp.), which is capable of considering conduction, convection and radiation heat transfers. The simulations imitated the real test structures and testing parameters, such as heating power and ambient temperature, precisely, although some simplifications of the simulated structures were made in order to keep the number of grid cells reasonable. FloTherm cannot realize round shapes due to gridding. Consequently, round features, such as microvias (Paper I), were replaced with rectangular blocks of equal volume. Electrical conductors, which are thin and narrow metallic layers and are thus not effective heat spreaders, were also omitted from the simulations when not located in the close vicinity of the LEDs.

An important factor leading to inaccuracy in the simulations is the validity of the material parameters used. With well-known materials, such as metals, the inaccuracy can be considered minor. However, in the case of alloys, such as solders, or mixed composites, such as phosphor encapsulant (Paper II) and FR4 insulation (Paper I), the inaccuracy in material parameters could affect the fidelity of the simulation results, especially if the material is in the critical part of the heat flow path.

Significant cause of uncertainty in simulations compared with measurements is the thermal interface quality, also discussed with thermal measurement in Section 4.1.1. In simulations all the interfaces are in perfect contact while in reality voids and other defects exists. This can cause simulated temperatures to be lower than measured values. In this thesis, the most critical interfaces are between the LED and the circuit board, and between the test structure and cooling device. The simulations were evaluated by comparing simulated temperatures with measured results. In general, they were in good agreement within a couple of degrees difference of each other. The largest difference of 3.5–7.7 °C between the simulations and measurements was discovered with the Cu MCPCB component (Paper I), including round microvias and an orthotropic FR4 insulation layer, realizing the major sources of inaccuracy in the simulations described above.

5. Thermal resistance at component level

Due to the cost and size benefits, high-power multichip chip-on-board (COB) LED components are currently the industry trend [5, 21]. The multichip component is a package with many chips located close together, while the chip-on-board defines that bare chips in contrast to packaged devices are directly mounted on and electrically interconnected to the final circuit board. Multichip component has much higher power than a single-chip LED component. It can provide more lumens and a wider light-emitting area when compared with a single-chip package while simultaneously producing more heat [5, 21].

In this chapter, the thermal resistance of the LED component is investigated with the multichip COB test structure introduced in Section 5.1. The chapter is based on Papers I and II. The research concentrates on improving the thermal performance of the component with a developed MCPCB substrate (Paper I). The effect of the phosphor encapsulant on the thermal resistance of a high-power COB LED structure is also discussed while a nearby phosphor packaging concept is introduced (Paper II). The test procedures are described in Section 5.2 and the major findings are reported in Section 5.3. Finally, some conclusions are given in Section 5.4.

5.1 Chip-on-board LED components

Copper-core MCPCB with copper-filled microvias under the LED chips through the insulation layer was developed for the multichip COB LED component. The thermal performance of the solution was compared with the same COB structure on an alumina substrate as a reference representing the common commercial solution. The multichip components consisted of a 9 x 9 array of blue chips (Epistar InGaN Venus Blue) with a 1.5 mm pitch. The array was symmetrically surrounded by four red chips (Epistar AlGaInP PN-series LED chip), one at each side of the array The Epistar chips were used because the blue chips had electrically insulating bottom. Also, as they are not the latest state-of-the-art in market, they are more affordable and easily available, that would make the component reasonable for certain applications and customers. The substrate size was 26 mm x 30.5 mm. To make the component tolerant against a single LED open or short failure, the

electrical connection of the chips was a combination of series and parallel connections, as illustrated in Figure 9. The true current through each LED in not know, as in reality, the current distribution within the LED array is different from the even distribution shown in Figure 9 due to the heat distribution and the performance variation between the LEDs. The chips were wire-bonded with Au wire and die-bonded on the substrates with silver-filled epoxy (Epoxy Technology H20E). The adhesive bonding is not the best choice for thermal performance. Here, since the research efforts concentrate on substrate, the LED joining does not make any difference, as the same adhesive method was used for both components used in the comparison. The test components are illustrated in Figure 10. (Paper I, Paper II)

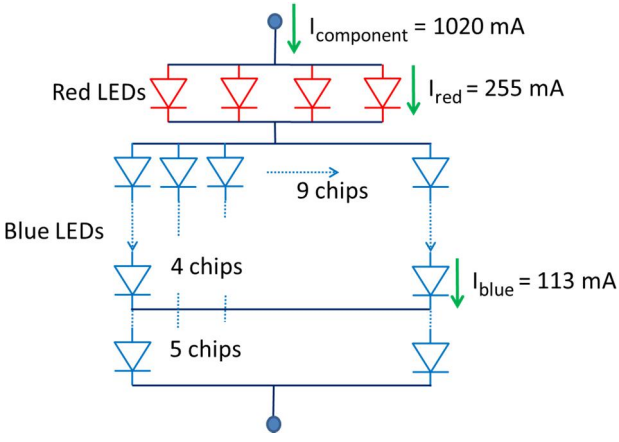

Figure 9. Simplified electrical circuit of the LED module. The I_{red} and I_{blue} are approximated based on even current distribution within the LED array. (Paper I, Paper II)

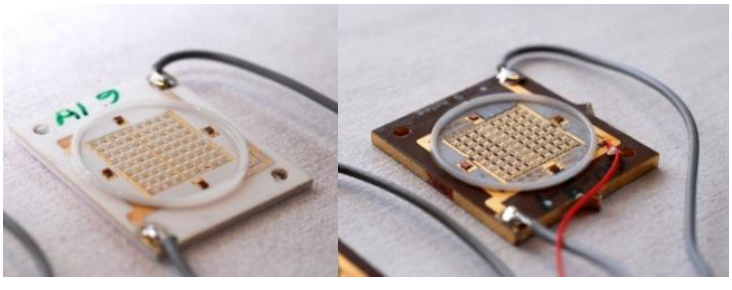

a) b)

Figure 10. a) Alumina and b) Cu MCPCB component used in the comparison. (Paper I, Paper II)

The reference substrate was 1.27 mm thick alumina with screen-printed electrical contacts on top. The Cu MCPCB had a 2 mm thick copper core and about 70 µm thick FR4 (IT-180, k = 0.88 W/mK) insulation layer with copper-filled microvias under each blue LED chip. The red LED chips had electrical contact on the bottom so thermal vias could not be used under them. The microvia was slightly cone shape with a diameter of approximately 90 µm. Different numbers and layouts of vias (4, 5 and 9 vias) were tested. The component configurations are illustrated in Figure 11 and via the configurations in Figure 12. The substrate thicknesses, 1.27 mm for the alumina and 2 mm for the Cu MCPCB, are typically used with the technologies. Thus, the component represents the standard substrate technology available. The layout and the LED array on Cu MCPCB and alumina substrates were identical. (Paper I)

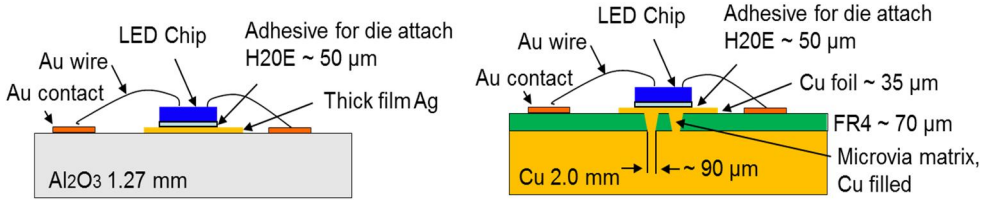

Figure 11. a) Alumina test structure and b) Cu MCPCB test structure with blue LEDs. (Paper I)

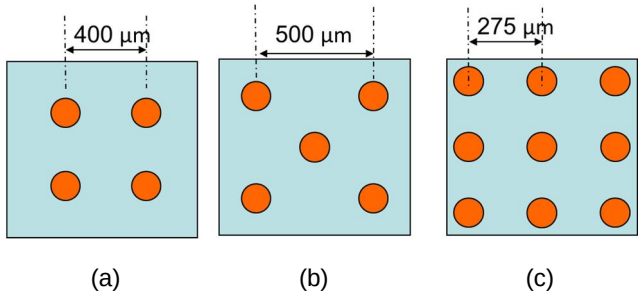

Figure 12. (a) 4 via configuration, (b) 5 via configuration and (c) 9 via configuration tested under the blue LED chips on Cu MCPCB component. (Paper I)

For the manufacturing of Cu MCPCB substrates, standard equipment commonly available in PCB shops was utilized. More details about the manufacturing process can be found in Paper I. The vias on the MCPCB module were realized after the lamination process with laser milling, which is a standard procedure and does not increase the manufacturing cost dramatically. Copper plating was used to fill the vias completely with copper. The use of copper as the core metal enables the

via processing. The thermal conductivity of the core is also higher compared with the aluminium core MCPCB. Unfortunately, the cost of the copper is higher as well. However, as the thermal vias provide a good thermal conduction path through the isolation layer, very low cost insulation material, FR4, can be used. In addition, thicker layers can be used to improve electrical isolation. (Paper I)

5.1.1 Phosphor packaging concepts

In contrast to previous studies [23–26], which concentrate on light extraction efficiency, the thermal performance of the COB LED component with different phosphor packaging concepts was studied. A nearby phosphor concept in which the phosphor is placed at a short distance from the LEDs is introduced and compared with phosphor directly dispensed on LED chips as illustrated in Figure 13. Contrary to the remote phosphor concept used in modules [23] or lamps [9], the structure is very small and flat. Thus, it could be more easily used with secondary optics and in applications with space limitations like automotive head lamps or downlights. The phosphor vehicle could also be used for sealing or physical protection of LEDs in demanding applications.

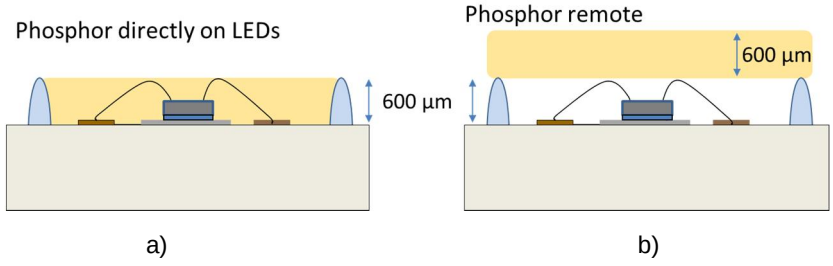

Figure 13. Test structure with (a) phosphor covering the LEDs and (b) a spacer holding the nearby phosphor plate at a short distance from the LEDs. (Paper II)

Three different phosphor packaging concepts were used in the comparison. The phosphor was dispensed directly onto the LED chips as illustrated in Figure 14a, the phosphor was dispensed on the nearby glass plate as illustrated in Figure 14b, and the phosphor was injection-moulded into plastics used as nearby plates as illustrated in Figure 14c. The alumina-based LED component illustrated in Figure 10a was utilized as the light source. Due to the lower absorption losses of the white substrate surface, it is more favourable in optical measurements than the developed Cu MCPCB component. In addition, the ceramic board would enable hermetic sealing.

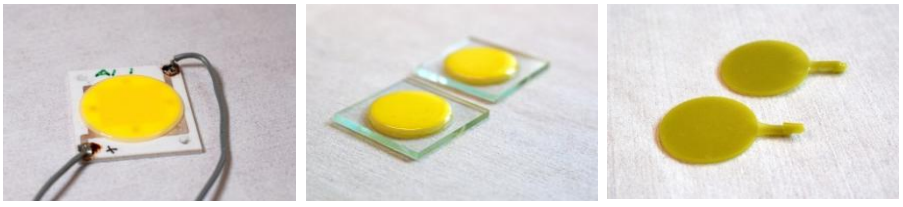

a) b) c)

Figure 14. (a) COB LED module with phosphor A10% covering the LEDs, (b) A10% and A12% phosphors on glass plates and (c) injection moulded plastic phosphor plates. (Paper II)

Commercial phosphor powder A (YAG:Ce) and an experimental phosphor powder B were used. To achieve warm white light (~3000 K), phosphor powder A was mixed with polymers with 10% and 12% mass per cent concentrations denoted accordingly. Phosphor powder B was mixed with the same polymers in very low concentration. The approximated mass per cent of phosphor B was less than 5%. The thickness of the dispensed phosphor directly on LEDs and on the nearby glass plate was approximately 600 µm. In the injection-moulded samples, the plate thickness was 2 mm, and phosphor A10% was used with PC Lexan 123R-111 plastic. The silicone (Hysol 3323) ring holding the dispensed phosphor in place was realized with a simple dispensing and curing process. In the nearby phosphor concept, the silicone ring was used as the spacer between the LED chips and the phosphor. (Paper II)

5.2 Testing procedures at component level

5.2.1 Thermal simulations

The 3D computational fluid dynamics simulation software FloTherm was used for the steady-state thermal simulations. The simulation models imitated the test structure dimensions and materials described in Section 5.1. Components were placed on 1 cm thick aluminium plate with a fixed temperature setting of 20 °C in the bottom that imitated the cold plate used in the measurements. The temperature of the surrounding air (ambient) was also 20 °C. The heating power in the simulations was determined by measuring blue chip array and red chip array separately. The heating power at the individual chips was obtained by subtracting the measured radiant power from the measured electrical power and allocating it to the solitary LED chips. For the alumina component, a heating power of 0.43 W was used for each red chip and 0.23 W for each blue chip. For the MCPCB component, the corresponding values were 0.40 W heating power at each red chip and 0.24 W heating power at each blue chip. As vast majority of the chips are blue they consume more than 90% of the total heating power of the component. The electrical power was the same for alumina and Cu MCPCB components, but the

radiant power on Cu MCPCB was lower than on the alumina due to the absorption losses of the darker colour surface. This contributed slightly higher heating power on Cu MCPCB component. In the simulations this extra power was allocated to the blue chips although in reality part of it is also absorbed into the board. (Paper I)

In simulations including phosphor, the alumina component was used as the light source. The total heating power was 27 W, consisting of 20.7 W heating power in the LED array and 6.3 W heating power in the phosphor that was attached to the whole volume of the phosphor material in the simulations. Thermal power values were selected based on measurements. The measured thermal power with and without phosphor for each sample is given in Table 6. (Paper II)

5.2.2 Thermal measurements

Thermal measurements were performed with the thermal transient tester T3Ster. The entire component consisting of 85 LED chips in an array was considered one heat source. The substrate was attached with screws and thermal paste to the 20 °C water-cooled cold plate performing as the test environment. Calibration was done with a sensor current of 20 mA for each component at temperatures from 20 °C to 80 °C in 10 °C steps. The average measured sensitivity coefficient of all the COB components without phosphor was -18.1 mV/K with a standard deviation of 1.3 mV/K, while the voltage of the modules was approximately 24.6 V. The phosphor concept study included 9 components from this group and the average measured sensitivity coefficient of them was -17.4 mV/K with a standard deviation of 1.1 mV/K. The sensitivity coefficients are for the entire LED array constituting the component. As the LEDs are the same with and without phosphor, the average sensitivity coefficients should be equal. Here, they slightly differ due to the different number of components used to calculate the averages, but the deviation is within the standard deviation of the total group. (Paper I, Paper II)The actual measurement was performed by driving the LED component first at a heating current of 1020 mA for 10 minutes and then another 10 minutes with a sensor current of 20 mA. Assuming even current distribution according to the electrical connection of LEDs (Figure 9), the heating current through each red LED chip was 255 mA and through each blue LED chip 113.3 mA. To determine the repeatability of the measurement and identify characteristic features in the structure function, more than 5 repeated measurements were done for a representative test structure using different drive currents and amounts of thermal paste between the component and the cold plate. The achieved standard deviation of thermal resistance in the repeatability tests was better than 0.02 K/W. (Paper I, Paper II)

The red and blue chips had different configuration and the Cu MCPCB structure was different under them (thermal vias lacking under the red chips). Thus, some additional tests were conducted measuring blue chips and red chips separately. The average measured sensitivity coefficient was -16.9 mV/K for the blue LED array and -1.6 mV/K for the red LED array. The measurements utilized the same set-up, and the calibration and measurement procedure described above. (Paper I)

5.3 Results and discussion on LED components

5.3.1 Chip-on-board substrate with enhanced thermal performance

The thermal simulation results comparing developed Cu MCPCB with reference alumina substrate are reported in Table 3. The insulating layer has a significant influence on the thermal performance of Cu MCPCB as the average temperature of the red LEDs on Cu MCPCB is 7 degrees higher than on the reference alumina component. Under the blue LEDs, copper-filled thermal vias are used on Cu MCPCB. Consequently, the average blue LED temperatures are lower on Cu MCPCB than on alumina. The average temperature of the blue LEDs with 9 via configuration Cu MCPCB is the lowest in the simulations. This is due to the largest number and density of vias under the LED. As illustrated in Figure 15, the LEDs in the middle of the array are warmer than the LEDs located in the side areas. This is caused by thermal interaction between the LEDs [21]. (Paper I)

Table 3. Thermal simulation results of the COB LED component with different substrate configurations ($I_{component}$ = 1020 mA). The component consisted of a 9 x 9 array of blue chips symmetrically surrounded by four red chips, one at each side of the array. (Paper I)

Substrate	Temperature, [°C] Average of blue LEDs	Temperature, [°C] Average of red LEDs
Alumina	46.9	35.4
Cu MCPCB, 4 vias per blue LED	41.3	42.3
Cu MCPCB, 5 vias per blue LED	41.0	42.3
Cu MCPCB, 9 vias per blue LED	39.7	42.3

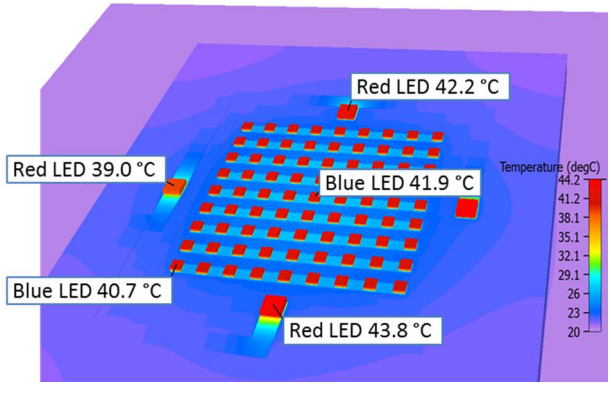

Figure 15. Simulated surface temperature on COB Cu MCPCB component with 4 microvias under each blue LED. (Paper I)

The thermal measurements of the multichip COB components revealed that up to 55% reduction in total thermal resistance was achieved with the Cu MCPCB solution compared with the alumina component. Altogether, 7 Cu MCPCB components and 7 alumina references were measured and the mean thermal resistances from the LED array to the bottom of the board are given in Table 4. A characteristic peak in the differential structure function was used to determine the component base as already illustrated in Section 4.1, Figure 7. The peak was identified to denote the component bottom by the method of making a controlled change in the test structure thermal resistance. (Paper I)

Table 4. Thermal measurement results of the COB component with different substrate configurations ($I_{component}$ = 1020 mA). There are no vias with red LEDs at any substrate as thermal vias could only be used under the blue LEDs. (Paper I)

	Component	**Average of blue LEDs**		**Average of red LEDs**	
Substrate	R_{th}, [K/W]	R_{th}, [K/W]	Temp. [°C]	R_{th}, [K/W]	Temp. [°C]
Alumina	1.12	1.14	48.3	8.1	32.7
Cu MCPCB, 4 vias	0.61	0.56	36.9	19.4	50.0
Cu MCPCB, 5 vias	0.59				
Cu MCPCB, 9 vias	0.50				

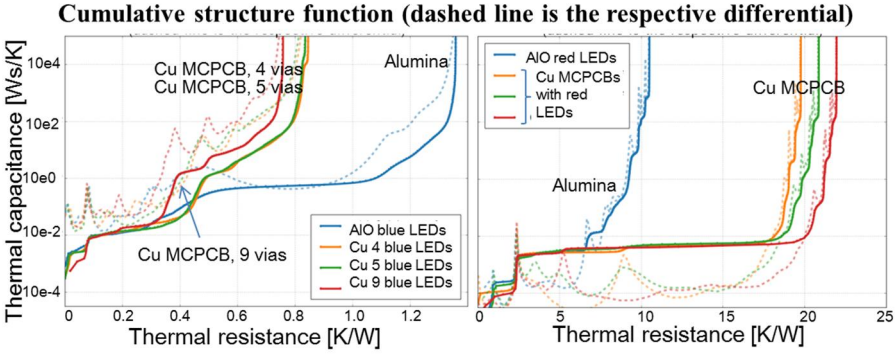

a) b)

Figure 16. Structure function of a) the blue LED array and b) the red LED array. The alumina component is indicated by the blue line. The Cu MCPCB component is indicated with red, green and orange line. Thermal vias are only located under the blue LEDs on Cu MCPCB (15a). (Paper I)

The blue and red LED arrays on alumina and Cu MCPCB components are separately compared in Table 4 and Figure 16. Considering the blue LEDs, the thermal performance of the developed Cu MCPCB is significantly better than the performance of the alumina reference. The Cu MCPCB component with 9 vias under each blue LED was measured with the lowest resistance of 0.48 K/W. This is well understood as the number and density of vias is considerably higher with 9 vias compared with 4 and 5 via versions between which no difference in thermal performance was distinguished. It should be noted, however, that for a solid comparison of different microvia configurations on Cu MCPCB, the number of samples is low. The situation is totally different considering red LEDs as there are no vias under the chips on the Cu MCPCB. Instead, there is a layer of FR4 with poor thermal conductivity. Consequently, the LED temperatures and thermal resistances are higher when compared with the alumina component. (Paper I) Regarding measurement inaccuracy, as described in Section 4.1.1, the variation in thermal interface quality to the cooling device is causing deviation in the temperature measurements (Table 4) and the total thermal resistance shown for the Cu MCPCB component in Figure 16b. The uncertainty in red LED array measurement is furthermore discussed in Paper I.

The thermal resistance of the component should be lower than the thermal resistances of the blue and red chips measured independently because, thermally, the blue and red chip arrays are in parallel [74]. However, the thermal balance of the component is difficult to analyse theoretically because the red and blue arrays are not independent of each other. They are closely situated and consequently heating each other, and the electrical circuit connecting the chips is a combination of series and parallel connections. This is also a cause for simulation inaccuracy, as the power distribution during the measurements could have differed from the even distribution assumed in the simulations. In addition, the factors related to material parameters and dimensions already discussed in Section 4.2 could also contribute to a difference when comparing simulations with measurements. Nonetheless, it can be stated that simulations and measurements agree that the enhanced thermal performance of Cu MCPCB component is due to copper-filled microvias under the blue LEDs. The thermal resistance of the module coincides with the thermal resistance of the blue chip array because it produces 92–93% of the thermal power of the module.

5.3.1.1 Radiant power

The radiant power was measured with an integrating sphere simultaneously with the heating phase of the thermal measurement. When calculating based on mean thermal resistance and average heating power on each component type, the average LED temperature advantage of Cu MCPCB components with 4, 5 and 9 vias over the alumina reference is 9.8 °C, 10,3 °C and 12,3 °C respectively. Since the average LED temperatures are higher on alumina boards, there should be less light emitted than on Cu MCPCB, as discussed in Section 2.1.1. However, this

was not discovered, as the average radiant power of the Cu MCPCB components and alumina components was 10.3 ± 0.5 W and 11.4 ± 0.3 W respectively. (Paper I)

When measured separately, the blue LEDs were on average 11,4 °C cooler on Cu MCPCB than on alumina. According to manufacturer datasheets, such reduction in ambient temperature (I_{blue} = 120 mA) would approximately constitute less than 2% increase in relative radiant flux of the blue LED. This is less than the standard deviation in the optical measurement, that explains why the achieved benefit in thermal resistance is not shown in light measurements. According to manufacturer datasheet, the red LEDs are more sensitive to temperature. Here, the red LED temperatures on developed Cu MCPCB component are actually higher than on reference alumina, because the thermal vias could not be used with them. Consequently, the red LED are emitting 12% less on Cu MCPCB than on alumina approximated based on equivalent ambient temperature reduction and I_{red} = 350 mA. However, as only 4 out of 85 LEDs in the component are red, the blue LEDs are dominating the total performance.

The result is also influenced by the substrate colour. The alumina component with white substrate reflects more light than the Cu MCPCB with a darker substrate surface due to absorption losses. This is a drawback of the Cu MCPCB technology introduced in this thesis and needs to be tackled by white masking [31], using a reflective concave cup under the LED array [21], or by changing the colour of the insulator material to make this technology commercially successful.

5.3.2 Effect of phosphor encapsulant on the thermal resistance of the COB LED component

Different phosphor packaging concepts were compared with thermal simulations, and the results are shown in Table 5. Without any encapsulant, the bare LED temperatures are 1–2 °C higher than when clear polymer encapsulant without the phosphor ingredient was used. In the case of phosphor covering the LEDs, the thermal power increase in phosphor concluded 2–3 °C increase in LED temperatures compared with clear polymer encapsulant. Also on components with nearby phosphor, the LEDs were only up to 1.7 °C warmer than bare LEDs, although the nearby plate heats up considerably as illustrated in Figure 17. In general, the maximum temperature in the polymer/phosphor layer exceeds the average LED temperature. This is because the maximum temperature is located where this layer and the warmest individual LED chip are in contact. In addition, self-heating in phosphor due to white light conversion losses occurs. (Paper II) The temperature distribution within the LED array has already been discussed in Section 5.3.1.

Table 5. Thermal simulation results with different phosphor packaging configurations on the COB LED component ($I_{component}$ = 1020 mA). (Paper II)

Packaging option	Temperature, [°C] Red LEDs (average)	Temperature, [°C] Blue LEDs (average)	Temperature, [°C] Polymer/phosphor (maximum)
Bare LEDs	35.4	46.9	-
Clear polymer covering the LEDs	34.4	44.9	46.2
Phosphor A10% covering the LEDs	36.7	48.1	50.0
Nearby phosphor with injection moulded plate	36.8	48.6	223
Nearby phosphor with glass plate	36.8	48.4	186

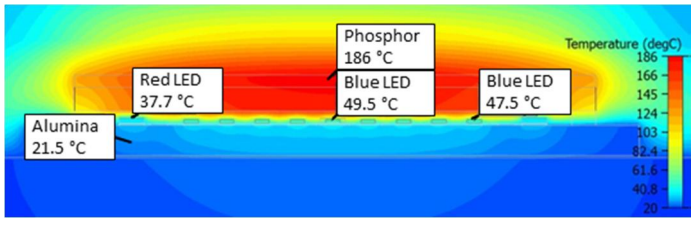

Figure 17. Simulated temperatures of the COB LED component with phosphor on nearby glass plate. (Paper II)

Thermal measurements with and without phosphor encapsulant on the COB LED component demonstrated that thermal resistance decreases with added encapsulant. The thermal resistance from the LED chips to a characteristic peak in the differential structure function within the thermal domain of the LED component was used in thermal analysis. This peak indicated as the comparable thermal resistance is shown in Figure 18 and the results obtained are listed in Table 6. The average temperature of a bare LED array without phosphor A ($I_{component}$ = 1.02 A) was 48.2 °C. After adding phosphor A, the average LED array temperature was 48.4 °C, although the thermal power increased by 29% due to the white light conversion losses in the phosphor. By adding the clear polymer encapsulant, the LED array temperature decreased by 2.6 °C, although there was a 12% thermal power increase. On samples with phosphor B, the situation is analogous to clear polymer encapsulant due to the very low phosphor concentration. (Paper II)

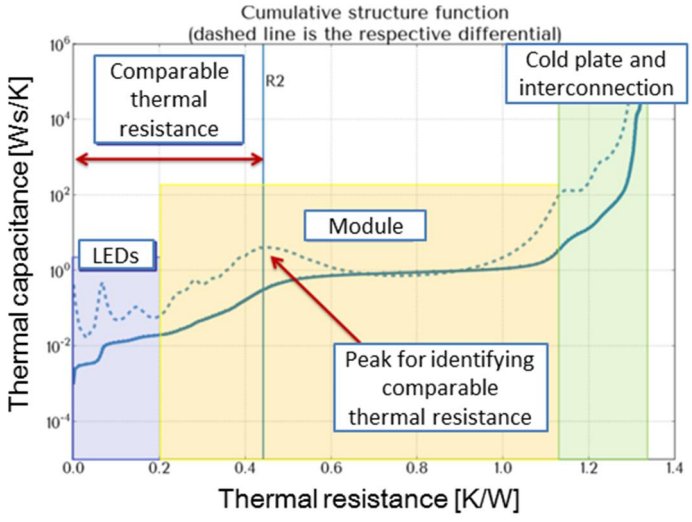

Figure 18. Thermal domains of the LED component and the comparable thermal resistance used in analysis. (Paper II)

Table 6. Optical and thermal measurement results with (w) and without (w/o) phosphor covering the LEDs ($I_{component}$ = 1020 mA). (Paper II)

Sample		Radiant power [W]			Thermal power [W]			Temperature of the LEDs, [ºC]			Comparable thermal resistance, [K/W]		
Phosphor		w/o	w	Change	w/o	w	Change	w/o	w	Change	w/o	w	Change
1.	A10%	11.3	5.5	-51%	20.9	26.8	28%	47.8	47.7	0%	0.44	0.34	-23%
2.	A10%	11.3	5.3	-53%	20.9	26.9	29%	48.6	49.5	2%	0.48	0.36	-25%
4.	A12%	11.4	5.2	-54%	20.9	27.1	29%	48.3	47.9	-1%	0.48	0.38	-20%
5.	B5%	11.8	9.5	-19%	20.8	22.4	7%	46.3	43.8	-6%	0.46	0.37	-19%
6.	B5%	11.9	9.9	-17%	20.1	22.1	10%	45.4	43.1	-5%	0.46	0.38	-17%
7*	- **	8.5	6.9	-18%	13.4	15.0	12%	39.2	36.6	-7%	0.50	0.40	-20%

* $I_{component}$ = 700 mA

** Clear polymer encapsulant

The thermal resistance of the component decreased with added encapsulant. The encapsulant creates a new heat conduction path as it overrides the air above the chip as illustrated in Figure 19. In this study, the path was good enough to compensate for the thermal power increase caused by the wavelength conversion in the phosphor encapsulant. Since the measured temperatures did not rise with added phosphor while the thermal power increased, the thermal resistance calculation for the module indicates lower values. The clear polymer encapsulant has

the same effect. Thermal simulations agree with these findings. In addition, simulations indicate that the maximum temperature in the phosphor encapsulant exceeds the average LED temperature as also reported in [79]. This is interesting as the thermal management of LED devices commonly concentrates on minimizing the LED junction temperature. In the future, the attention may turn more to thermal distribution within the phosphors that are already known to be very sensitive to temperature [5, 9, 26, 79].

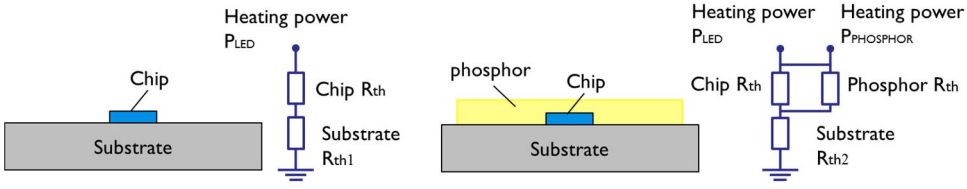

Figure 19. Simplified structure and thermal resistance model of a) component with bare LED and b) component with phosphor covering the LED. (Paper II)

There are some uncertainties in the simulations, as already discussed in Section 4.2. With regard to the phosphor encapsulant, there is inaccuracy in the location and volume of the generated power within the phosphor. In the simulations, the power is evenly distributed whereas in reality it is more likely to be located centrally and closer to the LEDs. The effect of the phosphor filler on the thermal properties of polymers and injection moulded plastic is also not considered in the simulations. However, according to the percolation theory [80], there is a drastic increase in thermal conductivity only after the filler is about 17% volume per cent of the total composite.

5.3.2.1 Optical measurements

An integrating sphere was used for radiant power and luminous flux measurements. Significant optical losses were measured with the nearby concept. When compared with dispensed phosphor samples the average luminous flux of nearby phosphor in glass components decreased down to 65%. The result was recorded with a drive current of 300 mA because the nearby plates could not tolerate the 1020 mA current used in thermal testing due to overheating. The absorption losses in the nearby plate were higher than expected, especially on the injection moulded samples, as the outcome was only 22% of the flux of the reference samples with dispensed phosphor although the light transmission of 88% is given for the material (PC Lexan 123R-111). (Paper II)

An inheritable feature of the nearby concept is that the LEDs occupy most of the module surface under the nearby phosphor plate. Thus, the LEDs themselves

will be the primary cause of backscattered light absorption [5, 24, 25, 78]. Losses due to substrate surface could be reduced using more reflective material under the LED array [21].

When used remotely, the phosphor can hardly utilize effective cooling provided for the LEDs. Optical filler with fitted refractive index between the nearby plate and LEDs would relieve the thermal issues and enhance the optical efficiency [5, 6, 78]. In this study, the nearby phosphor plate was practically insulated from substrate and the cold plate by the silicon ring spacer. Consequently, some serious thermal issues were demonstrated in the nearby phosphor samples with the 1020 mA drive current as in some cases the glass plates cracked and the plastic started to melt. Overheating was also reported by Luo *et al.* in [29]. The simulated temperature of ~190 °C at the nearby plate surface agrees with the thermocouple measured 180 °C. The heat is caused by white light conversion losses in the phosphor plates. As the LED temperatures were below 50 °C, they are not considered to heat the nearby plate significantly. (Paper II)

5.4 Conclusions at component level

The excellent thermal performance of the high-power COB LED component based on Cu MCPCB substrate was demonstrated. The performance was compared with the identical alumina component by means of thermal simulations and measurements, and a reduction of up to 55% in the thermal resistance from the LED source to the bottom of the substrate was indicated. The enhanced performance of the Cu MCPCB substrate is due to copper-filled thermal vias under the blue LED chips. (Paper I) The conclusion is coherent with the results of Lee *et al.* [45] who compared LED package temperatures with and without thermal contact through the anodized insulation layer. The thermal resistance corresponds to the via configuration – lower thermal resistance was shown on modules with a larger number and higher density of vias. The result coincides with the findings of Shin *et al.* [31] studying thermal vias on laminated PCBs and Yang *et al.* [37] concentrating on ceramic substrates. The LED chip itself constitutes the main part of the LED component cost. However, it is estimated that 20–30% of the cost of an LED component is attributed to the packaging materials and approximately 5–10% to manufacturing [5]. Here, horizontal LED chips with affordable price were used. The Cu MCPCB processing was relatively short and consisted of the standard steps of PCB manufacturing. In addition, the low-cost insulation material FR4 was used. Consequently, a cost-efficient and low thermal resistance COB LED component was demonstrated.

Thermal vias connect the LED directly to the metal core plate of the component, that explains the good thermal performance. Consequently, the via technology is only available for horizontal LEDs with electrically insulated bottom, and it is not compatible with vertical or flip-chip LEDs, which are more typical for high power solutions. The dark colour of the developed Cu MCPCB substrate is another challenge to tackle when targeting LED component market. For these reasons, the

developed Cu MCPCB might find better applications in other fields, such telecommunication, in future.

The effect of the phosphor packaging on the thermal performance of the high-power COB LED component was studied with simulations and measurement. It was demonstrated that encapsulant dispensed on the LED chips creates a new heat conduction path, as the encapsulant overrides the air above the chip. In the case of the encapsulant holding the phosphor particles, this path compensated the thermal power increase caused by the white light conversion losses in phosphor, and the temperatures on phosphor-coated LEDs and non-coated LEDs was measured to closely match. Furthermore, results indicate that LED temperatures could be decreased with clear encapsulant. In this case, the phosphor should be applied to some remote object. However, the study revealed optical absorption and thermal issues in the nearby phosphor concept introduced towards this target. (Paper II) Despite the challenges faced, the nearby concept is attractive for future research as it is of a small size and low cost compared with traditional remote phosphor solutions and provides the potential of integration with sealing or other mechanical/optical structures.

6. Thermal resistance in LED modules

Thermal performance improvements in high-power LED modules is studied in this chapter by comparing modules based on a novel thick-film insulated aluminium material system (IAMS) with the LED modules on commercial MCPCB. The chapter in based on Paper III. The MCPCB was selected as the reference because it is the most commonly used substrate in high-power LED modules [30, 31, 40]. Test structures are introduced in Section 6.1. The results are reviewed in Section 6.2 and concluded in Section 6.3.

6.1 Test modules

The test modules consisted of four Luxeon Rebel (LXML-PWC1-0100) LED components [18] soldered on a circuit board with an aluminium base plate and dimensions of 50 mm x 50 mm x 2 mm. The LED pitch was 20 mm. Testing included 24 modules in total: 9 modules on IAMS substrates with a ceramic insulating layer (IP 6075) and a polymer solder mask (denoted as an IAMS polymer),10 modules on IAMS substrates with a ceramic insulating layer (IP 6075) and a ceramic solder mask (denoted as IAMS ceramic), and 5 modules on commercial MCPCBs with a T-preg insulation layer (k = 3 W/mK) as a reference. The test modules are shown in Figure 20.

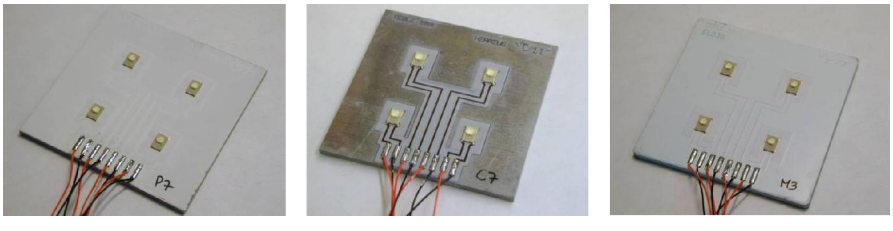

a) b) c)

Figure 20. a) IAMS module with polymer overglaze, b) IAMS module with ceramic overglaze and c) MCPCB reference module. (Paper III)

IAMS is a material system with screen printed dielectric, conductor and overglaze materials designed to be compatible with the aluminium substrate. More details on the IAMS manufacturing process can be found in Paper III. The test structures are presented in Figure 21. The Rebel LED has an electrically isolated thermal pad in the bottom of the component and most of the heat is transferred through it. Due to the screen film patterning of the IAMS circuit board, the thermal via could be made right under this pad as illustrated in Figure 21a. The via is the same size and shape as the thermal pad and it is filled with screen-printed silver (type C8829B) for good heat conduction. As already discussed with the component substrates, the utilization of thermal vias for heat management enables the use of lower cost insulation materials and thicker insulation layers for electrical isolation. With regard to IAMS technology, another advantage is that due to the additive printing process, the insulating layers and circuits can be used only where needed. This results in minimal material waste during substrate manufacturing compared with standard PCB and MCPCB manufacturing, in which sheets of copper are chemically etched away to create the circuit. (Paper III)

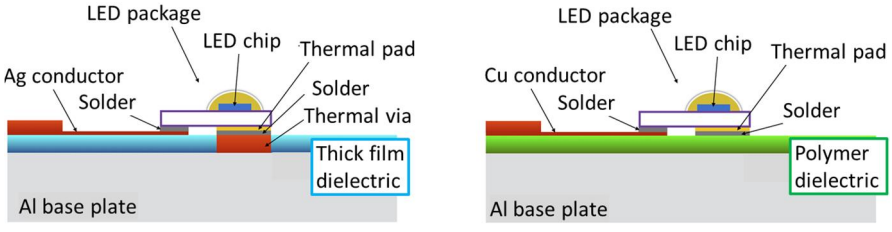

Figure 21. a) IAMS test structure, b) MCPCB test structure. (Paper III)

6.1.1 Thermal simulations

The goal of the simulations was to study the module with different substrate designs. Simulations were performed with FloTherm. The dimensions and material properties imitated the real test structures. The temperature of the surrounding air in the computational domain was 25 °C and a fixed setting of 25 ºC was also used in the module bottom imitating the cold plate used in the measurements. The heating power was 1.97 W per LED ($I_{component}$ = 700 mA), which coincided with the measured average heating power of LEDs on the IAMS boards. The thermal resistance of the LED component was matched to the measured 8 K/W.

Table 7 compares the simulated results of LED modules with different substrate configurations. The via is located underneath the thermal pad of the LED component. The optimum via size is 1.77 x 2.8 mm^2, which coincides with the thermal pad size of the LED. A larger via would increase the material costs due to the silver consumption but would not improve thermal performance. A smaller via would degrade the performance. The MCPCB with and without a heat spreading

layer is simulated as a reference. The results demonstrate a clear advantage of IAMS substrate over MCPCB technology. Without the heat spreading layers typically used with MCPCB substrates, the advantage is even more prominent. The simulations indicate that the thermal improvement of IAMS over MCPCB is due to the thermal via. Without the via, the LED temperatures on IAMS and MCPCB with heat spreading layers are in the same range. The dielectric layer of the IAMS board is thinner but has lower thermal conductivity compared with reference MCPCB. (Paper III) The conclusions agree with the findings at component level and the literature concluded in Section 5.4.

Table 7. Thermal simulation results of the LED module with different substrate configurations ($I_{component}$ = 700 mA). (Paper III)

	Via dimensions, [mm]	**LED temperature, [°C]**
IAMS without vias	-	53.6
IAMS with optimum via	1.77 × 2.8 × 0.06	45.2
IAMS with large via	3.0 × 4.0 × 0.06	45.1
IAMS with small via	1.0 × 1.0 × 0.06	48.2
MCPCB	-	51.2
MCPCB, no heat spreading layers	-	58.4

6.1.2 LED component soldering

Four LED components were soldered on each test substrate. The soldering was done with SnAgCu solder in a reflow oven. The solder was screen printed using 120 µm stencil and the LEDs were set in place by hand. All the samples were X-ray inspected after soldering. It was revealed that the IAMS Polymer samples suffered from voids more than the IAMS ceramic and reference MCPCB modules. Nonetheless, in general, the soldering quality was equal between the IAMS and MCPCB modules. Figure 22 illustrates an example of good soldering, bad soldering and typical soldering for each module type. (Paper III)

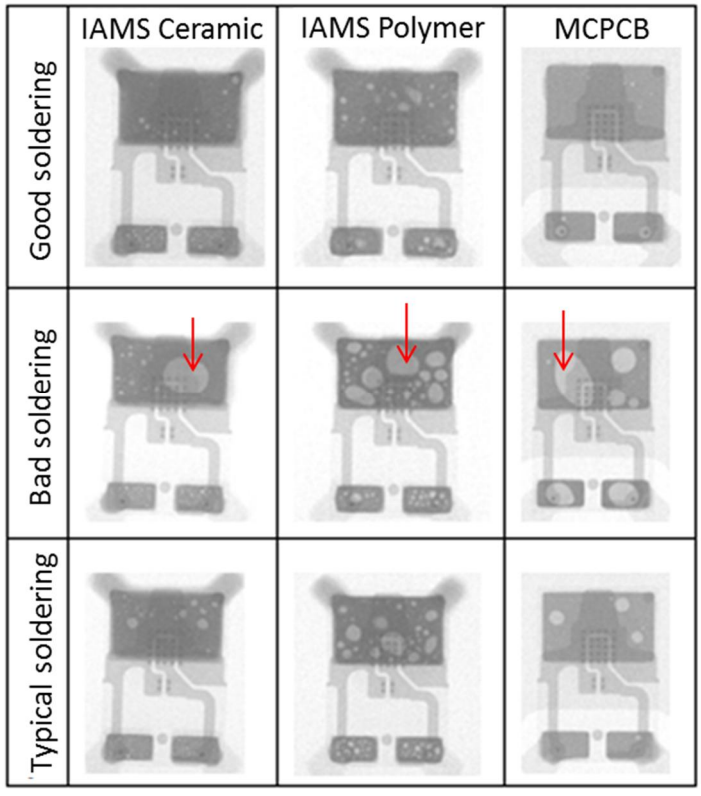

Figure 22. X-ray image of good soldering, bad soldering and typical soldering of each board type. The largest void in the thermal contact is indicated by a red arrow. (Paper III)

6.2 Results and discussion on LED modules

6.2.1 Measurement procedures

Temperature measurements were performed with the thermal transient tester T3Ster. The calibration was done with a sensor current of 10 mA at temperatures from 25 °C to 75 °C with 5 °C steps. The temperature coefficient of the LED forward voltage ranged from -1.8 mV/K to -1.2 mV/K. The actual measurement was made on a thermoelectric cooler that kept the bottom of the substrate at 25 °C. The module was first heated with a drive current of 700 mA for 10 minutes and then measured with a sensor current (10 mA) for another 10 minutes. The result was recorded for each LED on the module separately, although the entire module was measured at once. (Paper III)

To test repeatability of the measurement, three test substrates were measured twice. In repeated measurements, difference in total thermal resistance and LED temperature was less than 0.5 K/W and 1.1°C respectively. The amount of thermal paste and pressure in the substrate – the cold plate interface could have contributed this difference. The use of the characteristic feature in the structure function identified with the controlled change method instead of the total thermal resistance could have improved the accuracy. (Paper III)

The luminous flux and radiant power of the test modules were measured with an integrating sphere. The temperature of the LEDs and the luminous flux of the modules were recorded simultaneously, and the whole test module was measured at once. Consequently, the recorded luminous flux is the sum of 4 LEDs. The radiant power was recorded in a separate measurement in a similar manner. The measured radiant power of LEDs on each substrate was subtracted from the electrical power to calculate the total heating power. The average radiant power of an LED was 0.51 W on the IAMS ceramic, 0.55 W on the IAMS polymer and 0.53 W on the reference MCPCB. The average electrical power was 2.50 W for IAMS ceramic, 2.50 W for IAMS polymer and 2.38 for MCPCB. (Paper III)

6.2.2 Thermal resistance and LED junction temperature

Lower temperatures and thermal resistances were measured for modules with thick-film manufactured IAMS substrates than for modules with reference MCPCBs. The average LED junction temperature ($I_{component}$ = 700 mA) on the MCPCB was 53.1 °C with standard a deviation of 1.0 °C while it was 46.2 ± 0.8 °C on IAMS with polymer overglaze and 45.0 ± 1.5 °C on IAMS with ceramic overglaze. The mean value of the total thermal resistance from the LED junction to the bottom of the substrate for MCPCB was 15.5 K/W with a standard deviation of 0.4 K/W. The mean total thermal resistances for polymer and ceramic overglazed IAMS substrates were 11.2 ± 0.6 K/W and 10.4 ± 0.7 K/W respectively. Thus, among the polymer and ceramic overglazed IAMS substrates, the total thermal resistances from junction to module bottom were on average 4.3 K/W and 5.1 K/W lower than for the reference MCPCBs, which is a 28–33% reduction in the thermal resistance of the module. (Paper III)

The IAMS modules differ only by the solder mask material, which should have insignificant influence on the module's thermal performance. Instead, there was some variation in the LED soldering quality between the IAMS modules, which is considered to be the cause of the slightly higher temperatures and resistances on IAMS polymer modules compared with ceramic ones.

When considering only the thermal resistance of the substrate the advantage of the IAMS technology is even more prominent. In Figure 23 the thermal resistances of a sample of each module type are illustrated. A reduction of 46% and 67% in the substrate thermal resistance with IAMS technology is demonstrated when compared with MCPCB. However, the accurate location of the LED package – the substrate interface is hard to identify, causing some uncertainty in this conclusion. (Paper III)

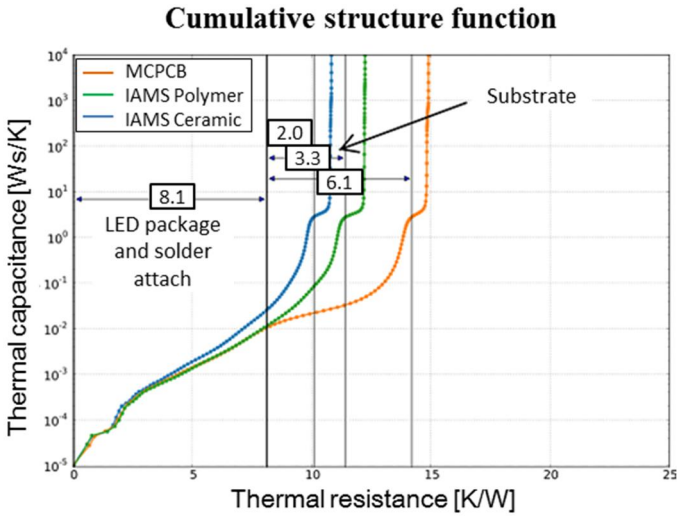

Figure 23. Structure function of an LED on MCPCB (orange), IAMS with polymer overglaze (green) and IAMS with ceramic overglaze (blue) modules. Thermal resistance of the LED component and different substrates are shown. (Paper III)

6.2.3 Luminous flux

The average luminous flux of the IAMS polymer, IAMS ceramic and MCPCB modules was 680 lm with a standard deviation of 23 lm, 657 lm ± 22 lm, and 681 lm ± 29 lm respectively. The LEDs on IAMS were on average 7–8 °C lower that on reference MCPCB module. Approximating based on manufacturer datasheet, such reduction in thermal pad temperature would constitute less that 1% increase in relative luminous flux, that explains why the reduced thermal resistance of IAMS modules is not shown in light measurements. Performance variations between LED components are also fairly large that shadows the results. The bin range of the luminous flux for the used LED component is about 30 lm at 700 mA [18]. (Paper III)

As already discussed in Section 5.3.1.1 with the LED components, the substrate colour affects the optical measurements due to absorption losses. This was also discovered here as the white modules (IAMS polymer and MCPCB) outperformed the darker colour IAMS ceramic.

6.3 Conclusions on LED modules

The IAMS substrate consists of an aluminium base plate with a screen-printed isolation layer and electrical contacts. In this study, a large thermal via through the insulation layer on IAMS substrate is realized and filled with screen-printed silver. The thermal contact of the LED component is soldered on top of the via. As a

result, 28–33% reduction in the thermal resistance from the LED junction to the bottom of the module was demonstrated compared with the standard MCPCB module. (Paper III) A similar test module has been realized by Heo *et al*. [30], reporting approximately 70% reduction in total thermal resistance compared with FR4 PCB and a 40% reduction compared with PCB with thermal vias for a 50W LED package prototype.

The average electrical power levels were slightly higher on the IAMS modules when compared with the MCPCB modules, indicating that there were more losses in the screen-printed conductors. This increases the heat load on the module, and implies that also the thermal conductivity of the metallizations may be low. However, this topic was not addressed in the current study and should be considered in future.

IAMS technology enables a purely inorganic substrate that would be beneficial in high reliability packaging and sealing of LEDs as well as other high-power devices. As the reliability of IAMS technology was not considered in this study and should be covered in future, especially because the high CTE of aluminium and the brittle character of the screen-printed ceramics might cause problems in real use environment.

7. Energy efficiency at luminaire and system level

In this chapter, performance improvement in high-power LED lighting is studied at luminaire and system level. The chapter is based on Paper IV. The aim of the research was to demonstrate energy savings in street lighting with advanced LED lighting technology without sacrificing end-user comfort. The target was set to use a pilot installation with commercial luminaires as a starting point to improve technical performance as well as user acceptance. As a result, an energy efficient street light designed for a pedestrian road is introduced in Section 7.1. The role of thermal management, among other aspects, such as optics design for end-user comfort, is discussed. In Section 7.2, a realization of a smart street lighting system is described, and energy savings with smart control in pedestrian street lighting is reviewed. The system consists of developed street lights with smart control, and it was implemented at the pilot installation site for performance evaluation in a real use environment.

7.1 Luminaire design and performance

A LED luminaire for pedestrian street lighting was developed to study energy efficiency in outdoor lighting application. The luminaire consists of aluminium tubes modified to house the LEDs, optics and control electronics. The luminaire is illustrated in Figure 24. Altogether 18 high-power LEDs (Cree XM-L) [19] were used. The LEDs were placed in two arrays, 9 LEDs each, along the tubular structure of the luminaire. Each LED was fitted with a free-form optical lens that was manufactured by glass moulding. (Paper IV)

The LED component had a rather cool correlated colour temperature (CCT) of 4600 K. The component selection was made based on the results of the user survey with commercial reference luminaires. As only mild preference for warm CCTs was discovered [81], a neutral CCT was chosen for the developed luminaire to reach higher energy efficiency. It could also be speculated that this choice may have a positive effect on the feeling of safety because cooler CCTs appear brighter in dark environments [60]. Light pollution or photobiological issues [82, 83] related to the blue-rich spectrum were not considered. The colour rendering index

of the LED component was also rather high (82) and was selected to achieve the true colours of nature (grass, snow) for a pleasant and inviting scene at the pilot installation, which took place in an outdoor recreation area. (Paper IV)

Figure 24. The smart LED luminaire for pedestrian street lighting. (Paper IV)

The technical performance of the developed luminaire was compared with commercial street lights. Four luminaires of each type were measured and the average values are listed in Table 8. More details of the commercial luminaires can be found in [81]. Commercial luminaires included high-pressure sodium (HPS), metal halide (MH) and three different types of LED luminaires (LED1, LED2 and LED3) denoted accordingly. The luminous efficacy of the commercial luminaires was 54–78 lm/W while the luminaire developed in this study achieved 96 lm/W. Thus, an energy saving of 19–44% was achieved through improved luminous efficacy compared with commercial luminaires. However, the comparison is not that straight forward, as the colour temperatures of the luminaires differ. The LEDs with cooler colour benefit from smaller losses of radiant power in the phosphor layer due to smaller stokes shift. Also, when calculating luminous flux, the match of the luminaire spectrum with the sensitivity of human eye effects the results.

Considering the measured LED junction temperature (Section 7.1.1), the approximated luminous efficacy of the selected LED is 117 lm/W [19]. This means that 18% of the luminous efficacy is lost in the luminaire. The main contributors are the driver electronics efficiency and optical losses. Compared with reference luminaires, the colour temperature of the developed luminaire is high (~4600 K). Assuming the efficacy loss of 18% in the developed luminaire, warm CCT (2600–3700 K) of the same LED would constitute luminaire efficacy of 80 lm/W, that is still the best in the test group, although close to the reference luminaire types LED1 and LED3 (~4000 K). It can be concluded, that the high luminous efficacy of

the developed luminaire is due to the high efficiency LED component with cool CCT. High efficacy driver, thermal management and optics realization also contributed good performance. (Paper IV) The commercial luminaires represent the technical status in 2011 while the developed street light was manufactured in 2012. Thus, compared with the LED luminaires, the developed street light has benefitted from the rapid development of LED technology.

Table 8. Laboratory measurement results of the pilot installation luminaires. (Paper IV)

Luminaire	P_{ele}, [W]	P_{rad}, [W]	P_{rad} / P_{ele}	Luminous flux, [lm]	Efficacy, [lm/W]	Colour temp., [K]	CRI
LED1	38.4	9.1	24%	2 950	77	4220	68
LED2	38.5	6.6	17%	2 070	54	2960	84
LED3	33.8	7.9	23%	2 650	78	3980	69
HPS	66.4	10.5*	16%	3 570	54	1880	23
MH	63.9	11.1*	17%	3 770	59	3300	72
Developed luminaire	30.5	9.4	31%	2 940	96	4610	82

* measured after 4900 burning hours

7.1.1 Thermal management of the luminaire

The objective of the thermal management was to guarantee acceptable LED temperatures for stable and efficient function of the luminaire. The thermal performance was measured with the thermal transient tester, T3Ster, in an air conditioned laboratory room with an ambient temperature of about 23 °C. The measurement was done with a sensor current of 20 mA and constant drive current of 720 mA delivering 4000 lm. The heating and cooling times were both 3.5 hours and the entire LED array was considered one heat source. Prior to the measurement, calibration was made by sinking the LED modules of the luminaire into the temperature-controlled water bath from 20 °C to 70 °C in 10 °C steps. The measured maximum LED array temperature of the developed luminaire was 40.4 °C. (Paper IV)

The thermal structure of the luminaire consists of the LED component (Cree XM-L) solder joined (SnAgCu) to a commercial MCPCB with T-preg dielectrics. Each LED had its own board of the size 30 mm x 30 mm. These kinds of modules were thermally connected with thermal paste and screws to the aluminium chassis of the luminaire that acted as the passive cooling device. In this arrangement, the LED modules were thermally in parallel on a common heat sink. Electrically all

LEDs were connected in series. With natural convection, the heat was transported from the luminaire chassis to the ambient. As shown in Figure 25, the thermal resistance of the convection from the chassis to the environment is about 0.7 K/W, which is greater than the total resistance of the other parts of the luminaire combined. The dielectric part of the module substrate is about 0.3 K/W. The module bottom interface was identified with controlled change method described in Section 4.1.1. Based on previous studies (Figure 23 in Section 6.2.2), some 50–70% of the thermal resistance of the module substrate could be reduced with advanced substrate technology. Calculating such an improvement for the dielectric part in Figure 25 would constitute 10–15% savings in the total thermal resistance of the luminaire. Despite this number only being an estimate, it clearly shows that at luminaire level, the thermal management of the LED components and modules is not capable of achieving major performance improvements alone. Instead, together with other features, such as optical design for end-user comfort and smart control for energy savings, an optimized solution could be achieved. (Paper IV)

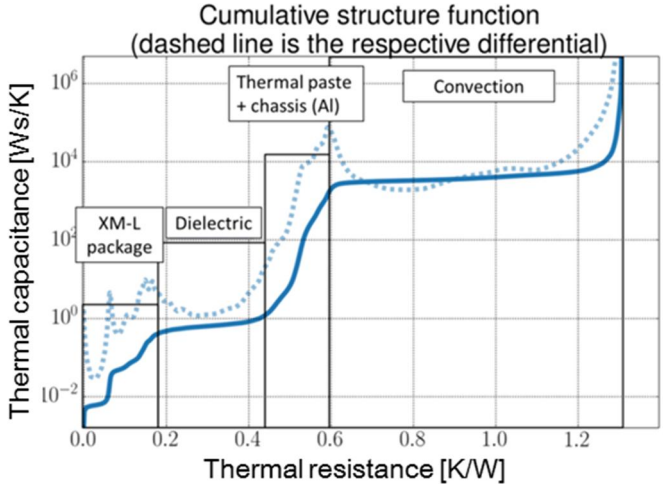

Figure 25. The structure function of the luminaire. The thermal domains of the luminaire are identified in boxes. The luminaire was measured as one heat source in which thermally the LEDs are in parallel on a common heat sink. (Paper IV)

Steady-state thermal simulations with FloTherm were used to analyse the temperatures in the worst case scenario, which was the maximum power (P_{heat} = 36 W, 4000 lm) in still air and 35 °C ambient temperature. The average LED temperature in the worst case scenario was 66 °C, which is well below the 135 °C maximum temperature of the LED component. The simulated model imitated the luminaire structure and was validated by comparing the results with the measurements. Good agreement was found as the average simulated LED temperature in 23 °C

ambient was 39.6 °C, which is only 0.8 °C different from the measured temperature. (Paper IV)

7.1.2 End-user feedback

The design of the luminaire utilized the technical and end-user feedback conclusions of the pilot installation with commercial luminaires [81]. The technical performance of the reference luminaires is already listed in Table 8. The end-user survey results suggested that the luminaire should be designed to avoid glare and that the spatial distribution of the luminous flux should give enough light on the verge of the road so that the neighbouring areas would also be partly illuminated. The lessons learned were incorporated into the optics design of the developed luminaire. To avoid glare, the luminous flux was mostly limited in gamma angles less than 75°. The average illuminating area was also large as the LEDs were spread along the tube structure with a 60 mm pitch, creating a sensation of a large area emitter. More details of the optical design of the luminaire are given in Paper IV.

The developed luminaires were installed on the pilot installation site on a pedestrian road in the City of Helsinki. The installation site was the same that was already occupied by the commercial luminaires of the first pilot installation. To compare, the user survey was repeated with the same procedures as in the reference study. The design strategy proved successful as the developed luminaire gained the highest overall score in the second user feedback survey, even though the cool tone of the light was not appreciated. With regard to the statement “the tone of the light is pleasant” in both surveys, users gave the lowest rating for the luminaire with the highest CCT. However, there were big differences in the luminaires and, consequently, many variables affected the opinions of the respondents. In the future, different properties should be examined separately so that user acceptance is more limited to specific properties, such as the tone of the light. More details of the survey can be found in Paper IV.

7.1.3 Discussion

Good performance with high CCT of the LED component is one of the main reasons for the high luminous efficacy of the street light introduced in this chapter. However, the choice of component could be re-evaluated as the higher CCT light tones received lower ratings in the user feedback survey than the warmer tones. Lower CCT would decrease efficacy [5] but would also be favourable for light pollution and photobiological reasons [82, 83].

The thermal structure of the luminaire succeeded in maintaining reasonably low LED temperatures. This was anticipated as the structure consisted of massive aluminium chassis functioning as the heat sink of the luminaire. Consequently, no advanced thermal management methods were needed as long as the LEDs were in good thermal contact with the chassis. The lower, the better is the rule of thumb regarding LED temperature. However, in this case, the LED temperatures were

lower (66 °C) than is typically considered sufficient even in the worst case scenario. Thus, the design could be improved by reducing the volume of aluminium in the luminaire chassis. This would increase the LED temperatures but rationalize the design due to the reduced material consumption and weight, which would be beneficial for installation and handling. An optimized solution would strip the aluminium to a minimum and balance the thermal performance with advanced substrates like the ones introduced in this thesis.

7.2 Smart street lighting system

Four luminaires introduced in Section 7.1 were installed on a pedestrian road in Helsinki. The luminaires incorporated sensors and low energy two-way wireless communication that were used for smart control, delivering different lighting modes. The luminaires also recorded data of their functions. The recorded data included ambient temperature, LED board temperature, light reflected from the road, direct light from the LEDs, pedestrian presence sensor activations and, most importantly, energy consumption. This data were delivered to a web page that also served as a user interface for remote control of the pilot installation.

7.2.1 Communication and control

The aim of the smart control design was to implement the functionality needed for the study. A passive infrared (PIR) sensor was used to detect the presence of the pedestrians. The PIR sensor was installed up in the lighting poles and aimed directly at the road. The luminaire light output was monitored with two ambient light level sensors. A direct light sensor was mounted on the LED module substrate to monitor changes in luminaire light output, and a reflected light sensor was aimed at the illuminated area to detect reflected light from the ground. A temperature sensor mounted on the LED module substrate monitored the changes in temperature. (Paper IV)

A robust field PC equipped with wireless communication capabilities was placed in the range of the luminaires to record the sensor data and control the luminaire functions. Radio communication was used between the luminaires and the field PC. The field PC was further connected to the Internet via a wireless modem so that the luminaires could be controlled and the sensor data analysed remotely. The system is illustrated in Figure 26. More details are described in Paper IV.

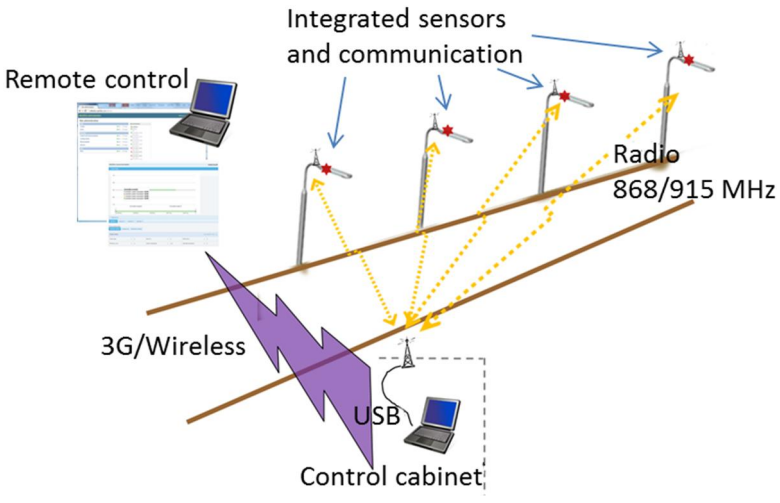

Figure 26. Communication and control system at the pilot installation site.

7.2.2 Energy savings with added intelligence

Three different lighting modes were used to study energy savings in pedestrian street lighting:

1. In the passive use mode, the smart luminaires were controlled as if they were standard street lights with no added intelligence. This mode was used as the reference point for energy savings achieved with smart control.
2. The light level sensing mode utilized a light sensor to keep the light levels on the ground stable regardless of the changes in the ambient conditions. Some energy savings were assumed during sunrise and sunset, but the main objective was to study the difference in energy consumption between summer and winter, as the amount of reflected light is totally different due to the snow in Finland.
3. The aim of the pedestrian sensing mode was to study the energy saving potential of dimming the street lighting levels at the quiet times of the night. The luminaires were dimmed by reducing the current by 50% and raised back to the state used in passive use mode when an approaching pedestrian was detected. In the passive use mode the power consumption was 30.5 W and when dimmed it was reduced to 17.1 W.

7.2.2.1 Light level sensing

The light reflected from the ground was recorded to study the possibility of using the changes in the luminance of the surroundings for energy savings in street lighting. This is of particular interest in Nordic countries where wintertime is long and dark but snowy. The light level sensing mode was realized by equipping the light sensor with the same optics as the LEDs. Thus, the monitored area coincided with the illuminated area. The data were recorded with fresh snow (March), inter-season (April) and with no snow (May). A major change in the lighting environment was discovered as the reflected light sensor value of 6.5 in the winter decreased to around 1 with the melting snow as shown in Figure 27. (Paper IV)

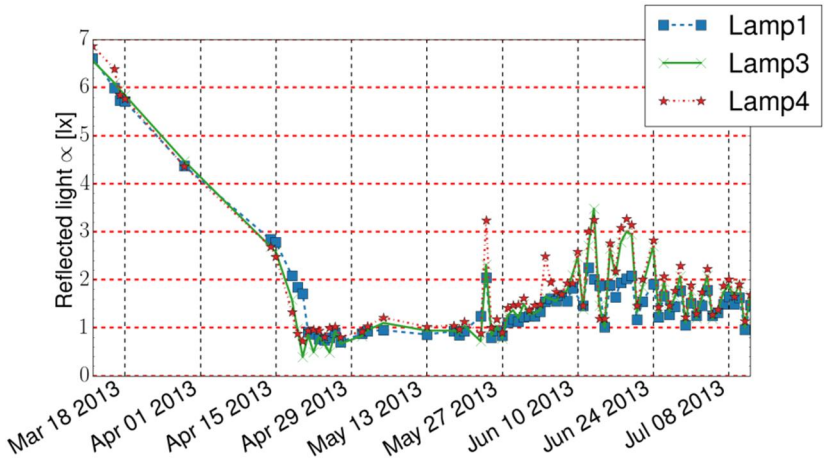

Figure 27. Daily median reflected light during melting snow season. The luminaires were operated in the passive use mode (Paper IV).

As illustrated in Figure 28, approximately 45% less power could be used during the night with fresh snow compared with the previous night with no snow on the road while maintaining the same reflected light value. In Helsinki, Finland, the average snow season lasts approximately 3 months while in Sodankylä, Lapland, the snow stays for 7.5 months [84]. This could mean significant energy savings in street lighting. For example, the City of Helsinki has 85,000 street lights that consume 54,000 MWh energy annually. The example shown in Figure 28 could realize estimated annual savings of 7,900 MWh and 0.8 M€ without losing the required light levels if light level sensing would be utilized generally. (Paper IV)

The energy saving potential of light level sensing at sunrise and sunset is demonstrated in Figure 29. The light level sensor detects the increase in natural light and the system controls the luminaire to lower the power until the specified minimum level is reached. Finally, the luminaire is turned off by the central control in the Helsinki area. Figure 29 shows that due to sunrise, the electrical power is gradually decreased down to 37% for about 30 minutes before it is turned off.

Compared with passive use, the median energy savings for 16 days was 28 Wh/day/luminaire when light level sensing was utilized at different sensor settings. These results suggest that instead of the widely used central control, more sophisticated solutions could generate major energy savings worldwide. (Paper IV)

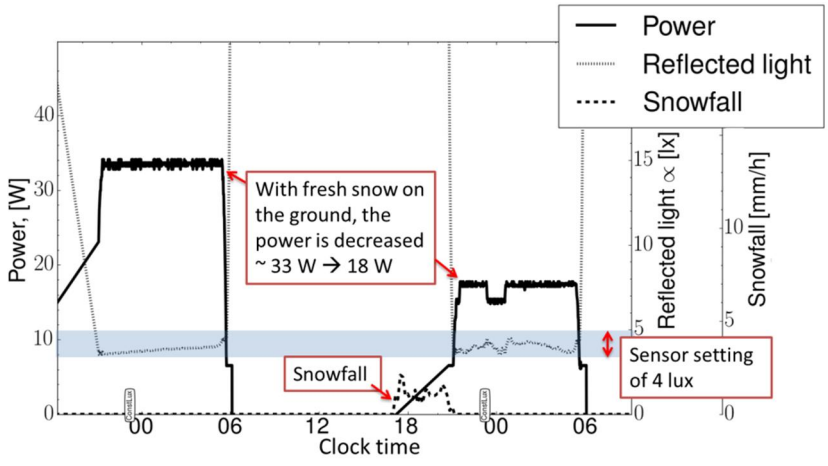

Figure 28. The power demand of the luminaire decreased after snowfall when the reflectivity of the surroundings was enhanced (Paper IV).

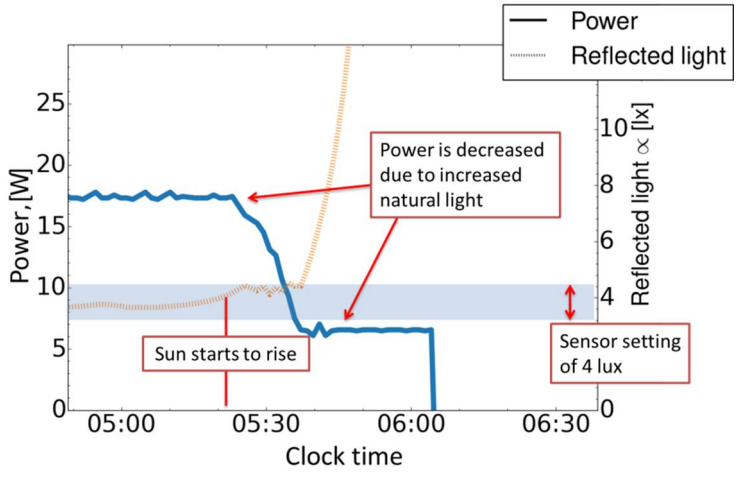

Figure 29. Power decrease in the morning during the natural light increase (Paper IV).

7.2.2.2 Pedestrian sensing

The energy saving potential of dimming the street light levels at the quiet times of the night was studied by operating luminaires in the pedestrian sensing mode. For comfort and safety reasons, the lighting cannot be completely turned off [52, 64–66] although that would pose the biggest energy savings. Here, the luminaires were dimmed to 50% drive current and raised back to passive use mode when an approaching pedestrian was detected. The set-up utilized PIR sensors integrated into the luminaires. Other luminaires were informed via wireless communication in case of detection. The system was constituted so that the pedestrian would not experience a change in the amount of light of the luminaire closest to him. Instead, the light level increased to the normal level ahead of the pedestrian and dimmed down 5 minutes after the last PIR detection. (Paper IV) The same kind of scenario was found acceptable by Haans *et al.* [65] and Viliunas *et al.* [66], according to whom pedestrians prefer having light in their immediate surroundings while light levels further away are less important.

An example showing the pedestrian sensing function is illustrated in Figure 30 in which the pedestrian sensing mode is compared with the passive use mode. The result was recorded in March 2013 when the lighting was turned on after 9 p.m. Consequently, only a few pedestrians appeared and all of them prior to midnight. During the five-day test period of pedestrian sensing, the luminaires in the pedestrian sensing mode operated on average at 40% lower power than in the passive use mode. (Paper IV)

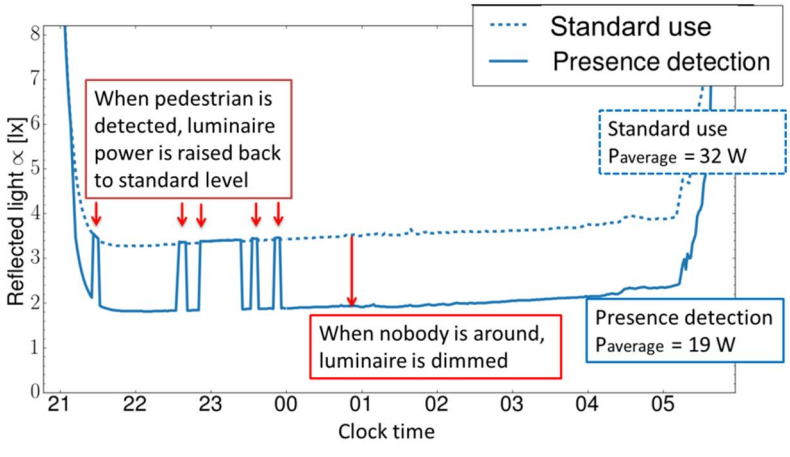

Figure 30. Detected light level on the road and average electrical power of luminaires in pedestrian sensing mode compared with passive use mode. The average is for 5 days (Paper IV).

The saving potential depends on the time delay used for dimming [56, 57]. A shorter delay would contribute to energy savings but might cause a negative user experience due to quicker changes in light level [55, 57]. The degree of dimming could have a similar effect. The saving potential is also dependent on the traffic volume of the road [61]. Fewer pedestrians contribute to greater energy savings. It could be concluded that there are always some quiet hours on pedestrian roads [61] that could provide energy savings by smart street lighting control. However, this method should be considered carefully as changes in light levels may have a negative effect on the user experience and could also cause problems with vandalism for instance [61].

7.2.3 Discussion

Power savings of more than 40% were demonstrated for pedestrian street lighting with smart control. The implementation was based on commercial state-of-art technology, so even bigger savings could be anticipated with advanced technology in the future. However, one of the main reasoning for street lighting is to prevent accidents and increase the safety and wellbeing of the citizens [52, 61, 64–66]. As all these aspects relate closely to the experience of end-users, the lighting cannot only be evaluated by technical performance numbers. Therefore, dimming scenarios and luminance distributions around pedestrians should be addressed in the future development of smart street lighting systems.

7.3 Conclusions at luminaire and system level

Street lighting was used as a case example for performance improvement in high-power LED lighting at luminaire and system level. An energy efficient street light for pedestrian roads was realized. Energy efficiency is achieved via high-efficacy driver and LED components of cool CCT. Optics design contributed good efficacy and succeeded in incorporating the main features considered for positive user experience. (Paper IV)

Thermal analysis of the luminaire structure revealed that the design would benefit slightly from the advanced thermal solutions introduced in this thesis for LED components and modules. This is due to the massive aluminium chassis of the luminaire, which is able to provide efficient cooling by means of natural convection. In the case of reducing the size and weight of the chassis, advanced substrates could be used to balance the thermal performance to acceptable LED temperatures. (Paper IV)

At system level, energy saving possibilities with smart control in pedestrian street lighting were studied. In snowy conditions, a 45% electrical power decrease was shown compared with power consumption with no snow on the road, while maintaining the same luminance (measured reflected illuminance from the road). Dimming the street light with increasing natural light during sunrise demonstrated a 63% power decrease for about 30 minutes. For adaptive lighting set to respond to the presence of pedestrians, the five-day average electrical power reduction

was 40%. (Paper IV) The demonstrated savings are bigger than that reported for traditional street lighting technology with a fixed dimming schedule [68] but smaller than that proposed with dynamic control [61, 70].

It can be concluded that a large amount of energy could be saved with smart control. What is more, these kinds of savings can be experienced on top of the improvements already achieved at component, module or luminaire level. This is a great opportunity for energy savings in street lighting, and big changes in lighting practices are anticipated in the near future. In addition, there are major refurbishment needs in the near future for legislative reasons such as the European Union Ecodesign Directive (2005/32/EY) about to ban many lamp types widely used in street lighting [60, 85] that will induce this development.

8. Conclusions and future work

High-power LED lighting technology development at component, module, luminaire and system level was studied in this work. The main thesis in the research was that

- *thermal resistance can be reduced with thermal vias in the LED substrate, and*
- *energy savings can be achieved by controlling the lighting according to lighting environment and person presence.*

Achieved results along with some considerations for future research are concluded in this chapter. Thermal resistance related to thermal vias and phosphor packaging is discussed in Sections 8.1 and 8.2, respectively. Energy savings with smart control is reviewed in Section 8.3.

8.1 Reduced thermal resistance with thermal vias

The main focus of this thesis is on reducing thermal resistance of high-power LED devices. The thesis addresses this issue at component, module and luminaire level, and the achieved improvement in the total thermal resistance is concluded in Table 9. The resulting reduction in thermal resistance is due to thermal vias in the insulation layer of the substrate under the heat source. For the luminaire the reduction is estimation as no advanced substrate was used in the luminaire realization. The estimation is based on module-level results as the reference substrate in the LED module studies coincides with the one used in the luminaires.

As shown in Table 9, the test structures used at component, module and luminaire levels differ in many aspects. It is shown, that the thermal vias are most effective in small devices with high power density. However, there are also other features in the realized test structures contributing to the achieved result. The main features are discussed with future considerations in the following sections 8.1.1 and 8.1.2. Finally, in Section 8.1.3, ways to benefit from the results are described.

Table 9. Achieved reduction in total thermal resistance compared with standard substrate technology.

	Component Paper I	**Module** Paper III	**Luminaire** Paper IV
Heating power, [W]	21	7.9	36
LED pitch, [mm]	1.5	20	60
Substrate area, [cm^2]	7.9	25	162
P_{heat} / $A_{substrate}$ [W/cm^2]	2.7	0.3	0.2
Thermal resistance reduction	Up to 55%	Up to 33%	~10 %–15%

8.1.1 Location of the via

As introduced in Chapter 2, the primary heat transfer mechanism away from the LEDs is conduction, as the width of the light emission spectrum is narrow and far from the infrared region. Also, the surface area of the chip is small for convection and radiation heat transfer. To enhance conduction, thermal vias on the LED component and module substrates are proven as a viable solution. From Table 9 it is evident that the thermal vias are most effective when used in direct contact with LEDs as was the case at component level. This is well understood as the substrate constitutes a major part of the total thermal resistance of the component as illustrated in Figure 7. In the modules, the vias were realized on component-carrying circuit boards. The heat source, which was a packaged LED component, introduced additional interfaces between the LED chip and the thermal via and, consequently, the improvement was less than the thermal resistance reduction at component level. The thermal via locations at component and module level are compared in Figure 31. The result coincides with the findings of Wu *et al.* [21], who concluded that improving heat dissipation problems at package level is more efficient than at board or system level due to the closest location of the heat source.

Thermal vias connecting the LED chip directly to the heat spreading metal core plate of the substrate (Figure 31a) explains the good thermal performance, but limits the availability of the solution to LEDs with electrically insulated bottom. Consequently vertical or flip-chip LEDs, which are more typical for high power solutions, cannot be used. For those LEDs, the vias should be realized in the following packaging layer (Figure 31b) referred as module level in this thesis.

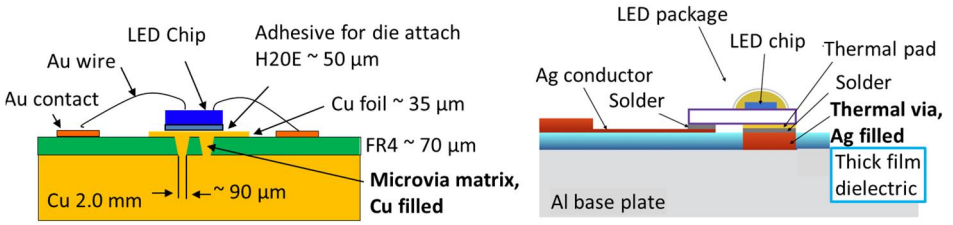

Figure 31. a) Microvias under the LED chip on the Cu MCPCB component substrate (Paper I) compared with b) thermal via under the LED package on the IAMS module board (Paper III).

The large size and LED pitch resulted in low heat power density on the luminaire. A massive aluminium chassis functioning as the heat sink also provided effective passive cooling for the LEDs. Consequently, the luminaire did not benefit much from the advanced module substrates with thermal vias. The thermal resistance of the luminaire is dominated by convection from the luminaire chassis to the environment (Figure 25) and the thermal resistance of the module circuit board represents only a small part of the total resistance. Thus, the thermal improvement at module level would only lead to minor improvements in the total thermal resistance of the luminaire.

8.1.2 Quality of the via fill

It can be concluded from Table 9 that the thermal vias are most effective in small devices with high power density. However, the via fill material and quality may also influence the resulting improvement. At component level, the micro vias were realized on a copper-based MCPCB and a copper-plating process was utilized for the via fill. Such a solution enables a compact thermal path through the thermal via, as illustrated in Figure 32a, and the thermal conductivity of the copper in the via fill can be approximated to be close to the normal copper conductivity (k = 385 W/mK).

Investigations of microvias at component level concluded that the thermal resistance is determined by the number and density of vias under the heat source. Thus, it could be assumed that the large area (5 mm^2) of the thermal via studied at module level would provide the ultimate solution with the optimized via coverage under the heat source. However, the reduction in thermal resistance was less than that achieved at component level. One reason for this could be the voids discovered in the soldering of the LEDs, indicating difficulty in flat-filling the large-area via. The voids increase the contact resistance from the LED to the thermal via, which reduces the efficiency of the cooling solution. A similar discovery was reported by Yang *et al*. [37] who concluded that the thermal resistance is not just

determined by the volume ratio of the thermal via but also the effective contact thermal resistance from the LED to the via surface.

In addition, as filled with screen-printed silver the material consistency in the large-area via may not be as favourable as in copper-filled microvias. An example of a copper-plated via plug compared with a screen-printed silver via is given in Figure 32. It can be seen that the screen-printed via fill is prone to being more porous, leading to reduced thermal conductivity compared with bulk material (k = 377 W/mK). In this work, when driven with the constant current, slightly higher electrical power was discovered on screen-printed modules than on reference modules with copper-plated MCPCB. This indicates that resistance was higher in screen-printed silver when compared with plated copper, which implies that also the thermal conductivity of the via plug is lower. However, the quality of metallization was not a topic in the current study and should be considered in future research.

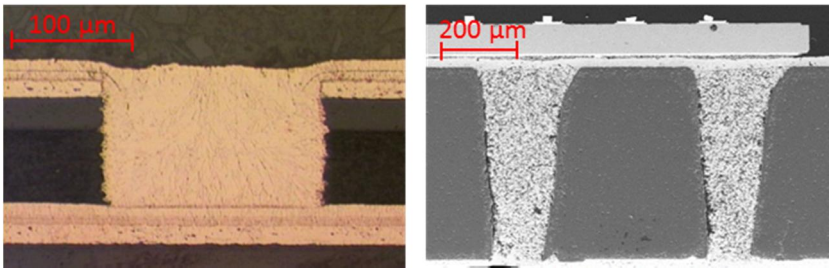

a) b)

Figure 32. a) Copper-plated via fill compared with b) thick-film silver-filled via.

8.1.3 Benefit

The demonstrated improvement in the total thermal resistance of the LED components and modules concluded in Table 9 resulted in ~10 °C decrease in the average LED temperature. As discussed in Section 2.1.1 such a reduction should generate improved optical efficiency. Unfortunately, this was not experienced in this study. As the testing was performed with active cooling, the absolute temperatures of the LEDs were rather low (< 50 °C), which explains the negligible optical efficacy improvement. The effect of absorption losses was also discussed, as the developed solutions differed from the reference components and modules by their darker substrate colour. In the future, to reveal the optical performance improvement, the testing at some elevated ambient temperature, 65 °C, for instance would be useful. The surfaces of the test structures should also be more similar for a fair comparison.

Besides targeting lower LED temperatures for improved reliability and performance, reduced thermal resistances could be utilized to drive the components and

modules with a higher current without increasing the LED temperature. The drive current should be limited under the so-called efficiency droop region in which the radiative efficiency of InGaN LEDs is saturated [7]. Considering a similar temperature increase and up to 55% reduction in the thermal resistance demonstrated in this work, the heating power could be more than doubled according to the definition of thermal resistance introduced in Section 4.1. This could be exploited through increased optical power or reduced cost of the solution as fewer LEDs could be used in the luminaire. In addition, some efficiency increase could be experienced as driver electronics is typically designed to function more efficiently at higher power levels.

Another way to benefit from reduced thermal resistance would be to decrease the cooling capacity without sacrificing the acceptable LED temperatures. In practice, this would mean reducing the size and weight of the luminaire as the vast majority of the LED luminaires utilize passive cooling with a heat sink. Reduced thermal resistance at component and module level would therefore have a positive impact on the cost of the luminaire, as material consumption would be decreased and the handling and installation of the luminaire would be easier. Practical examples of increased optical power and reduced heat sink size with reduced thermal resistance of the substrate are shown in Figure 33 [86].

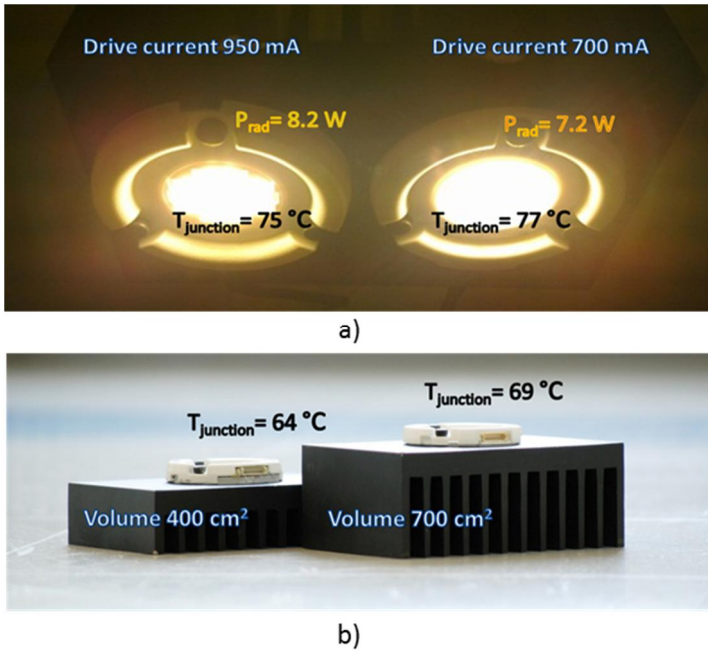

Figure 33. Increased optical power on the same heat sink (a), and reduced heat sink size with the same drive current (b) of a LED module utilizing advanced substrate technology (left) compared with a commercial LED module (right) [86].

8.2 Phosphor packaging

Phosphor used in combination with blue LEDs is a common way to produce white light for lighting applications. Phosphor packaging was studied in this work as part of the thermal management of the LED component. It was shown that phosphor encapsulant dispensed over the LEDs has a positive effect on the thermal resistance they experience. However, this did not reduce LED temperatures because the encapsulant holding the phosphor also added a thermal load in the component due to the white light conversion losses. The result was contrary to expectations [9, 14, 79] since it was assumed that by adding heat load, the phosphor would degrade the thermal performance of the LED component.

With regard to the introduced nearby phosphor concept, results indicate that sufficient cooling should be provided for the nearby plate to make the concept viable. Although the research did not achieve a breakthrough in performance improvement, it generated some interesting aspects for future development. If features appreciated in remote phosphor solutions could be incorporated into devices with smaller dimensions, the solution may be able to tackle some fabrication issues of LED components and modules [5] by simplifying the phosphor handling process, reducing phosphor material consumption or improving the phosphor material homogeneity.

8.3 Energy savings with smart control

In LED components and modules, thermal management is one of the key issues to solve for improved device performance [5, 7, 9]. However, at luminaire and system level, improvements in a certain sector, such as thermal management, can only contribute a limited amount (Table 9) as the performance is a more diversified combination of various design aspects and use conditions [5, 21]. Therefore this thesis concentrated on energy efficiency as the measure of the achievements at luminaire and system level. This is reasonable also from a global perspective, as, due to the environmental concerns, the whole lighting industry strives for energy savings in lighting [7, 8].

Showing the potential of advanced LED lighting technology, luminous efficacy of 96 lm/W was demonstrated in this thesis for a developed luminaire.. Compared with commercial street light references, the CCT of the developed luminaire was higher that contributed to the higher luminous efficiency. (Paper IV)

Street lighting case examples of different dimming scenarios in a real use environment revealed additional power savings of more than 40% with smart control reacting to lighting environment and person presence. (Paper IV) The result was attained by just dimming down the excess light. In other words, the light level on the road remained standard whenever needed and only the light that was wasted (i.e. excess lumens due to natural light or high flux when nobody was around) was removed. The result was in the expected range based on literature reviews [61, 68–70],

although, in many aspects, these studies diverge from what was introduced in this thesis.

Lighting can be considered a service for the person executing some task like reading or jogging [4, 8]. Lighting is therefore also an experience, and the performance evaluation needs to be expanded from a technical perspective to also cover the end-user aspects. In fact, user acceptance, like light quality and appearance, luminaire outlooks and usability, could be a major factor in the commercial success of a common consumer product, such as a luminaire. In this thesis, user feedback from a pilot installation with commercial luminaires was utilized in the design of the demonstrator luminaire. The approach was successful, as the developed luminaire received the highest overall score in the comparing end-user feedback study. However, the smart control scenarios tested in this thesis were not included in the user survey. This is an increasingly important topic to study in the future as smart control can change the amount, appearance and distribution of light around the user.

References

[1] Holonyak, N., and Bevacqua, S. F. 1962. Coherent (visible) light emission from $Ga(As_{1-x}P_x)$ junctions. Applied Physics Letters, Vol. 1, No. 4, pp. 82–83.

[2] Nakamura, S., Mukai, T., and Senoh, M. 1991. High-power GaN P-N junction blue-light-emitting diodes. Japanese Journal of Applied Physics, Vol. 30, No. 12A, pp. L1998–L2001.

[3] Nakamura, S., Senoh, M., and Mukai, T. 1993. High-power InGaN/GaN doubleheterostructure violet light emitting diodes. Applied Physics Letters, Vol. 62, No. 19, pp. 2390–2392.

[4] Haitz, R., and Tsao, J. Y. 2011. Solid-state lighting: 'The case' 10 years after and future prospects. Physica Status Solidi A, Vol. 208, No. 1, pp. 17–29.

[5] Liu, Z., Liu, S., Wang, K., and Luo X. 2009. Status and prospects for phosphor-based white LED packaging. Frontiers Optoelectronics China, Vol. 2, No. 2, pp. 119–140. Doi: 10.1007/s12200-009-0011-2.

[6] Krames, M. R., Shchekin, O. B., Mueller-Mach, R., Mueller, O. G., Zhou, L., Harbers, G., and Craford, M. G. 2007. Status and Future of High-Power Light-Emitting, Diodes for Solid-State Lighting. Journal of display technology, Vol. 3, No. 2, pp. 160–175.

[7] Crawford, M. H. 2009. LEDs for Solid-State Lighting: Performance Challenges and Recent Advances. IEEE journal of selected topics in quantum electronics, Vol. 15, No. 4, pp. 1028–1040.

[8] Tsao, J. Y., Saunders, H. D., Creighton, J. R., Coltrin M. E., and Simmons, J. A. 2010. Solid-state lighting: an energy-economics perspective. Journal of physics D: applied physics, Vol. 43, No. 35, pp. 1–17. Doi: 10.1088/0022-3727/43/35/354001.

[9] Lasance, C. J. M., and Poppe, A. 2014. Thermal Management for LED Applications. Springer Science+Business Media, NewYork. Doi:10.1007/978-1-4614-5091-7.

[10] Lighting the way: Perspectives on the global lighting market, Second edition. 2012. McKinsey & Company.

[11] Saunders, H. D., and Tsao, J. Y. 2012. Rebound effects for lighting. Energy Policy, Vol. 49, pp. 477–478.

[12] Singh, J. 1996. Optoelectronics, An introduction to materials and devices. The McGraw-Hill Companies, Inc. USA.

[13] Sergent, J. E., and Krum, A. 1998. Thermal Management Handbook for Electronic Assemblies. McGraw-Hill, New York, USA.

[14] Narendran, N., Gu, Y., Freyssinier, J. P., Yu, H., and Deng, L. 2004. Solid-state lighting: failure analysis of white LEDs. Journal of Crystal Growth, Vol. 268, No. 3–4, pp. 449–456.

[15] Hu, J., Yang, L., and Shin, M. W. 2007. Mechanism and thermal effect of delamination in light-emitting diode packages. Microelectronics Journal, Vol. 38, No. 2, pp. 157–163.

[16] Reliability and Lifetime of LEDs, Application Note. 2013. OSRAM Opto Semiconductors GmbH. (http://catalog.osram-os.com/catalogue/catalogue.do;jsessionid=55E4DA283D95D517F61641FDF2C966EA?act=downloadFile&favOid=020000010003e0ac000200b6, downloaded 12.2.2014).

[17] Evaluating the Lifetime Behavior of LED Systems. The path to a sustainable luminaire business model, White Paper WP15 20121218. Philips Lumileds, (http://www.philipslumileds.com/uploads/167/WP15-pdf, downloaded 12.2.2014).

[18] LUXEON Rebel General Purpose White Portfolio, Technical Datasheet DS64. 2012. Philips Lumileds Lighting Company, (http://www.philipslumileds.com/uploads/28/DS64-pdf, downloaded 12.2.2014).

[19] Cree® XLamp® XM-L LEDs, Product Family Data Sheet, CLD-DS33 Rev 9A. 2010–2013. (http://www.cree.com/products/pdf/xlampxm-l.pdf, downloaded 25.9.2013).

[20] Bridgelux RS Array Series, Product Data Sheet DS25. 2012. Bridgelux, Livermore, CA, USA. (http://www.led-tech.de/produkt-pdf/bridgelux/Bridgelux-RS-Rectangle-Array.pdf, downloaded 12.2.2014).

[21] Wu, H.-H., Lin, K.-H., and Lin, S.-T. 2012. A study on the heat dissipation of high power multi-chip COB LEDs. Microelectronics Journal, Vol. 43, No. 4, pp. 280–287.

[22] Kim, B.-H., and Moon, C. 2012. Comparison of the thermal performance of the multichip LED packages. IEEE Transactions on Components, Packagaging and Manufacturing Technology, Vol. 2, No. 11, pp. 1832–1837.

[23] Hoelen, C., Borel, H., de Graaf, J., Keuper, M., Lankhorst, M., Mutter, C., Waumans, L., and Wegh, R. 2008. Remote phosphor LED modules for general illumination: Toward 200 lm/W general lighting LED light sources. Proceedings of the SPIE, Vol. 7058, id. 70580M, pp. 1–10.

[24] Narendran, N., Gu, Y., Freyssinier-Nova, J. P., and Zhu, Y. 2005. Extracting phosphor-scattered photons to improve white LED efficiency. Physica Status Solidi A, Vol. 202, No. 6, pp. R60–R62.

[25] Liu, Z., Liu, S., Wang, K., and Luo, X. 2009. Optical analysis of phosphor's location for high-power light-emitting diodes. IEEE Transactions on Device and Materials Reliability, Vol. 9, No. 1, pp. 65–73.

[26] Moon, K.-M., An, S.-H., Kim, H.-K., Chae, J.-H., and Park, Y.-J. 2010. Phosphor concentration and geometry for high power white light emitting diode. Proceedings of the SPIE, Vol. 7617, No. 76171Y, pp. 1–8.

[27] Halonen, L., and Lehtovaara, J. 1992. Valaistustekniikka. Gummerus kirjapaino, Jyväskylä, Finland.

[28] Leung, M. 2012. Fair comparison of white LEDs and remote phosphor guides design choice. Leds Magazine, Vol. 1, pp. 56–64.

[29] Luo, X., Fu, X., Chen, F., and Zheng, H. 2013. Phosphor self-heating in phosphor converted light emitting diode packaging. International Journal of Heat and Mass Transfer, Vol. 58, No. 1–2, pp. 276–281.

[30] Heo, Y. J., Kim, H. T., Nahm, S., Kim, J., Yoon, Y. J., and Kim, J. 2012. Ceramic-metal package for high power LED lighting. Frontiers of Optoelectronics, Vol. 5, No. 2, pp. 133–137.

[31] Shin, H. W., Lee, H. S., and Jung, S. B. 2011. Analysis on Thermal Resistance of LED Module with Various Thermal Vias. In: 18th IEEE International Symposium on the Physical and Failure Analysis of Integrated Circuits (IPFA), Incheon, Korea, 4–7 July 2011.

[32] Barcena, J., Maudes, J., Vellvehi, M., Jorda, X., Obieta, I., Guraya, C., Bilbao, L., Jiménez, C., Merveille, C., and Coleto, J. 2008. Innovative packaging solution for power and thermal management of wide-bandgap semiconductor devices in space applications. Acta Astronautica, Vol. 62, No. 6–7, pp. 422–430.

[33] Lei, T. G., Calata, J. N., Ngo, K. D. T., and Lu, G.-Q. 2009. Effects of large-temperature cycling range on direct bond aluminum substrate. IEEE Transactions on Device and Materials Reliability, Vol. 9, No. 4, pp. 563–568.

[34] Schulz-Harder, J., and Meyer, A. 2007. Hermetic packaging for power multichip modules. In: European Conference on Power Electronics and Applications (EPE), Aalborg Denmark, 2.–5. Sept. 2007, pp. 1–10.

[35] iNEMI Technology Roadmaps, Interconnection substrates – ceramic, crystalline photovoltaic cell & module technology. 2013.

[36] Lin, S. C., Huang, R.-F., and Chiu, C. H. 2009. Investigation of Thermally Conductive Ceramic Substrates for High-Power LED Application. In: Microsystems, Packaging, Assembly and Circuits Technology Conference (IMPACT), Taipei, Taiwan, 21–23 Oct. 2009, pp. 589–592.

[37] Yang, L., Jang, S., Hwang, W., and Shin, M. 2007. Thermal analysis of high power GaN-based LEDs with ceramic package. Thermochimica Acta, Vol. 455, No. 1–2, pp. 95–99.

[38] Jordá, X., Perpiñá, X., Vellvehi, M., and Coleto, J. 2008. Power-substrate static thermal characterization based on a test chip. IEEE Transactions on Device and Materials Reliability, Vol. 8, No. 4, pp. 671–679.

[39] Di Pascoli, S., Bagnoli, P. E., and Casarosa, C. 1999. Thermal analysis of insulated metal substrates for automotive electronic assemblies. Microelectronics Journal, Vol. 30, No. 11, pp. 1129–1135.

[40] Cho, H. M., and Kim, H. J. 2008. Metal-core printed circuit board with alumina layer by aerosol deposition process. IEEE Electron Device Letters, Vol. 29, No. 9, pp. 991–993.

[41] Holmes, J. D., Stone, D. A., and Foster, M. P. 2010. Effect of inter-layer interface quality on electrical and thermal characteristics of IMS. In: 5th IET International Conference on Power Electronics, Machines and Drives (PEMD 2010), Brighton, UK, 19–21 April 2010, pp. 1–4.

[42] Sim, J.-K., Ashoka, K., Ra, Y.-H., Im, H.-C., Baek, B.-J., and Lee, C.-R. 2012. Characteristic enhancement of white LED lamp using low temperature co-fired ceramic-chip on board package. Current Applied Physics, Vol. 12, No. 2, pp. 494–498.

[43] Asai, S., Funaki, M., Sawa, H., and Kat, K. 1993. Fabrication of an insulated metal substrate (IMS), having an insulating layer with a high dielectric constant. IEEE Transactions on Components, Hybrids, and Manufacturing Technology, Vol. 16, No. 5, pp. 499–504.

[44] Horng, R.-H., Hong, J.-S., Tsai, Y.-L., Wuu, D.-S., Chen, C.-M., and Chen, C. J. 2010. Optimized thermal management from a chip to a heat sink for high-power GaN-based light-emitting diodes. IEEE Transactions on Electron Devices, Vol. 57, No. 9, pp. 2203–2207.

[45] Lee, M.-H., Lee, T. J., Lee, H. J., and Kim, Y.-J. 2010. Design and fabrication of metal PCB based on the patterned anodizing for improving thermal dissipation of LED lighting. In: Microsystems Packaging Assembly and Circuits Technology Conference (IMPACT), Taipei, Taiwan, 20–22. Oct. 2010, pp. 1–4.

[46] Godbold, C. V., Sankaran, V. A., and Hudgins, J. L. 1997. Thermal analysis of high-power modules. IEEE Transactions on Power Electronics, Vol. 12, No. 1, pp. 3–11.

[47] Park, J. K., Lee, Y. K., Choi, S. H., Shin, S. H., and Choi, M. S. 2011. Formation of through aluminum via for noble metal PCB and packaging substrate. In: Electronic Components and Technology Conference (ECTC), Lake Buena Vista, Florida, USA, May 31 – Jun. 3 2011, pp. 1787–1790.

[48] Mu, D., and Jin, Y. 2000. Study of anodized Al substrate for electronic packaging. Journal of Materials Science: Materials in Electronics, Vol. 11, No. 3, pp. 239–242.

[49] Heo, Y. J., Kim, H. T., Kim, K. J., Nahm, S., Yoon, Y. J., and Kim, J. 2013. Enhanced heat transfer by room temperature deposition of AlN film on aluminum for a light emitting diode package. Applied Thermal Engineering, Vol. 50, No, 1. pp. 799–804.

[50] Kim, Y.-W., Kim, J.-P., Kim, J.-B., Kim, M.-S., Sim, J.-M., Song, S.-B., and Hwang, N. 2009. Thermal analysis of a package substrate with filling viaholes for COB LED manufacturing. Journal of the Korean Physical Society, Vol. 54, No. 5, pp. 1873–1878.

[51] Taylor, S. 2010. MCPCB's and thermal interface material considerations for high power LED lighting applications. OSRAM LED light for you (LLFY) System design Workshop, 28. Oct., 2010. San Diego, USA. (http://www.

slideshare.net/OSRAMLEDlight/llfy-workshop-oct-20101-for-publish, downloaded 12.2.2014).

[52] Mullner, R., and Riener, A. 2011. An energy efficient pedestrian aware smart street sighting system. International Journal of Pervasive Computing and Communications, Vol. 7, No. 2, pp. 147–161.

[53] European Commission. 2011. Lighting the Future, Accelerating the Deployment of Innovative Lighting Technologies, COM (2011) 889 final.

[54] Atici, C., Özcelebi, T., and Lukkien, J. J. 2011. Exploring user-centered intelligent road lighting design: A road map and future research directions. IEEE Transactions on Consumer Electronics, Vol. 57, No. 2, pp. 788–793.

[55] Dubois, M. C., and Blomsterberg, Å. 2011. Energy saving potential and strategies for electric lighting in future North European, low energy office buildings: A literature review. Energy and Buildings, Vol. 43, No. 10, pp. 2572–2582.

[56] Galasiu, A. D., Newsham, G. R, Suvagau, C., and Sander, D. M. 2001. Energy saving lighting control systems for open-plan offices: a field study. Leukos, Vol. 4, No. 1, pp. 7–29.

[57] Pigg, S., Eilers, M., and Reed, J. 1996. Behavioral Aspects of Lighting and Occupancy Sensors in Private Offices: A Case Study of a University Office Building. In: 1996 ACEEE Summer Study on Energy Efficiency in Buildings. Pacific Grove, CA, USA, 25–31 Aug. 1996, Vol. 8, No. 18, pp. 8161–8170.

[58] Disruptive technologies: Advances that will transform life, business, and the global economy. 2013. McKinsey Global Institute, McKinsey & Company.

[59] Street Lighting Retrofit Projects: Improving Performance, while Reducing Costs and Greenhouse Gas Emissions. White paper. 2010. Clinton Climate Initiative, Outdoor Lighting Program. (http://www.dvrpc.org/energyclimate/eetrafficstreetlighting/pdf/CCI_EE_Streetlighting_White_Paper.pdf, downloaded 12.2.2013)

[60] Boyce, P. R., Fotios, S., and Richards, M. 2009. Road lighting and energy saving. Lighting Research and Technology, Vol. 41, No. 3, pp. 245–260.

[61] Lau, S. P., Merrett, G. V., and White, N. M. 2013. Energy-Efficient Street Lighting through Embedded Adaptive Intelligence. In: International Conference on

Advanced Logistics and Transport (ICALT 2013), Sousse, Tunisia, 29–31 May 2013, pp. 53–58.

[62] Chiogna, M., and Mahdavi, A. 2012. Energy efficiency of alternative lighting control systems. Lighting Research and Technology, Vol. 44, No. 4, pp. 397–415.

[63] Williams, A., Atkinson, B., Garbesi, K., Page, E., and Rubinstein, F. 2012. Lighting controls in commercial buildings. Leukos, Vol. 8, No. 3, pp. 161–180.

[64] Fotios, S. 2013. LRT Digest 1 Maintaining brightness while saving energy in residential roads. Lighting Research and Technology, Vol. 45, No. 1, pp. 7–21.

[65] Haans, A., and de Kort, Y. A. W. 2012. Light distribution in dynamic street lighting: Two experimental studies on its effects on perceived safety, prospect, concealment, and escape. Journal of Environmental Psychology, Vol. 32, No. 4, pp. 342–352.

[66] Viliûnas, V., Vaitkevicius, H., Stanikunas, R., Vitta, P., Bliumas, R., Auskalnyte, A., Tuzikas, A., Petrulis, A., Dabasinskas, L., and Zukauskas, A. 2013. Subjective evaluation of luminance distribution for intelligent outdoor lighting. Lighting Research and Technology. Doi: 10.1177/1477153513491760.

[67] Wojnicki, I., Ernst, S., Kotulski, L., and Sedziwy, A. 2014. Advanced street lighting control. Expert Systems with Applications, Vol. 41, No. 4, pp. 999–1005.

[68] Chung, H. S. H., Ho, N. M., Hui, S. Y. R., and Mai, W. Z. 2005. Case study of a highly-reliable dimmable road lighting system with intelligent remote control. In: European Conference on Power Electronics and Applications (EPE), Dresden, Germany, 11–14 Sep. 2005, pp. 1–10.

[69] Sun, J.-H., Su, J.-F., Zhang, G.-S., Li, Y., and Zhao, C. 2010. An energy-saving control method based on multi-sensor system for solar street lamp. In: 2010 International Conference on Digital Manufacturing & Automation (ICDMA), Changsha, China, 18–20 December 2010, Vol. 1, pp. 192–194.

[70] Intelligent street lighting at TU Delft saves up to 80% on energy. 2011. Delft University of Technology. (http://www.tvilight.com/wp-content/uploads/2010/03/02.-Intelligente-straatverlichting-TU-Delft_06-juli-2011_EN.pdf, downloaded 12.2.2014).

[71] Viraktamath, S. V., and Attimarad, G. V. Power saving mechanism for street lights using wireless communication. 2011. In: International Conference on Signal Processing, Communication, Computing and Networking Technologies (ICSCCN), Thuckalay, India, 21–22 July 2011. Pp. 282–285.

[72] Blackburn, D. L. 2004. Temperature Measurements of Semiconductor Devices – A Review. In: Twentieth Annual IEEE Semiconductor Thermal Measurement and Management Symposium (SEMI-THERM), San Jose, CA, USA, 9–11 March 2004. Pp. 70–80.

[73] Technical Guide: Integrating Sphere Radiometry and Photometry. 2006. Labsphere, Inc., North Sutton, NH, USA.

[74] Kim, L., and Shinh, M. W. 2007. Thermal resistance measurement of LED package with multichips. IEEE Transactions on Components and Packaging Technology, Vol. 30, No. 4, pp. 632–636.

[75] T3Ster Thermal Transient Tester Technical Information. 2011. Mentor Graphics Corporation, Wilsonville, OR, USA.

[76] Szekely, V., and Van Bien, T. 1988. Fine structure of heat flow path in semiconductor devices: A measurement and identification method. Solid-State Electronics, Vol. 31, No. 9, pp. 1363–1368.

[77] Implementation of the Electrical Test Method for the Measurement of Real Thermal Resistance and Impedance of Light-Emitting Diodes with Exposed Cooling. 2012. Standard JESD51-51.

[78] Liu, Z.-Y., Liu, S., Wang, K., and Luo, X.-B. 2010. Studies on optical consistency of white LEDs affected by phosphor thickness and concentration using optical simulation. IEEE Transactions on Components and Packaging Technology, Vol. 33, No. 4, pp. 680–687.

[79] Hu, R., Luo, X., and Zheng, H. 2012. Hotspot Location Shift in the High-Power Phosphor-Converted White Light-Emitting Diode Packages. Japanese Journal of Applied Physics, Vol. 51, pp. 1–4.

[80] Furgel', I., Molin, O., and Borshch, V. 1992. Thermal conductivity of polymer composites with a disperse filler. Journal of Engineering Physics and Thermophysics, Vol. 62, No. 3, pp. 335–340.

[81] Paakkinen, M., Tetri, E., and Halonen, L. User evaluation of pedestrian way lighting, Light and Engineering, accepted to be published.

[82] Falchi, F., Cinzano, P., Elvidge, C. D., Keith, D. M., and Haim, A. 2011. Limiting the impact of light pollution on human health, environment and stellar visibility. Journal of Environmental Management, Vol. 92, No. 10, pp. 2714–2722.

[83] Žukauskas, A., Vaicekauskas, R., and Vitta, P. 2012. Optimization of solid-state lamps for photobiologically friendly mesopic lighting. Applied Optics, Vol. 51, No. 35, pp. 8423–8432.

[84] Finish Meteorological Institute web site: http://ilmatieteenlaitos.fi/lumitilastot (accessed 2 July 2013).

[85] Komission asetus (EY) N:o 245/2009. 2009. Euroopan unionin virallinen lehti, FI L 76/17. (http://eur-lex.europa.eu/LexUriServ/LexUriServ.do?uri=OJ:L:2009:076:0017:0044:Fi:PDF, downloaded 13.2.2014).

[86] Moilanen, V., Juntunen, E., Tapaninen, O., Sitomaniemi, A., Jokelainen, K., Heikkinen, V., and Aikio, J. 2012. Different LED interconnection methods and their effects on LED modules and luminaires, case studies with MCPCBs and beyond. Invited talk in: Strategies in Light Europe, 18–20 Sept. 2012, Munich, Germany.

PUBLICATION I

Copper-Core MCPCB with Thermal Vias for High-Power COB LED Modules

In: IEEE Transactions on Power Electronics
2014, (29)3, pp. 1410–1417.

Copper-Core MCPCB With Thermal Vias for High-Power COB LED Modules

Eveliina Juntunen, Olli Tapaninen, Aila Sitomaniemi, Markku Jämsä, Veli Heikkinen, Mikko Karppinen, and Pentti Karioja

***Abstract*—To improve thermal performance of high-power chip-on-board multichip LED module, a copper-core metal core printed circuit board (MCPCB) substrate with copper filled microvias is introduced. As a reference, the performance is compared with alumina module with the same layout by means of thermal simulations and measurements. Up to 55% reduction in the thermal resistance from the LED source to the bottom of the substrate is demonstrated. The excellent performance of the Cu MCPCB module is due to copper-filled microvias under the blue LED chips that occupy the majority of the multichip module. The conclusion was verified by measuring increased thermal resistances of red chips without thermal vias on the Cu MCPCB module. However, as the blue LEDs dominate the thermal power of the module, they also dominate the module thermal resistance. The thermal resistance was demonstrated to correspond with the number of vias as lower thermal resistance was measured on modules with larger number of vias. The Cu MCPCB was processed in standard PCB manufacturing and low cost material, FR4, was utilized for the electrical insulation. Thus, the solution is potentially cost-effective despite the higher cost of copper in comparison with aluminum that is the most commonly used MCPCB core material.**

***Index Terms*—Dielectrics and electrical insulation, light emitting diodes (LEDs), multichip modules, substrates, thermal analysis.**

I. Introduction

LIGHT emitting diodes (LEDs) are solid-state light sources that are overriding traditional solutions in many applications like backlighting, communications, signage, and general illumination. Environmental reasons, such as energy efficiency, long lifetime, and lack of mercury content, are promoting the LED replacement over the traditional lighting solutions. Also, features like small size, ease of control, quick start-up even in low temperatures, and low UV radiation level are appreciated among lighting industry [1]–[3].

Manuscript received January 2, 2013; revised March 15, 2013; accepted April 16, 2013. Date of current version September 18, 2013. This work was supported in part by Tekes, Finnish Funding Agency for Technology and Innovation, and Infotech Oulu Doctoral Program. Recommended for publication by Associate Editor A. Lindemann.

E. Juntunen, O. Tapaninen, A. Sitomaniemi, V. Heikkinen, M. Karppinen, and P. Karioja are with the VTT Technical Research Centre of Finland, 90571 Oulu, Finland (e-mail: eveliina.juntunen@vtt.fi; olli.tapaninen@vtt.fi; aila.sitomaniemi@vtt.fi; veli.heikkinen@vtt.fi; mikko.karppinen@vtt.fi; pentti.karioja@vtt.fi).

M. Jämsä is with Aspocomp, 02150 Espoo, Finland (e-mail: Markku.Jamsa@aspocomp.com).

Color versions of one or more of the figures in this paper are available online at http://ieeexplore.ieee.org.

Digital Object Identifier 10.1109/TPEL.2013.2260769

General lighting calls for high luminosity. Reaching for high luminous flux tends to increase power density in LED devices as more and more LEDs are packaged in a small space. This poses a challenge for thermal management of LED devices that would benefit from lower junction temperature with increased efficacy, lifetime, and light quality [4]–[6].

In a chip-on-board (COB) multichip module, LED chips are located closely with each other on a common substrate. COB defines that the LED sources are bare chips directly mounted and electrically interconnected on to the final substrate in contrast to using individually packaged LED components on the substrate. Metal core printed circuit board (MCPCB), insulated metal substrate (IMS), or ceramics are typically used as substrates [7], [8].

Ceramics can tolerate hazardous circumstances and enable multilayer structures and hermetic packaging. Consequently, ceramics are used as substrates for demanding applications like automotive or space [9], [10]. Unfortunately, thermal conductivity of common ceramics (alumina, LTCC) is low ($k = 3, \ldots,$ 30 W/mK). AlN and BeO conduct heat well ($k = 180, \ldots,$ 280 W/mK), but they are expensive compared with alumina and LTCC. In addition, BeO is toxic and as such an environmental and health risk [11].

MCPCB and insulated metal substrate techniques offer good thermal performance with reasonable cost [12]. They consist of a typically 1–3-mm-thick metal core with an electrically insulating layer on top. The core is used as a mechanical support while enabling effective thermal spreading. Typical core metals copper and aluminum are good thermal conductors ($k = 240, \ldots,$ 390 W/mK). Due to lower cost and weight, aluminum boards are more widespread although copper excels in thermal conductivity [12]–[16]. In addition, all kind of milling is easier for aluminum compared to copper. For the insulating layer, there are different materials and techniques available. Thin (35–125 μm) organic dielectric realized with lamination process is typical for MCPCB, while electrical interconnections are made with deposited copper [12], [13], [15], [16]. Inorganic insulation layers are available with IMS technique. Electrochemical anodization is a traditional IMS technique. Typically, anodic film thickness of about 20–40 μm is required for high impedance insulation layer. To form electrical conductors, there are various plating, printing, and sputtering methods available [17], [18].

Attempts to improve thermal performance of MCPCB and IMS concentrate on the insulation layer, since the electrical insulator materials (polymer, ceramic compositions) are poor thermal conductors [13]. Thermal conductivity can be enhanced by charging the polymer resin with thermally conductive ceramic

particles. Alumina particles are typically used [13], [14]. In addition, thermal performance is affected by thickness and interface quality of the insulation layer to the surrounding structure [12], [13], [16]. The challenge is to develop insulation layers with low thermal resistance but sufficient electrical isolation, because the voltage level on LED modules can be high. Unfortunately, all these enhancements tend to increase the cost of the MCPCB and IMS boards.

Thermal vias under the heat source could be an effective heat management solution as reported for ceramic substrates in [19] and [20] and IMS in [21]. Also, for PCBs, a significant thermal performance enhancement with thermal vias is reported [22]. With MCPCB, thermal vias are not typically available since the lamination process is too inaccurate to realize the vias on the insulation layer before lamination (by piercing). In addition, copper-filled thermal vias cannot easily be made on aluminum core MCPCB that is most commonly used due to processing reasons. On Cu-core MCPCB, some thermal via solutions utilizing laser drilling exist [23].

In this paper, a COB LED module using copper-core MCPCB with microvias through the FR4 insulation layer under the LED chips is introduced. Thermal performance of the module is compared with alumina module as a reference. The vias on the MCPCB module are realized after the lamination process with laser milling, which is a standard procedure in circuit board manufacturing. Thus, it does not increase manufacturing cost dramatically. The microvias are copper filled for good thermal contact. The use of copper as the core metal enables the via processing. Also, thermal conductivity of the core is higher compared to the aluminum core MCPCB. Some concerns about cost of Cu MCPCB solution exist. However, as the thermal vias provide a good thermal conduction path through the isolation layer, very low cost insulation material, FR4, can be used. In addition, thicker layers can be used to improve electrical isolation.

II. Test Structure Design

A. Test Modules

The multichip modules consisted of 9×9 array of blue chips of size 0.61 mm $\times$ 0.61 mm $\times$ 0.15 mm (Epistar InGaN Venus Blue) with 1.5-mm pitch that was symmetrically surrounded with four red chips of size 1.066 mm $\times$ 1.066 mm $\times$ 0.225 mm one at each side of the array (Epistar AlGaInP PN-series LED chip). The substrate size was 26 mm $\times$ 30.5 mm. The electrical connection of the chips was a combination of series and parallel connections illustrated in Fig. 1 to make the module tolerant against single LED open or short failure. The chips were wire-bonded with Au wire and die-bonded on the substrates with silver-filled epoxy (Epoxy Technology H20E). The test modules are illustrated in Fig. 2.

The alumina module consisted of 1.27-mm-thick alumina with screen-printed electrical contacts on top. The Cu MCPCB had 2-mm-thick copper core and some 70-μm-thick FR4 (IT-180, $k = 0.88$ W/mK) insulation layer with copper-filled microvias under each blue LED chip. The red LED chips had electrical contact on bottom, so thermal vias could not be used

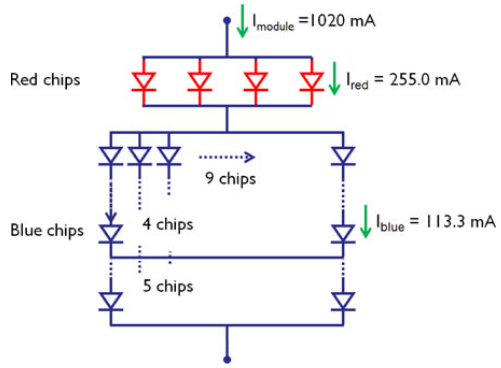

Fig. 1. Simplified electrical circuit of the LED module.

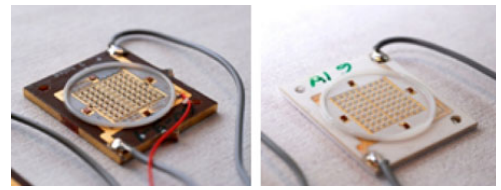

Fig. 2. (Left) Cu MCPCB module and (right) alumina module.

under them. The microvia was slightly cone shape with diameter around 90 μm. Different number and layout of vias (four, five, and nine vias) were tested. The different module configurations are illustrated in Fig. 3 and via configurations in Fig. 4. The substrate thicknesses, 1.27 mm for the alumina and 2 mm for the Cu MCPCB, are typically used with the technologies. Thus, the modules represent standard substrate technology available. The layout and the LED array on Cu MCPCB and alumina substrates were identical.

Manufacturing of Cu MCPCB had a limited number of processing steps and standard equipment available commonly in PCB shops was utilized. First, the copper plate was chemically treated to enable sufficient surface topography for Cu-epoxy adhesion. Then, the Cu plate was laminated together with FR4 glass-epoxy sheet and thin surface foil. FR4 is common dielectric capable of operating at elevated temperatures. Thicknesses between 50 and 100 μm are typical. The purpose of the surface foil is to enable circuit formation on the top of the insulating FR4 layer. After lamination, the Cu MCPCB panel was laser milled according to the desired design to realize microvias. Milling locally removes the surface foil, dielectric, and also thin Cu layer from the top of the Cu core plate. In general, mechanical drilling, cavity milling (laser or mechanical), hole drilling by laser, or any combination of these could be used. The following step was copper plating in order to fill the small vias completely by copper. Finally, the panel was ready for circuit layer patterning which is typically a combination of photo resist process, Cu/Sn pattern plating, and etching. In this stage, the panel is already electrically functional but needs some finishing steps like solder mask printing and final finish for contact areas. Also, separation

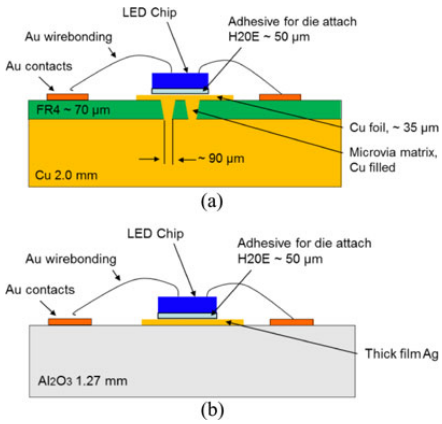

Fig. 3. (a) Cu MCPCB and (b) alumina test structure with blue LEDs.

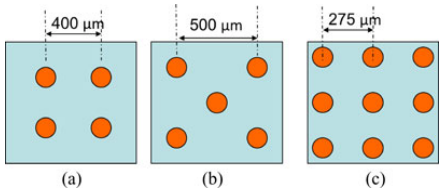

Fig. 4. (a) Four via configuration (b) Five via configuration (c) Nine via configuration tested under the blue LED chips on Cu MCPCB module.

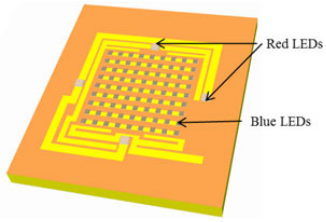

Fig. 5. LED module layout in the thermal simulations.

of the circuitry from the manufacturing panel and testing and final quality control is required.

B. Thermal Simulations

3-D computational fluid dynamics simulation software (FloTHERM, Mentor Graphics Corporation, Wilsonville, OR, USA) was used for the steady-state thermal simulations. Conduction, convection, and radiation heat transfer were included in the simulations. The simulated structure imitated measured modules and is illustrated in Fig. 5. Material properties used are listed in Table I. The temperature of the surrounding air (ambient) was 20 °C and the size of the computation domain was 16 cm × 16 cm × 16 cm (x, y, z). Cell size of the solution grid was 1.6 μm–5.3 mm, being at its finest with the smallest structural details. Modules were placed on 1-cm-thick aluminum plate with a fixed temperature setting 20 °C in the bottom that imitated the cold plate used in the measurements.

TABLE I
THERMAL SIMULATION PARAMETERS

Simulated structure		Material	Thermal conductivity (W/(mK))	Layer thickness (µm)
Alumina module	Substrate	Alumina	25	1270
	Conductors	Screen printed silver	320	25
	Adhesive	H20E	3	50
MCPCB module	Core	Copper	385	2000
	Dielectric	FR4, IT-180	0.88	70
	Conductors	Copper	385	35
	Adhesive	H20E	3	50
LEDs	Blue chips	Sapphire	23.1*	150
	Red chips	Silicon	151**	225

*k = 23.1 in plane, 25.1 through plane.
**k = 117.5 – 0.42 x (temperature (°C) – 100 (°C)).

TABLE II
THERMAL SIMULATION RESULTS

Substrate	Average temperature T [°C] Red LEDs	Average temperature T [°C] Blue LEDs
Alumina	35.4	46.9
Copper MCPCB, 4 vias per blue LED	42.3	41.3
Copper MCPCB, 5 vias per blue LED	42.3	41.0
Copper MCPCB, 9 vias per blue LED	42.3	39.7

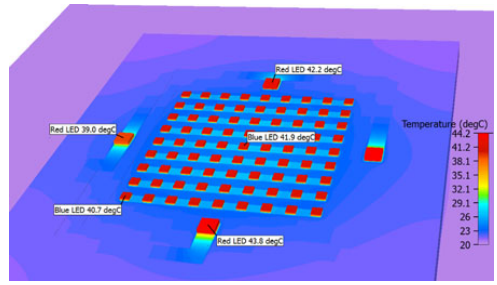

Fig. 6. Simulated surface temperatures on COB Cu MCPCB module with four microvias under each blue LED.

Heating power at the module was obtained by subtracting the measured radiant power from the measured electrical power and allocated to solitary LED chips. For the alumina module, heating power of 0.43 W was used in the simulations for each red chip and 0.23 W for each blue chip. For the MCPCB module, the corresponding values were 0.40 W heating power at each red chip and 0.24 W heating power at each blue chip. The results are reported in Table II. As illustrated in Fig. 6, the LED temperatures vary depending on their location in the LED array—the LEDs in the middle of the array are warmer than the LEDs located at side areas. This is caused by thermal interaction between the LEDs.

The insulating layer has a detrimental effect on thermal performance of Cu MCPCB as the average temperature of the red LEDs is 7° higher when compared with alumina module. Under blue LEDs, copper-filled thermal vias are used on Cu MCPCB. Consequently, the average temperature of the blue LEDs with nine via configuration Cu MCPCB is the lowest in simulations. This is due to the largest number and density of vias under the LED.

III. Measurement Procedure

A. Thermal Measurements

Thermal measurements were performed with a thermal transient tester (T3Ster, Mentor Graphics Corporation) utilizing temperature dependence of the semiconductor forward voltage for thermal characterization of device packages. T3Ster records the junction temperature of the LED as a function of time and calculates the thermal transient response of the structure. From this response, the cumulative structure function is processed. The cumulative structure function is a 1-D description of the thermal path from the heat source to surrounding ambient. Differential structure function is the derivative of the cumulative structure function. It can be described as the product of volumetric thermal capacitance c, thermal resistance r, and cross-sectional area A of the heat flow path, as shown in (1). Here, the entire chip array was considered as heat source, while the ambient was the 20 °C cold plate used in the measurements. Thus, the result describes the thermal path from the LED array to the ambient and the thermal resistance seen by individual chips cannot be distinguished [24], [25]

$$\frac{dC_\Sigma}{dR_\Sigma} = crA^2. \tag{1}$$

Sensitivity coefficient was determined with a sensor current of 20 mA for each module in a calibration measurement using temperature-controlled thermostat chamber. Voltage over the module was recorded from 20 °C to 80 °C with 10 °C steps and a line was fitted to the measurement points using least square method. The average measured sensitivity coefficient of all modules was −18.1 mV/K with a standard deviation of 1.3 mV/K. Voltage of the modules at 20 mA current was around 24.6 V.

The actual measurement was performed on a water-cooled cold plate at 20 °C driving the LED module first at a heating current of 1020 mA for 10 min and then another 10 min with the sensor current (20 mA). The voltage change over the LED array was recorded and corresponding temperatures were calculated with the sensitivity coefficients. Assuming even current distribution according to the electrical connection of LEDs (see Fig. 1), the heating current through each red LED chip was 255 mA and through each blue LED chip was 113.3 mA. The measurement procedure followed JESD51-51 [25] standard and is described more in detail in [21].

The red and blue chips had different configuration and the Cu MCPCB structure was different under them (thermal vias lacking under the red chips). Thus, some additional tests were made measuring blue chips and red chips separately. The average measured sensitivity coefficient was −16.9 mV/K for the blue LED array and −1.6 mV/K for the red LED array. The measurements utilized the same setup and the calibration and measurement procedure was the same as described above.

TABLE III
Radiant and Electrical Power of the Modules ($I_{\mathrm{module}} = 1020$ mA)

LED module			Blue LEDs		Red LEDs	
	Radiant power, Prad [W]	Electrical power, Pele [W]	Prad [W]	Pele [W]	Prad [W]	Pele [W]
MCPCB	10.3 ± 0.5	32.6 ± 0.2	9.5	30.8	0.47	2.1
Alumina	11.4 ± 0.3	32.3 ± 0.6	10.4	30.8	0.47	2.2

± denotes standard deviation.

B. Radiant Power Measurements

Radiant power of the modules was measured with a 0.5-m diameter integrating sphere (type: UMBB-500, Gigahertz Optik) by placing the module in the opening of the sphere wall so that the light was guided into the sphere. The measurement setup was calibrated to take into account the nonideal nature of the sphere surface [26]. The radiant power of the LED modules was recorded in conjunction with the heating phase of the thermal measurements. The average measured radiant and electrical power of seven alumina modules and seven Cu MCPCB modules is listed in Table III. Blue and red LED arrays were measured separately and average values of four Cu MCPCB and three alumina substrates are listed in Table III. Measured radiant power of each module at the heating current was subtracted from the electrical power to calculate the total heating power.

IV. Results and Discussion

A. Thermal Measurements

The results of thermal measurements of the multichip modules are listed in Table IV. Characteristic changes in structure function are used to detect the thermal domains of the module. In many cases, where the heat flow path consists of materials with similar thermal conductivity, the thermal domains are difficult to distinguish. The differential structure function brings out even the small changes and is therefore used for comparative analysis. Here, a characteristic peak in differential structure function is used to determine module base as illustrated in Fig. 7. The peak is identified to be the module base by making a controlled change in module structure. In this case, the amount of thermal paste between the module base and the cold plate was varied. The location of the change in structure function coincides with the part of the structure that was altered. Thus, by changing the module base–cold plate interface quality and by comparing the structure function curves, the peak defining the interface can be identified. The comparison of structure functions of different types of modules is illustrated in Fig. 8 in which the curves are moved to overlap at 0.1 K/W for solid comparison.

Considerably, lower thermal resistances were measured in Cu MCPCB modules than in the reference alumina modules. The mean value of thermal resistance from the LED array to the bottom of the alumina module was 1.12 K/W with standard

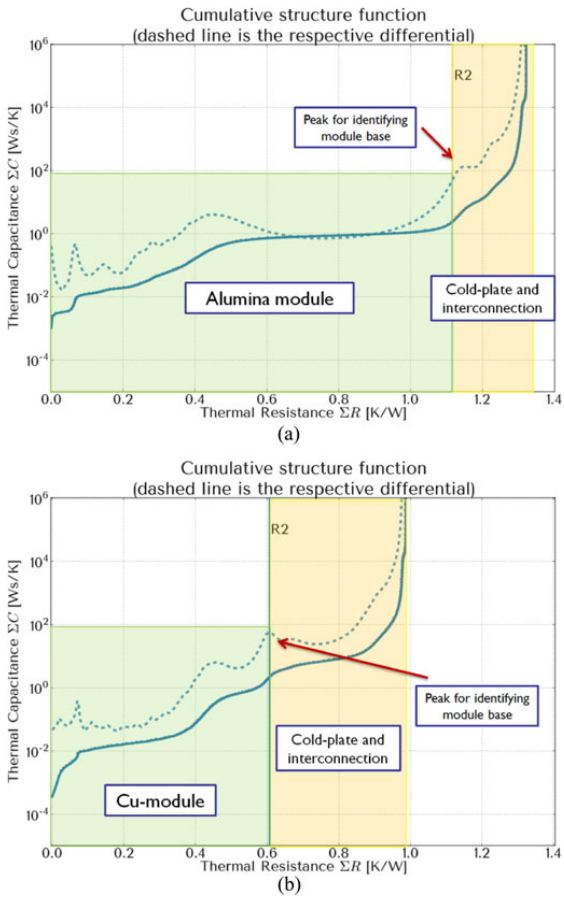

Fig. 7. Area indicating the thermal resistance from the chip array to module base for (a) alumina and (b) Cu MCPCB module.

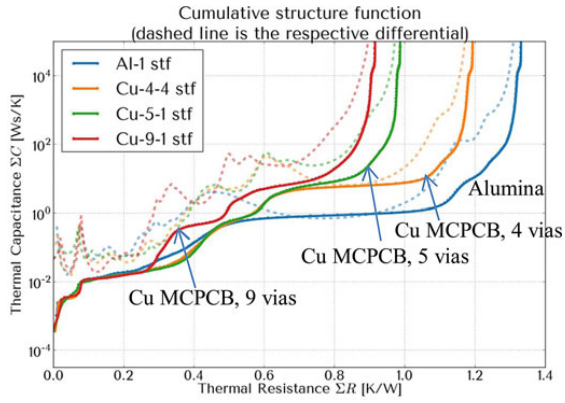

Fig. 8. Structure function of alumina module (blue) and Cu MCPCB module with nine vias (red), five vias (green) and four vias (orange) under a blue LED chip. Dashed lines are differential structure functions.

TABLE IV
THERMAL RESISTANCE OF THE MODULES ($I_{\mathrm{module}} = 1020$ mA)

ID	Substrate	Thermal resistance, chips to module base R [K/W]	Average R [K/W]
Al-1	Alumina	1.12	1.12
Al-2	Alumina	1.15	
Al-3	Alumina	1.12	
Al-4	Alumina	1.13	
Al-5	Alumina	1.09	
Al-6	Alumina	1.06	
Al-7	Alumina	1.17	
Cu-4-1	MCPCB, 4 vias	0.67	0.61
Cu-4-2	MCPCB, 4 vias	0.56	
Cu-4-4	MCPCB, 4 vias	0.60	
Cu-5-1	MCPCB, 5 vias	0.61	0.59
Cu-5-2	MCPCB, 5 vias	0.58	
Cu-9-1	MCPCB, 9 vias	0.50	0.50
Cu-9-2	MCPCB, 9 vias	0.50	

TABLE V
THERMAL RESULTS OF THE BLUE CHIP ARRAY ($I_{\mathrm{module}} = 1020$ mA)

ID,	Substrate	Temperature [°C]	Thermal resistance, chips to module base, R [K/W]
Al-3-blue	Alumina	47.6	1.10
Al-4-blue	Alumina	49.4	1.18
Al-7-blue	Alumina	48.0	1.13
Cu-4-4-blue	MCPCB, 4 vias	37.2	0.59
Cu-5-1-blue	MCPCB, 5 vias	37.5	0.58
Cu-5-2-blue	MCPCB, 5 vias	37.4	0.58
Cu-9-2-blue	MCPCB, 9 vias	35.5	0.48

deviation of 0.04 K/W. The mean thermal resistance for Cu MCPCB with four, five, and nine vias under blue LED chip was 0.61, 0.59, and 0.50 K/W respectively. Thus, up to 55% reduction in module thermal resistance was achieved with Cu MCPCB solutions.

The multichip module consisted of blue and red chips. The thermal vias could only be used under the blue chips due to their electrically isolated bottom. Thus, with some modules, the blue and red chips were measured separately. The results of blue LEDs are listed in Table V and compared in Fig. 9 in which the curves are moved to overlap at 0.1 K/W for solid comparison. The LED array temperature is approximated as measured temperature change $\Delta T + T_{\mathrm{ambient}}$ that is the 20 °C cold plate. The results of red LEDs are compared in Fig. 10 in which the curves are moved to overlap at 2.5 K/W for solid comparison.

If only the blue LEDs are measured, the temperature and thermal resistance are considerably lower on Cu MCPCB than on alumina module. The average temperature of the blue LED array ($I_{\mathrm{total}} = 1020$ mA) on Cu MCPCB was 36.9 °C, while it was 48.3 °C on alumina module. The mean thermal resistance of the blue chip array on Cu MCPCB was 0.56 K/W, while it was 1.14 K/W on alumina module. For solid comparison of different microvia configurations on Cu MCPCB, the number of samples is low. Still, the version with nine vias can be detected as the one with lowest resistance. This is well understood as the number and density of vias is considerably higher with nine

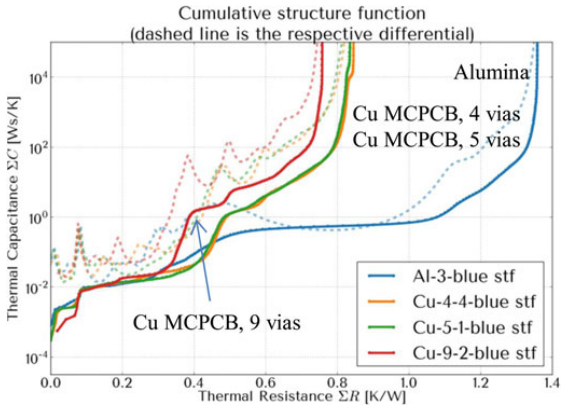

Fig. 9. Structure function of the blue chip array on alumina module (blue) and on Cu MCPCB module with nine vias (red), five vias (green), and four vias (orange) per chip.

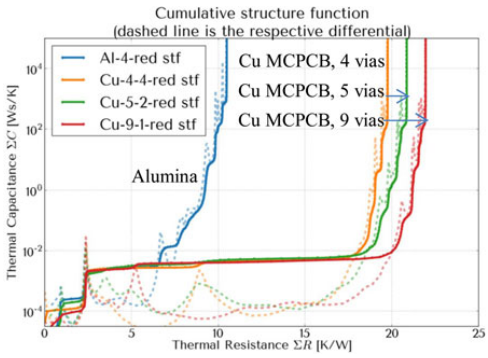

Fig. 10. Structure function of the red chip array on alumina module (blue) and Cu MCPCB module with nine vias (red), five vias (green), and four vias (orange).

vias compared with four and five via versions between which no difference in thermal performance can be distinguished.

The situation is totally different considering red LEDs, as there are no vias under the chips on Cu MCPCB. Instead, there is a layer of FR4 with poor thermal conductivity. Consequently, temperatures are higher when compared with the alumina module. The red LED array ($I_{\mathrm{total}} = 1020$ mA) on Cu MCPCB was 50.0 °C, while it was only 32.7 °C on alumina module. The thermal resistance of red chips on Cu MCPCB was 19.4 K/W, while it was 8.1 K/W on alumina module. These numbers represent the average of three modules measured both with Cu MCPCB and alumina substrate. It should be noted however that the red LED measurement data are much noisier than blue LED measurement data. The measurement setup was optimized for the whole module of high forward voltage (∼32 V) with voltage resolution of 4 mV. This caused lower temperature resolution for the red LED array measurement using the same setup because the forward voltage (∼2 V) was significantly less than the whole module voltage. Calculation of the structure function involves numerical derivation which exaggerated this noise. Still, the measurement demonstrates that the excellent thermal performance of the Cu MCPCB module is due to the thermal vias under the blue chips. As the vast majority of the chips of the multichip module are blue, they are dominating the thermal resistance of the entire module.

On alumina module, the average simulated red and blue chip temperature was within 1.4–2.7 °C difference from measured LED array temperatures. This is considered fairly accurate as series and parallel connection of the LEDs causes some inherent inaccuracy to the simulation as well as measurement. Closely situated LEDs affect each other thermally (see Fig. 6) which can cause variation in LED performance and thus change the current distribution within the LED array. Consequently, the actual heating power distribution during the measurements could have differed from even distribution assumed in the simulations. In addition, the biggest difference between simulations and measurements is with red LEDs. There is inaccuracy in the red LED array measurement that could have contributed to this difference.

Aforementioned differences between the simulations and measurement relate to the Cu MCPCB modules as well. On Cu MCPCB, the measured average red LED array temperature was 7.7 °C higher when compared with average simulated values. A potential cause of this is the thermal conductivity and thickness of FR4 layer. FR4 is a glass-epoxy material and presumed to be orthotropic. The thermal conductivity of the FR4 given in the material datasheet might not be valid in all directions [27]. For the blue LEDs on Cu MCPCB, the average simulated temperatures were 3.5–4.2 °C higher than measured. As the copper-filled thermal vias are managing the thermal performance, the simulation parameters of FR4 insulation are not as critical. Due to the laser milling utilized in the manufacturing, the vias were slightly cone shaped. In the simulations, the vias were approximated with rectangular blocks.

The thermal resistance of the entire module should be lower than thermal resistances of the blue and red chips measured independently, because thermally the blue and red chip arrays are in parallel [28]. However the thermal balance of the module is difficult to analyze theoretically because red and blue arrays are not independent from each other: they are closely situated and consequently heating each other and the electrical connections of the chips are a combination of series and parallel connections. Here, the thermal resistance of the module coincides with the thermal resistance of the blue chip array because it produces 92%–93% of thermal power of the module.

The total thermal resistance of the module varies significantly with the thermal contact quality between the module base and the cold plate, as demonstrated in Fig. 11. Thermal paste and screw attachment were used in these measurements. Changes in paste amounts and pressure can cause measurement inaccuracy because the paste was applied and the screws were fastened by hand. High power and small size of the module induce the effect. To eliminate this inaccuracy, thermal resistance from the chips to the module base is used instead of total thermal resistance. A characteristic peak in the differential structure function is used to determine module base. Occasionally, this interface is hard to find, causing error to the listed results. Still, the procedure is considered more accurate than using the total thermal

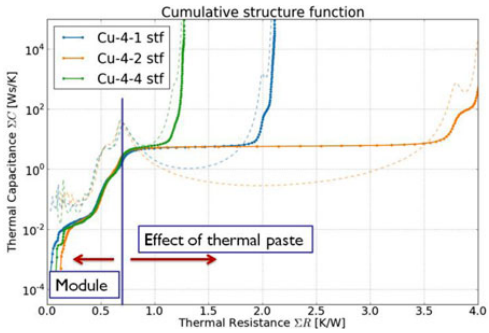

Fig. 11. Structure function comparison of same type Cu MCPCB modules with different module–cold-plate interface quality. Curves have been moved to overlap at 0.7 K/W for solid comparison.

resistances. The repeatability of a single thermal measurement was verified with five repeated measurements of alumina module Al-9. Average thermal resistance of the module was 1.021 K/W with a standard deviation of 0.012 K/W. The deviation is 1% of the mean.

Because T3Ster system principle of measurement is based on the assumption of 1-D heat flow, multidimensionality of the heat flow can cause uncertainty on measurements. However, in this measurement, as the substrate area is relatively small and the active cooling forces the heat to flow essentially in one dimension, the effect of the uncertainty can be considered low.

B. Radiant Power Measurements

As the LED temperatures are higher on alumina boards, there should be less light emitted than on Cu MCPCB because LED efficacy decreases with increasing junction temperature. However, this was not discovered, as the average radiant power of a Cu MCPCB module and an alumina module was 10.3 W and 11.4 W, respectively. The result could be explained by variation in LED performance and the substrate color because the alumina module with white substrate reflects more light than Cu MCPCB module with darker substrate due to absorption losses. The similar results have been reported also in our previous studies [21]. This is a drawback of the Cu MCPCB technology proposed in this paper and needs to be tackled by white masking or by changing the color of the insulator material to make this technology commercially successful.

V. Conclusion

In this paper, excellent thermal performance of high-power COB LED module based on a Cu MCPCB substrate with copper-filled microvias is reported. The performance is compared with alumina module with the same layout by means of thermal simulations and measurements and up to 55% reduction in the thermal resistance from the LED source to the bottom of the substrate is indicated. The Cu MCPCB processing was relatively short and consisted of standard steps of PCB manufacturing. In addition, low-cost insulation material FR4 was used. Consequently, good potential to develop a cost efficient and excellent thermal performance substrate for this application is demonstrated.

The enhanced performance of the Cu MCPCB LED module is due to copper-filled thermal vias under the blue LED chips. There are also some red chips without thermal vias on the Cu MCPCB module that experience increased thermal resistance in comparison with alumina module. However, as the vast majority of the chips on the module are blue, they dominate the module thermal resistance. The thermal resistance corresponds to the number and density of vias—lower thermal resistance was measured on modules with larger number and higher density of vias. In the future, the authors will concentrate on the enhancement of the optical performance and characterization of environmental reliability of the proposed Cu MCPCB technology.

Acknowledgment

The authors would like to thank J. Ollila, J. Kumpuniemi, and V. Moilanen for their expertise and valuable work for this study. They would also like to thank the following organizations: Aspocomp, BraggOne, Inkron, Laser Components, Lumichip, Modulight, Papula-Nevinpat, Selmic, Tampere University of Technology, Vaisala, and Valukumpu for cooperation in Produla project.

References

[1] D. L. DiLaura, K. W. Houser, R. G. Mistrick, and G. R. Steffy, *The Lighting Handbook: Reference and Application*, 10th ed. New York, NY, USA: Illuminating Engineering Society, 2011, Ch. 7.5.

[2] Life-cycle assessment of energy and environmental impacts of LED lighting products Part I: Review of the life-cycle energy consumption of incandescent, compact fluorescent, and LED lamps, Navigant Consulting, Inc., Chicago, IL, USA, Tech. Rep., Aug. 2012.

[3] R. Haitz and J. Y. Tsao, "Solid-state lighting: 'The case' 10 years after and future prospects," *Physica Status Solidi (a)*, vol. 208, no. 1, pp. 17–29, Jan. 2011.

[4] "Reliability and lifetime of LEDs," OSRAM Opto Semiconductors GmbH, Regensburg, Germany, Application Note, 2011.

[5] "Evaluating the lifetime behavior of LED systems," Philips Lumileds, San Jose, CA, USA, 2011, White paper.

[6] "XLamp LED reliability," Cree Inc., Durham, NC, USA, Application note, 2011.

[7] "Bridgelux RS array series product data sheet DS25," Bridgelux Inc., Livermore, CA, USA, 2012.

[8] "PhlatLight® wWhite LED Iillumination Pproducts, CBM-360 Seriesseries," Luminus Devices, Inc., Billerica, MA, USA, Product data sheet, 2011.

[9] J. Barcena, J. Maudes, M. Vellvehi, X. Jorda, I. Obieta, C. Guraya, L. Bilbao, C. Jiménez, C. Merveille, and J. Coleto, "Innovative packaging solution for power and thermal management of wide-bandgap semiconductor devices in space applications," *Acta Astron.*, vol. 62, pp. 422–430, Mar.–Apr. 2008.

[10] T. Jeong, K. H. Kim, S. J. Lee, S. H. Lee, S. R. Jeon, S. H. Lim, J. H. Baek, and J. K. Lee, "Aluminum nitride ceramic substrates-bonded vertical light-emitting diodes," *IEEE Photon. Technol. Lett.*, vol. 21, no. 13, pp. 890–892, Jul. 2009.

[11] "Interconnection Ssubstrates – Cceramic," IMAPS-CII / iNEMI Technology Roadmaps, Jan. 18, 2005.

[12] X. Jordà, X. Perpiñà, M. Vellvehi, and J. Coleto, "Power-substrate static thermal characterization based on a test chip," *IEEE Trans. Device Mater. Rel.*, vol. 8, no. 4, pp. 671–679, Dec. 2008.

[13] S. Di Pascolia, P. E. Bagnolia, and C. Casarosab, "Thermal analysis of insulated metal substrates for automotive electronic assemblies," *Microelectron. J.*, vol. 30, pp. 1129–1135, 1999.

[14] H. M. Cho and H. J. Kim, "Metal-core printed circuit board with alumina layer by aerosol deposition process," *IEEE Electron Device Lett.*, vol. 29, no. 9, pp. 991–993, Sep. 2008.

[15] G. Liu, Y. Shi, Y. Z. Tao, and S. Cao, "Measurement and significance of the effective thermal conductivity of the dielectric in an IMS," in *Proc. Microsyst. Packag. Assem. Circuits Technol. Conf.*, Taipei, Taiwan, Oct. 20–22, 2010, pp. 1–4.
[16] J. D. Holmes, D. A. Stone, and M. P. Foster, "Effect of inter-layer interface quality on electrical and thermal characteristics of IMS," in *Proc. 5th IET Int. Conf. Power Electron., Mach. Drives*, 2010, pp. 1–4.
[17] D. Mu and Y. Jin, "Study of anodized Al substrate for electronic packaging," *J. Mater. Sci.: Mater. Electron.*, vol. 11, pp. 239–242, 2000.
[18] X. Shao, Y. Cai, H. Li, and M. Wu, "Research of heat dissipation of RGB-LED backlighting system on LCD," in *Proc. 7th IEEE Int. Conf. Ind. Informat.*, 2009, pp. 807–812.
[19] M. A. Zampino, R. Kandukuri, and W.K. Jones, "High performance thermal vias in LTCC substrates," in *Proc. Intersoc. Conf. Thermal Thermomech. Phenomena Electron. Syst.*, 2002, pp. 179–185.
[20] V. Heikkinen, E. Juntunen, K. Kautio, A. Kemppainen, P. Korhonen, J. Ollila, A. Sitomaniemi, T. Kemppainen, T. Kutilainen, and H. Sahavirta, "High-brightness LED modules on alumina substrates," *Adv. Microelectron.*, vol. 34, pp. 12–16, Jul.–Aug. 2007.
[21] E. Juntunen, A. Sitomaniemi, O. Tapaninen, R. Persons, M. Challingsworth, and V. Heikkinen, "Thermal performance comparison of thick-film insulated aluminum substrates with metal core PCBs for high-power LED modules," *IEEE Trans. Compon., Packag., Manuf. Technol.*, vol. 2, no. 12, pp. 1957–1964, Dec. 2012.
[22] Y.-W. Kim, J.-P. Kim, J.-B. Kim, M.-S. Kim, J.-M. Sim, S.-B. Song, and N. Hwang, "Thermal analysis of a package substrate with filling via-holes for COB LED manufacturing," *J. Korean Phys. Soc.*, vol. 54, no. 5, pp. 1873–1878, May 2009.
[23] S. Taylor. (2010, Oct. 28). MCPCB's and thermal interface material considerations, in *Proc. OSRAM LLFY Workshop*, pp. 36–39. [Online]. Available: http://www.ledlightforyou.com/Downloads/data/Publications/Bergquist-MCPCBs-and-Thermal-Interface-Material-Considerations-for-High-Power-LED-Lighting-Applications-SanDiego-Oct.2010.pdf
[24] "T3Ster thermal transient tester technical information," Mentor Graphics Corporation, Wilsonville, OR, USA, 2011.
[25] *Implementation of the Electrical Test Method for the Measurement of Real Thermal Resistance and Impedance of Light-Emitting Diodes With Exposed Cooling*, JESD51–51, 2012.
[26] "Technical guide: Integrating sphere radiometry and photometry," Labsphere, Inc., North Sutton, NH, USA, 2006.
[27] J. E. Sergent and A. Krum, *Thermal Management Handbook for Electronic Assemblies*. New York, NY, USA: McGraw-Hill, 1998.
[28] L. Kim and M. W. Shinh, "Thermal resistance measurement of LED package with multichips," *IEEE Trans. Compon. Packag. Technol.*, vol. 30, no. 4, pp. 632–636, Dec. 2007.

Eveliina Juntunen received the M.Sc.(Tech.) degree in electrical engineering from the University of Oulu, Oulu, Finland, in 2004.

In 2004, she joined the VTT Technical Research Center of Finland, Oulu, where she is currently a Research Scientist in the Lighting and Integration Solutions Team. Her research interests include the area of reliability of electronics packaging including thermal management and environmental testing. Since 2007, she has been focusing on these topics from the LED lighting point of view.

Olli Tapaninen received the M.Sc. degree in physics from the University of Oulu, Oulu, Finland, in 2011.

Since 2011, he has been with the VTT Technical Research Centre of Finland, Oulu, as a Research Scientist, where he is involved in research on LED lighting. He was with Sodankylä Geophysical Observatory, Oulu, as a Research Assistant, where he was involved in research on space physics. His current research interests include thermal transient measurements and thermal analysis of high-power LED packages and systems.

Aila Sitomaniemi received the M.Sc. degree in physics from the University of Oulu, Oulu, Finland, in 2001.

She joined the VTT Technical Research Centre of Finland, Oulu, in 1998. Her first research area was computer networks. Since 2006, she has been involved in research on optics-related electronic modules, at first concentrating on optical simulations on LED lighting. Her major research field is thermal management in electronics including thermal design, simulations, and characterization.

Markku Jämsä received the M.Sc. degree in mechanical engineering from the Helsinki University of Technology, Helsinki, Finland, in 1985.

After graduation, he was with Finnish mining company Outokumpu. Since 1988, he has been working in printed circuit board (PCB) industry, mainly for Aspocomp, Espoo, Finland, and its predecessors where he has been responsible for PCB design, production management, quality, and sales. He is currently a Senior manager at Aspocomp, where he is responsible for European and overseas clients, technical customer service, and PCB technology for customer projects. Aspocomp is a PCB company producing printed circuit boards for electronics industry. Aspocomp has two printed circuit factories in Finland, specialized in high-density interconnect and other high-technology PCBs.

Veli Heikkinen received the M.Sc.(Tech.), Lic.Sc.(Tech.), and D.Sc.(Tech.) degrees in electrical engineering from the University of Oulu, Oulu, Finland, in 1986, 1999, and 2004, respectively.

He is a Senior Scientist with the VTT Technical Research Centre of Finland, Oulu. His research interest includes the optoelectronic module integration.

Mikko Karppinen received the M.Sc. degree in engineering physics from the Helsinki University of Technology, Helsinki, Finland, in 1998, and the D.Sc. degree in technology (optoelectronics) from the University of Oulu, Oulu, Finland, in 2008.

Since 1998, he has been with the VTT Technical Research Centre of Finland, Oulu, where he became a Scientist and Team Leader during 2005–2009, and is currently a Senior Scientist. At VTT, he has carried out research on photonics technologies and also managed several national and international R&D projects. In 2001, he was a Visiting Researcher at the University of Ottawa, Ottawa, Canada. He has authored or coauthored more than 40 journal or reviewed conference papers. His research interests include fabrication, hybrid integration, and packaging of photonics devices, for applications including optical interconnections, sensors, and lighting.

Pentti Karioja received the M.Sc., Lic.Sc.(Tech.), and D.Sc.(Tech) degrees in electrical engineering from the University of Oulu, Oulu, Finland, in 1981, 1993, and 1997, respectively.

After having worked for three years for Rauma Repola, he joined VTT Electronics, Oulu, in 1985. In 1993, he joined the Optical Sciences Center, University of Arizona, as a Visiting Scholar for a one-year period, where in 1996, he spent five months finishing his doctoral thesis. From 1998 to 2005, he was the Group Manager at VTT, where he was the Customer Manager in 2006 and 2007. In 2000, he was a Chief Research Scientist at VTT, where in 2006, he became a Research Professor for a five-year period with focus on module integration. In 2011, his position was renewed with the focus on photonics solutions. He has authored or coauthored 22 journal papers and has 5 patents or patent applications.

PUBLICATION II

Effect of Phosphor Encapsulant on the Thermal Resistance of a High-Power COB LED Module

In: IEEE Transactions on Components, Packaging and Manufacturing Technology 2013, (3)7, pp. 1148–1154.

Effect of Phosphor Encapsulant on the Thermal Resistance of a High-Power COB LED Module

Eveliina Juntunen, Olli Tapaninen, Aila Sitomaniemi, and Veli Heikkinen

***Abstract*— With their many advantages, such as small size, energy efficiency, and long lifetime, light emitting diodes (LEDs) are conquering the lighting world. Blue LEDs, because of their high efficiency, are commonly used and a phosphor is used to convert blue light into white light. The remote phosphor concept has gained attention since it promises to deliver better efficacy than solutions in which the phosphor is applied directly on the LEDs. In this paper, the effect of phosphor packaging on the thermal performance of a high-power chip-on-board LED module is studied. Both simulations and measurements show that, despite the added thermal load caused by white light conversion losses in the phosphor, the average temperature of the phosphor-coated LEDs matches with that of noncoated LEDs. The phosphor encapsulant generates a parallel heat conduction path which reduces the thermal resistance from the LED chips to ambient and compensates the thermal power increase.**

***Index Terms*— Light emitting diodes LEDs, multichip modules, phosphors, thermal analysis.**

I. Introduction

DRIVEN by increasing environmental concerns and cost of energy, light emitting diodes (LEDs) are conquering the lighting world. Nowadays, LEDs are used in applications such as display backlighting, communication, signage, and increasingly in general illumination. Besides the environmental benefits of low energy consumption, long lifetime, and the absence of mercury, features such as small size, easy controllability also at low-temperature circumstances, and low UV radiation level are appreciated in the lighting industry [1], [2].

Multichip module is a package with many chips located closely with each other, whereas chip on board (COB) defines that bare chips in contrast to packaged components are directly mounted on and electrically interconnected to the final circuit board. A common method of realizing high-power multichip COB LED modules is the use of chips emitting blue light along with a phosphor applied on top it to convert the emitted light into white light. The phosphor material covers the entire LED and is held in its place with a support ring [3], [4].

The remote phosphor concept has gained much attention because it promises to deliver 30%–60% more efficacy than solutions with phosphor-coated LEDs [5]–[7]. In the remote phosphor designs, the phosphor is moved away from the immediate vicinity of the LED chips and placed on a secondary optic or diffuser. Blue LEDs are used because of their high efficiency. Conversion from blue light to white light generates heat, and by removing the phosphor from the LED chip this extra heat load is extracted from the LED itself. Heat is detrimental to LEDs [8]–[10] and thus remote phosphor design is beneficial for increased efficacy and lifetime of the LEDs. Also, phosphors are temperature sensitive [1], so removing the heat load that the LED is causing on the phosphor is another significant benefit [11].

A typical remote phosphor solution consists of a plate covering a mixing chamber at the bottom of which the LEDs are located [5], [12]. Thus the dimensions of the light engine are relatively large, and the small size of the LED components is not utilized. Another drawback is that the cost of the solution can be high [12]. To make the conversion from blue light to white light, the required phosphor layer is typically relatively thick (>100 μm) and, while rather large surfaces are coated, the consumption of the phosphor material could be high.

In contrast to previous studies [5]–[7], [11], concentrating on the light extraction efficiency, this paper reports the thermal performance of a COB LED module with different phosphor packaging concepts. A nearby phosphor, where the phosphor plate is placed at a short distance from the LEDs, is introduced and compared with phosphor directly dispensed on the LED chips. Contrary to the remote phosphor concept, the proposed structure is very small and flat. Thus it could be more easily used with secondary optics and in applications with space limitations such as automotive head lamps. In addition, the phosphor vehicle could be used for sealing or physically protecting the LEDs in demanding applications.

The first nearby concept consists of a phosphor that is dispensed on a glass plate located in front of the LEDs. The process is quick and easy, and the volume of the slot is optimized so that the phosphor consumption is minimized. In the second nearby phosphor concept, the phosphor is included as one of the injection-molding ingredients. Thus the amount of phosphor in a sample can be controlled, and the molded piece designed to serve some other functions as well, such as secondary optics or mechanics.

II. Test Structure Design

A. Test Modules

The COB LED modules consisted of a 9×9 array of blue chips (Epistar InGaN Venus Blue) with 1.5 mm pitch that

Manuscript received December 21, 2012; revised March 15, 2013; accepted April 15, 2013. Date of publication June 4, 2013; date of current version July 2, 2013. This work was supported in part by Tekes, the Finnish Funding Agency for Technology and Innovation, and Infotech Oulu Doctoral Program. Recommended for publication by Associate Editor X. Luo upon evaluation of reviewers' comments.

The authors are with the Department of Photonic Devices and Measurement solutions, VTT Technical Research Centre of Finland, Oulu 90571, Finland (e-mail: eveliina.juntunen@vtt.fi; Olli.Tapaninen@vtt.fi; aila.sitomaniemi@vtt.fi; veli.heikkinen@vtt.fi).

Color versions of one or more of the figures in this paper are available online at http://ieeexplore.ieee.org.

Digital Object Identifier 10.1109/TCPMT.2013.2260796

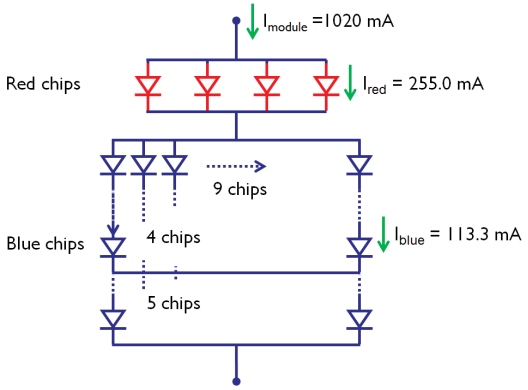

Fig. 1. Simplified electrical circuit of the LED module.

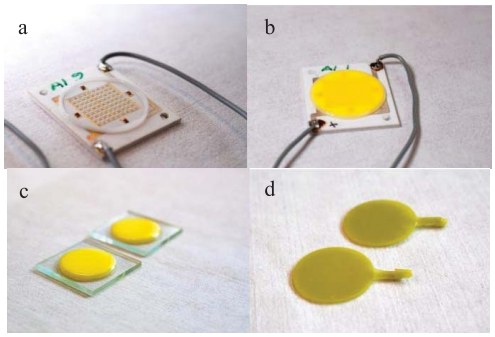

Fig. 2. (a) COB LED module without phosphor. (b) COB LED module phosphor A1covering the LEDs. (c) A1 and A2 phosphors on glass plates. (d) Injection-molded plastic phosphor plates.

was symmetrically surrounded with four red chips (Epistar AlGaInP PN-series LED chips). The size of the red LED chips was 1.066 × 1.066 × 0.225 mm and size of the blue LED chips was 0.61 × 0.61 × 0.15 mm. The chips were wire-bonded with gold and die-bonded with silver-filled epoxy (Epoxy Technology H20E) on alumina substrates of size 26 × 30.5 mm and thickness 1.27 mm. Combination of series and parallel electrical connections of the chips was used to make the module tolerant against single LED open or short failure, as depicted in Fig. 1.

The test module is illustrated in Fig. 2(a). Three different phosphor packaging concepts were studied. The phosphor was dispensed directly on the LED chips, as illustrated in Fig. 2(b), dispensed on the glass as illustrated in Fig. 2(c), and injection-molded in plastics as illustrated in Fig. 2(d). A commercial phosphor powder A (YAG:Ce) and an experimental phosphor powder B were used. Phosphor powder A was mixed with polymers to achieve 10% and 12% mass percent concentrations, denoted as A1 and A2, respectively. The concentrations were selected according to the phosphor supplier's recipe to achieve white light. Phosphor powder B was mixed with the same polymers to achieve very low mass percent to see

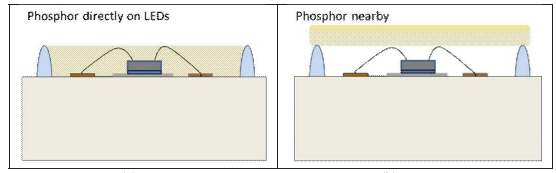

Fig. 3. Test structure with (a) phosphor covering the LEDs and (b) with spacer holding the nearby phosphor plate at a short distance from the LEDs.

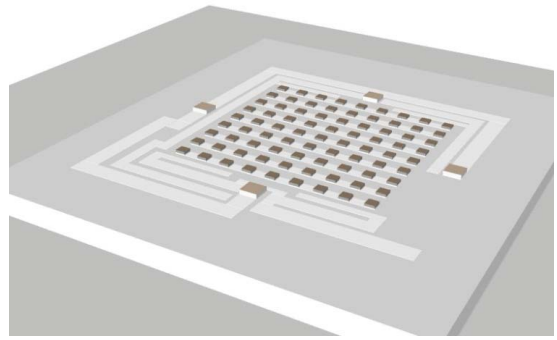

Fig. 4. LED module layout in the thermal simulations.

whether the phosphor filler would affect the thermal performance of the phosphor–polymer composite in comparison with a clear polymer encapsulant. The approximate mass percent of phosphor B was 5%, denoted as B1. The thickness of the dispensed phosphor directly on LEDs and on the nearby glass plate was around 600 μm to gain white light (~3000 K). For the injection-molded plate phosphor, A1 (10% mass percent) was used with PC Lexan 123R-111 plastic. The plate thickness was 2 mm.

The test structure configuration is presented in Fig. 3. The silicone (Hysol 3323) ring around the chips holding the phosphor in place was realized with a simple dispensing and curing process. In the nearby phosphor concept the silicone ring was used as the spacer between the LED chips and the phosphor.

B. Thermal Simulations

3-D computational fluid dynamics software (FloTHERM, Mentor Graphics Corp.) was used to perform the steady-state thermal simulations. Conduction, convection, and radiation were all considered. The temperature of the surrounding ambient (air) was 20 °C, and the size of the computation domain was 16 × 16 × 16 cm (x, y, z). The cell size of the solution grid varied from 1.6 to 5.3 mm, being finest in structural details with smallest dimensions. The simulated structure represented the test module and is illustrated in Fig. 4. The properties of the materials used are listed in Table I. Modules were placed on a 1-cm-thick aluminum plate with a temperature setting of 20 °C at the bottom, imitating the cold plate used in the measurements.

TABLE I
THERMAL SIMULATION PARAMETERS

Simulated Structure		Material	Thermal Conductivity (W/(mK))	Layer Thickness (μm)
Board	Substrate	Alumina	25	1270
	Conductors	Screen-printed silver	320	25
	Adhesive	H20E	3	50
LEDs	Blue chips	Sapphire	23.1*	150
	Red chips	Silicon	151**	225
Phosphor	Support ring	Silicone	0.25	600
	Polymer/ phosphor A1	Polymer	0.68	600
	Injection molded nearby plate	LEXAN 123R pc	0.19	2000
	Glass plate	Glass	1.05	1000
	Phosphor A1 on glass	Polymer	0.68	600

* $k = 23.1$ in plane, 25.1 through plane.
** $k = 117.5 - 0.42x$ [temperature (°C) – 100 (°C)].

TABLE II
THERMAL SIMULATION RESULTS ($P_{\text{LEDs}} = 20.7$ W, $P_{\text{Phosphor}} = 6.3$ W)

Module Option	Average Temperature T [°C] Red LEDs	Average Temperature T [°C] Blue LEDs	Maximum Temperature of the Polymer/Phosphor Layer
Bare LEDs	35.4	46.9	—
Clear polymers covering the LEDs	34.4	44.9	46.2
Phosphor A1 covering the LEDs	36.7	48.1	50.0
LEDs with injection-molded nearby phosphor plate	36.8	48.6	223
LEDs with phosphor on nearby glass plate	36.8	48.4	186

Heating power for the simulations was chosen based on the measurements. The total heating power in the simulations was 27 W, consisting of 20.7 W heating power in the LED array and 6.3 W heating power in phosphor. In compliance with the measurements, a heating power of 0.427 W was used for each red chip and 0.234 W for each blue chip. The heating power of the phosphor was attached to the whole volume of the material layer that contained phosphor.

Table II compares the simulated temperatures with different phosphor concepts. The clear polymer encapsulant is simulated to lower the average LED temperatures by 2 °C. The encapsulant overrides the air above the chip and creates a parallel heat conduction path. Consequently the LED temperatures indicate lower values. In case of the phosphor covering the LEDs the path partly compensates the thermal power increase, resulting in only a slight increase of the LED temperatures. On modules with nearby phosphor the LEDs are only ~1.7 °C warmer than the bare LEDs without phosphor although the nearby plate heats up considerably as illustrated in Fig. 5. The maximum simulated temperatures at the nearby plates are 223 °C in the injection molded plate and 186 °C in the phosphor on the glass plate. Also when the phosphor is dispensed directly on the LEDs, the maximum phosphor temperature exceeds the average LED temperature. The maximum temperature of the clear polymer is attained when the polymer and the warmest individual LED chip are in contact. Consequently this temperature is also higher than the average LED temperatures.

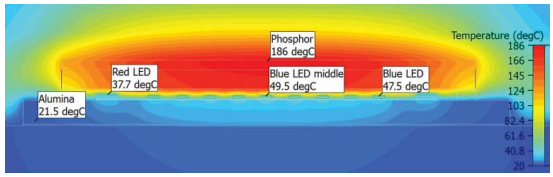

Fig. 5. Simulated temperatures of the COB LED module with phosphor on nearby glass plate.

III. MEASUREMENT PROCEDURE

A. Thermal Measurements

Thermal measurements were performed with a thermal transient tester (T3Ster, Mentor Graphics Corp.) which uses the temperature dependence of the semiconductor forward voltage for thermal characterization of semiconductor packages [13] The T3Ster records the junction temperature of the LED as a function of time and calculates the thermal transient response of the structure. The response curve is processed to a cumulative structure function [14], which is a 1-D description of the thermal path from the heat source to the surrounding environment. The differential structure function is the derivative of the cumulative structure function. It can be presented as the product of volumetric thermal capacitance c, thermal resistance r, and cross-sectional area A of the heat flow path, given by

$$\frac{dC_\Sigma}{dR_\Sigma} = crA^2. \tag{1}$$

These two functions are used to determine the thermal domains of the LED module. In cases where the heat flow path consists of materials with similar thermal conductivity, the cumulative structure function does not show notable features and the thermal domains are difficult to distinguish. The differential structure function brings out even the small changes as peaks and valleys and is therefore used for comparative analysis. Here, the entire chip array was considered as the heat source and the environment was the 20 °C cold plate used in the measurements. Thus the thermal resistance of individual chips is not established.

The sensitivity coefficient for each module was determined in a calibration measurement using temperature-controlled chamber and a small sensor current of 20 mA. The voltage

of the module was recorded from 20 °C to 80 °C with 10 °C steps, and a line was fitted to the measurement points describing the dependence between voltage of the module and temperature at the sensor current. The average measured sensitivity coefficient of the nine modules was −17.4 mV/K with a standard deviation of 1.1 mV/K, while the voltage of the modules was 24.6 V.

After the calibration, the module was placed on a water cooled cold plate at 20 °C. First, the LED module was driven with a heating current of 1020 mA. Assuming an even current distribution (Fig. 1), the heating current through each red LED was 255.0 mA and through each blue LED was 113.3 mA. After a stabilization time of 10 min, the heating current was switched to the sensor current (20 mA) and the voltage change over the LED module was recorded and corresponding temperatures according to the sensitivity coefficients were calculated. The measurement procedure followed JESD51-51 standard [15], which is described more in detail in [16].

B. Optical Measurements

An integrating sphere with a diameter of 0.5 m (type: UMBB-500, Gigahertz Optik) was used for radiant power and luminous flux measurements. A calibration coefficient was measured to take into account the nonideal nature of the sphere's surface [17]. Radiant power was measured simultaneously with the heating phase of the thermal measurement. Luminous flux was calculated according to the radiant power measurement.

The measured radiant power of each module was used to calculate the actual heating power from the electrical power. The average radiant power of the eight LED modules without phosphor was 11.4 W with a standard deviation of 0.3 W while average electrical power was 32.6 W with a standard deviation of 0.1 W. It was discovered that the nearby phosphor plates heated up too much with 1020 mA drive current. Thus additional light measurements were performed with a drive current of 300 mA. The measurement procedure was the same as described above.

IV. Results and Discussion

A. Thermal Measurements

Characteristic changes in the structure function were used to identify the thermal domains of the module, as illustrated in Fig. 6, which presents the cumulative and differential (dashed line) structure function of an LED module. The interconnection of the LED module to the cold plate has a significant impact on the temperature and the total thermal resistance of the module, which causes inaccuracies in locating the interfaces in repeated measurements. For example, on comparing measurements with and without the thermal paste between the module and the cold plate, the total thermal resistance changed from 0.95 to 3.44 K/W. To eliminate this uncertainty, the thermal resistance from the chips to a characteristic peak in the differential structure function within the thermal domain of the LED module was used in the thermal analysis, indicated as comparable thermal resistance in Fig. 6.

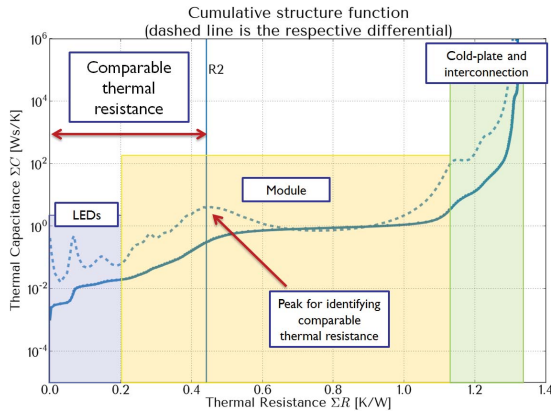

Fig. 6. Thermal domains of the LED module and the comparable thermal resistance used in the analysis.

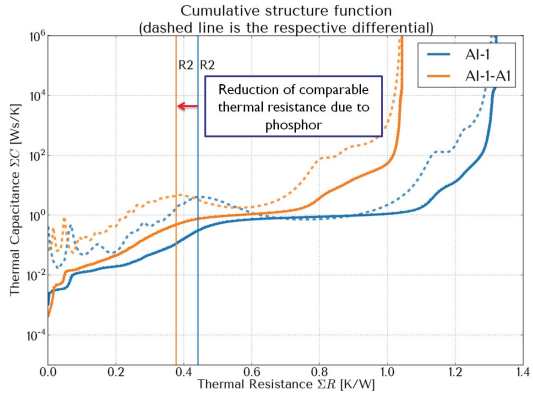

Fig. 7. Structure function comparison of modules before (blue) and after (orange) dispensing phosphor A1 over the LED chips.

The results of thermal measurements are listed in Table III. The temperature of the LED array is the measured temperature change plus the 20 °C of the cold plate. The average LED array temperature without phosphor A (Imodule = 102 A) was 48.2 °C. After adding the phosphor A, the average LED array temperature was 48.4 °C although the thermal power increased by 29% due to the white light conversion losses. A pair of structure functions comparing the module with and without dispensed phosphor A is presented in Fig. 7. On samples with phosphor B, the thermal power change was only 7%–10% because the radiant power absorption was lower than with phosphor A. Considering the clear polymer encapsulant the LED array temperature reduced by 2.6 °C although there was a 12% thermal power increase.

The thermal resistance of the module decreased with added phosphor. The phosphor encapsulant creates a new heat conduction path as the phosphor overrides the air above the chip as illustrated in Fig. 8. The path is good enough to compensate the thermal power increase caused by wavelength conversion

TABLE III
THERMAL MEASUREMENT RESULTS WITH AND WITHOUT PHOSPHOR COVERING THE LEDS ($I_{module} = 1.02$ A)

Module	Added Phosphor	Radiant Power [W]			Thermal Power [W]			Temperature of the LEDs, [°C]			Comparable Thermal Resistance, [K/W]		
		Without phosphor	With phosphor	Change (%)	Without	With	Change (%)	Without	With	Change (%)	Without	With	Change (%)
Al-1	A1	11.3	5.5	−51	20.9	26.8	28	47.8	47.7	0	0.44	0.34	−23
Al-2	A1	11.3	5.3	−53	20.9	26.9	29	48.6	49.5	2	0.48	0.36	−25
Al-4	A2	11.4	5.2	−54	20.9	27.1	29	48.3	47.9	−1	0.48	0.38	−20
Al-5	B1	11.8	9.5	−19	20.8	22.4	7	46.3	43.8	−6	0.46	0.37	−19
Al-6	B1	11.9	9.9	−17	20.1	22.1	10	45.4	43.1	−5	0.46	0.38	−17
Al-8@ 700mA	Clear polymers	8.5	6.9	−18	13.4	15.0	12	39.2	36.6	−7	0.50	0.40	−20

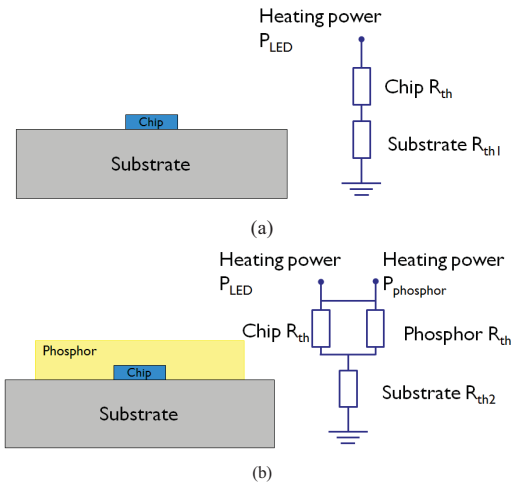

Fig. 8. Simplified structure and thermal resistance model of (a) module with bare LED and (b) module with phosphor covering the LED.

in the phosphor. Since the measured temperatures did not rise with the added phosphor while the thermal power increased, the thermal resistance calculation for the module indicates lower values. The clear polymer encapsulant has the same effect.

Thermal simulations agree with measurements as the average simulated blue chip temperature is within 0.4 °C–1.7 °C difference from measured LED array temperature with and without the phosphor A. There are some uncertainties in simulations due to inaccuracy in material parameters. Especially, the effect of the phosphor filler on the thermal properties of polymers and the injection molded plastic is not considered in simulations However according to percolation theory [18], there is drastic increase in thermal conductivity only after the filler is about 17% volume percent of the total composite. Also some uncertainty is caused by the location and volume of the generated power within the phosphor. In the simulations the power is evenly distributed whereas in reality it is more likely to be located more centrally. In addition, the actual current distribution within the LED array consisting of series and parallel connections is likely to be affected by thermal coupling between the closely located LEDs causing some inherent inaccuracy in the simulations as well as in the measurements. Instead, in the simulations and in decoding of the measurements the current is supposed to be distributed evenly within the LED array.

To determine the repeatability of the measurement and to identify characteristic features in structure function, seven repeated measurements were carried out for module Al-1 with dispensed phosphor A1 using different drive currents and different amounts of thermal paste between the module and the cold plate. The paste is applied using a syringe and the module is fastened on the cold plate by hand, which could cause measurement inaccuracy due to changes in paste amount and pressure. The average comparable thermal resistance of the module in the repeatability test was 0.36 K/W with a standard deviation of 0.02 K/W.

A factor causing uncertainty on measurements of the structure function is multidimensionality of the heat flow. The T3Ster system principle of measurement is based on the assumption of 1-D heat flow, although in reality some spreading inside the LED module occurs. Here, since the LED array occupies a significant portion of the module and the active cooling forces the heat essentially in one direction, this uncertainty is considered reasonable. In addition, the spreading resistance and the phosphor resistance are described as parallel heat flow paths with parallel resistance networks. Thus the measured structure function is considered a representation of a 1-D equivalent circuit of the more complex physical system.

B. Optical Measurements

The results of the optical measurements with 300-mA drive current and phosphor A are listed in Table IV. The phosphor B concentration was so low that the color of light was not comparable and consequently it is not considered here.

The optical measurements indicate bigger losses in nearby concept caused by optical absorption and thermal issues. An inheritable feature of the nearby concept is that the LEDs occupy most of the module surface under the nearby phosphor plate. Thus the LEDs themselves will be the primary

TABLE IV
LIGHT MEASUREMENT RESULTS ($I_{module} = 300$ mA)

ID	Phosphor	Radiant Power, [W]	Luminous Flux [lm]	Efficacy [lm/W]	Color Temp. [K]	CRIa
Phosphor covering the LEDs						
Al-1	A1	1.97	635	73	2870	68
Al-2	A1	1.97	638	72	2854	68
Al-3	A2	1.89	618	70	2809	67
Al-4	A2	1.85	615	70	2762	66
Al-8	Clear polymer	3.02				
Al-9	—	3.55				
Nearby phosphor						
Plastic-1	A1	0.38	140	16	3152	67
Plastic-2	A1	0.39	143	16	3311	69
Plastic-3	A1	0.40	153	17	3381	67
Glass-1	A1	1.12	391	45	2958	65
Glass-2	A2	1.11	389	44	2883	64

cause of backscattered light absorption [19]. It would help if the surfaces under the nearby plate, the LED chips and substrate surface could be made more reflective. In addition, a filler material with matched refractive index between the nearby phosphor and the chips would enhance the optical efficiency [19].

The optical absorption in the nearby phosphor structures was large. Especially the losses were higher than expected on injection-molded samples although a light transmission of 88% is given for the material (PC Lexan 123R-111). This is one of the main challenges to making the method successful. Still the nearby concept is considered interesting because it might enable the use of a smaller size of the light module and lower phosphor consumption compared with the remote phosphor concept. Also in comparison with traditional phosphor coating on LEDs, the nearby concept is attractive because it provides the potential of integration with sealing or other mechanical/optical structures. Therefore, the injection molding tests demonstrated are considered as possibly promising future prospects and a subject of further research, although the performance values reported in this paper are poor.

When used remotely, the phosphor can hardly utilize effective cooling provided for the LEDs. An optical filler between the nearby plate and LEDs would relieve the thermal issues as well. Here, the nearby phosphor plate is practically insulated from the cold plate by the silicon ring spacer. Consequently some serious thermal issues are demonstrated in nearby phosphor concept as in some cases the plastic started to melt. Similar results were reported in [20]. Also cracks on glass plates were discovered with high drive current. The simulated temperature of ∼190 °C at the nearby plate surface agrees with that measured by a thermocouple of 180 °C. The heat is caused by conversion losses in phosphor plates. As the LED temperatures are below 50 °C they are not considered to heat the nearby plate significantly.

V. CONCLUSION

In this paper, the effect of phosphor packaging on the thermal performance of a high-power COB LED module was presented. When phosphor was used directly on the LEDs, the thermal losses of white light conversion caused an additional heating of the LED chips. However, both simulations and measurements showed that the average junction temperature of the phosphor-coated LEDs equaled that of noncoated LEDs. The phosphor encapsulant created a new heat conduction path as the phosphor overrided the air above the chip. Here, the new path compensated the thermal power increase in the phosphor.

ACKNOWLEDGMENT

The authors would like to thank J. Ollila, J. Kumpuniemi, and M. Karppinen for their expertise and valuable contribution they made for this research. They would also like to thank the following organizations: Aalto University, Alppilux, Aspocomp, BraggOne, City of Helsinki, City of Jyväskylä, Enerpoint, Ensto Finland, Hella Lighting Finland, Helvar, Herrmans, Inkron, Laser Components, Lumichip, Modulight, MTG-Meltron, Oplatek, Papula-Nevinpat, Sabik, Selmic, Senaatti-kiinteistöt, Tampere University of Technology, Vaisala, Valopaa, Valukumpu, and YIT for co-operation in Produla and AthLEDics projects.

REFERENCES

[1] R. Haitz and J. Y. Tsao, "Solid-state lighting: 'The case' 10 years after and future prospects," *Phys. Status Solidi A*, vol. 208, no. 1, pp. 17–29, Jan. 2011.
[2] D. L. DiLaura, K. W. Houser, R. W. Mistrick, and G. R. Steffy, *The Lighting Handbook*, 10th ed. New York, NY, USA: Illuminating Engineering Society, 2011, ch. 7.5.
[3] *Bridgelux RS Array Series, Product Data Sheet DS25*, Bridgelux, Livermore, CA, USA, 2012.
[4] B.-H. Kim and C. Moon, "Comparison of the thermal performance of the multichip LED packages," *IEEE Trans. Compon., Packag., Manuf. Technol.*, vol. 2, no. 11, pp. 1832–1837, Nov. 2012.
[5] C. Hoelen, H. Borel, J. de Graaf, M. Keuper, M. Lankhorst, C. Mutter, L. Waumans, and R. Wegh, "Remote phosphor LED modules for general illumination: Toward 200 lm/W general lighting LED light sources," *Proc. SPIE*, vol. 7058, no. 70580M, pp. 1–10, Aug. 2008.
[6] N. Narendran, Y. Gu, J. P. Freyssinier-Nova, and Y. Zhu, "Extracting phosphor-scattered photons to improve white LED efficiency," *Phys. Status Solidi A*, vol. 202, no. 6, pp. R60–R62, May 2005.
[7] Z. Liu, S. Liu, K. Wang, and X. Luo, "Optical analysis of phosphor's location for high-power light-emitting diodes," *IEEE Trans. Device Mater. Rel.*, vol. 9, no. 1, pp. 65–73, Mar. 2009.
[8] *Reliability and Lifetime of LEDs, Application Note*, Osram, Munich, Germany, 2011.
[9] *Evaluationg the Lifetime Behavior of LED Systems, White Paper*, Philips Lumileds, San Jose, CA, USA, 2011.
[10] *Cree XLamp LED Reliability, Application Note*, Cree, Vermilion, AB, Canada, 2011.
[11] K.-M. Moon, S.-H. An, H.-K. Kim, J.-H. Chae, and Y.-J. Park, "Phosphor concentration and geometry for high power white light emitting diode," *Proc. SPIE*, vol. 7617, no. 76171Y, pp. 1–8, Jan. 2010.
[12] M. Leung, "Fair comparison of white LEDs and remote phosphor guides design choice," *Leds Mag.*, vol. 1, pp. 56–64, Jul.–Aug. 2012.
[13] *T3Ster Thermal Transient Tester Technical Information*, Mentor Graphics Corporation, Wilsonville, OR, USA, 2011.
[14] V. Szekely and T. Van Bien, "Fine structure of heat flow path in semiconductor devices: A measurement and identification method," *Solid-State Electron.*, vol. 31, no. 9, pp. 1363–1368, 1988.
[15] *Implementation of the Electrical Test Method for the Measurement of Real Thermal Resistance and Impedance of Light-Emitting Diodes with Exposed Cooling*, Standard JESD51-51, 2012.

[16] E. Juntunen, A. Sitomaniemi, O. Tapaninen, R. Persons, M. Challingsworth, and V. Heikkinen, "Thermal performance comparison of thick-film insulated aluminum substrates with metal core PCBs for high-power LED modules," *IEEE Trans. Compon., Packag. Manuf. Technol.*, vol. 2, no. 12, pp. 1957–1964, Dec. 2012.
[17] *Technical Guide: Integrating Sphere Radiometry and Photometry*, Labsphere, Inc, North Sutton, NH, USA, 2006.
[18] I. Furgel', O. Molin, and V. Borshch, "Thermal conductivity of polymer composites with a disperse filler," *J. Eng. Phys. Thermophys.*, vol. 62, no. 3, pp. 335–340, 1992.
[19] Z.-Y. Liu, S. Liu, K. Wang, and X.-B. Luo, "Studies on optical consistency of white LEDs affected by phosphor thickness and concentration using optical simulation," *IEEE Trans. Compon. Packag. Technol.*, vol. 33, no. 4, pp. 680–687, Dec. 2010.
[20] X. Luo, X. Fu, F. Chen, and H. Zheng, "Phosphor self-heating in phosphor converted light emitting diode packaging," *Int. J. Heat Mass Transf.*, vol. 58, pp. 276–281, Mar. 2013.

Eveliina Juntunen received the M.Sc. (Tech.) degree in electrical engineering from the University of Oulu, Oulu, Finland, in 2004.

She joined VTT, Oulu, in 2004, where she is a Research Scientist with the Lighting and Integration Solutions. Since 2007, she has been focusing on LED lighting point of view. Her current research interests include reliability of electronics packaging including thermal management and environmental testing.

Olli Tapaninen received the M.Sc. degree in physics from the University of Oulu, Oulu, Finland, in 2011.

He has been with the VTT Technical Research Centre of Finland, Oulu, since 2011, as a Research Scientist researching LED lighting. He was previously with Sodankylä Geophysical Observatory, Oulu, as a Research Assistant involved in research on space physics. His current research interests include thermal transient measurements and thermal analysis of high-power LED packages and systems.

Aila Sitomaniemi received the M.Sc. degree in physics from the University of Oulu, Oulu, Finland, in 2001.

She joined VTT Technical Research Centre of Finland, Oulu, in 1998. Her first research was computer networks. Since 2006, she has been involved in research on optics related electronic modules, at first concentrating on optical simulations on LED lighting. Her major field is thermal management in electronics including thermal design, simulations and characterization.

Veli Heikkinen received the M.Sc. (Tech.), Lic.Sc. (Tech.), and D.Sc. (Tech.) degrees in electrical engineering from the University of Oulu, Oulu, Finland, in 1986, 1999, and 2004.

He is a Senior Scientist with the VTT Technical Research Centre of Finland, Oulu. His current research interests include optoelectronic module integration.

PUBLICATION III

Thermal Performance Comparison of Thick-Film Insulated Aluminum Substrates With Metal Core PCBs for High-Power LED Modules

In: IEEE Transactions on Components, Packaging and Manufacturing Technology 2012, (2)12, pp. 1957–1964.

Thermal Performance Comparison of Thick-Film Insulated Aluminum Substrates With Metal Core PCBs for High-Power LED Modules

Eveliina Juntunen, Aila Sitomaniemi, Olli Tapaninen, Ryan Persons, Mark Challingsworth, and Veli Heikkinen

***Abstract*— Evolution of lumens per watt efficacy has enabled exponential growth in light-emitting diode (LED) lighting applications. However, heat management is a major challenge for an LED module design due to the necessity to conduct heat away from the LED chip. Elevated chip temperatures cause adverse effects on LED performance, lifetime, and color. This paper compares the thermal performance of high-power LED modules made with two types of circuit boards: novel substrates based on insulated aluminum material systems (IAMSs) technology that inherently allows using thermal vias under the LEDs and traditional metal core printed circuit boards (MCPCBs) commonly used with high-power LED applications. IAMS is a thick-film insulation system developed for aluminum that cannot handle temperature higher than 660 °C. The coefficient of thermal expansion of IAMS pastes is designed to match with aluminum, which minimizes any bowing. The thermal via underneath the LED enables excellent thermal performance. More than 7 °C reduction in LED junction temperature at 700-mA drive current and 27% reduction in the total thermal resistance from the LED junction to the bottom of the substrate were demonstrated for the IAMS technology when compared with MCPCB. When considering only the thermal resistance of the substrate, reductions of around 70% and 50% were obtained. This versatile and low-cost material system has the potential to make LEDs even more attractive in lighting applications.**

***Index Terms*— Dielectrics and electrical insulation, light-emitting diodes (LEDs), substrates, thermal analysis, thermal management, thick films.**

I. Introduction

CONSTANT increase of packaging density has driven the electronics industry for decades to develop better substrates for thermal management of high-power devices. The revolution of light-emitting diode (LED) lighting induces this development because the extreme requirements on thermal performance come with low cost expectations. LEDs are solid-state light sources that are increasingly used in many applications such as display backlighting, communications, medical services, signage, and general illumination. LEDs have a high potential to replace lamp-based light sources in many applications due to their better energy efficiency and long lifetime. LEDs are also eco-friendly products with no mercury and low health impact due to low UV radiation. In addition, features like small size, ease of control and lack of low-temperature startup problems have guided the way of LED lighting success [1]–[3]. The heat flux of high-power LEDs can be four times larger than that of conventional electronics, such as central processing units [4]. This is a severe challenge, because with lower junction temperature the LEDs will perform longer and better, will be brighter, and will have higher efficacy. In addition, LED manufacturers report thermal aging effects of packaging materials such as color changes of the white packages or aging of the silicone lenses [5]–[7].

Metal core printed circuit board (MCPCB) and insulated metal substrate (IMS) are the commonly used substrates with good thermal performance and low costs [8]. Both substrates use a metal core that serves as a mechanical support and thermal spreader with an electrically insulating layer on the top surface, and in literature their meanings cross. Here, MCPCB typically refers to a 1–3-mm-thick metal core structure with organic dielectric layer composition. The dielectric on the top surface is a thin (35–125 μm) polymer-based layer, over which the copper for the electrical interconnections is deposited [9]–[12]. The material of the base metal is usually aluminum, which has a high bulk thermal conductivity and light weight, although different metals, such as steel and copper, are also used [9].

Thermal properties of the MCPCB are mainly determined by the insulating layer, since the polymer has a very low thermal conductance compared with the base metal [9]. Thermal vias through the laminated dielectrics are not typically available due to alignment inaccuracy of the lamination process. Also, the processing of Cu-filled thermal vias on Aluminum core MCPCB is difficult. Thus, in order to increase the thermal performance, much effort has been made to develop insulating layers. There are two basic methods available—either to develop thermal properties of the material or to develop thinner insulating layers. To enhance the thermal performance, one common way is to charge the polymer resin with thermally conductive ceramic particles [13]. The effective thermal conductivity value of the dielectric layer strongly depends on the materials used, their relative proportions, the microscopic structure of the ceramic particles, and the quality of the interface with the metal layers [8], [9], [14].

Manuscript received November 1, 2011; revised May 15, 2012; accepted June 9, 2012. Date of publication September 4, 2012; date of current version December 3, 2012. Recommended for publication by Associate Editor M. Arik upon evaluation of reviewers' comments.

E. Juntunen, A. Sitomaniemi, O. Tapaninen, and V. Heikkinen are with the VIT Technical Research Centre of Finland, Oulu 90571, Finland (e-mail: eveliina.juntunen@vtt.fi; aila.sitomaniemi@vtt.fi; Olli.Tapaninen@vtt.fi; veli.heikkinen@vtt.fi).

R. Persons and M. Challingsworth are with the Thick Film Division, Heraeus Materials Technology, LLC, West Conshohocken, PA 19428 USA (e-mail: Ryan.Persons@heraeus.com; Mark.Challingsworth@heraeus.com).

Color versions of one or more of the figures in this paper are available online at http://ieeexplore.ieee.org.

Digital Object Identifier 10.1109/TCPMT.2012.2206390

Typically, alumina particles are used [9], but more exotic materials like barium titanate [14] and diamond [15] are also reported. The challenge with thin insulation layers is the electrical isolation, because the voltage on LED fixtures can be high. With very thin layers, like 38 μm, the layer quality is questionable as up to 35% variation in overall dielectric thickness has been reported [11], which results in unpredictable problems with thermal performance and electrical isolation [3], [10], [11], [12]. Another problem with MCPCBs is that they are subject to delamination at high temperatures [2].

IMS technique is very similar to MCPCB. Here, IMS refers to metal, typically aluminum, substrate with an inorganic insulation layer. This system produces a purely inorganic substrate with a high potential for reliable, high-power LED packaging [16]. The most traditional IMS technique is electrochemical anodization. Anodic film thickness of around 20–40 μm is usually needed to provide high-impedance insulation layer [16], [17]. There are various methods to form electrical conductors on anodized aluminum. Electroless plating, metal paste screen printing/sintering, and sputtering are representative approaches [2], [16], [17]. As with MCPCB, the thermal improvements of IMS solutions concentrate on the insulation layer. For example, the aerosol deposition process is reported with good results for high-power LED heat dissipation [13].

An effective solution would be thermal vias conducting the heat from the component directly to the metal core through the insulation layer. There are some studies reported to develop vertical connections [16], [18], but the efforts were made for multilayer substrate purposes more than thermal improvements of IMS boards. Lee *et al.* [3] introduces a patterned anodizing method to connect the lead frame of the LED package directly to the metal substrate. The test structure and setup is very simple. Still the potential of the thermal solution is clearly demonstrated [3]. Also, a significant thermal performance enhancement with filled thermal vias compared with MCPCB is reported in [4].

In this paper, an insulated aluminum material system (IAMS) substrate is introduced for high-power LED modules. The package consists of an aluminum base plate with screen printed isolation layer and electrical contacts. Under the thermal contact of the LED, a large thermal via is used. To our knowledge, this is the first time that a commercial-scale available [19] screen printed IMS is introduced with direct thermal contacts through the insulation layer. There is a constant struggle to develop insulation materials with low thermal resistance but high electrical isolation. This is a big challenge because it increases the costs of the MCPCB and IMS boards [4]. With the suggested IAMS technology, where the thermal via is managing the thermal performance, lower cost materials could be used for the isolation. As there is no need to pursue thin layers for thermal management reasons, thicker insulation layers can be used, which is favored for electrical isolation. In addition, due to the additive printing process, insulating layers can be used only where needed, resulting in minimal material waste during the circuit manufacturing compared to MCPCBs where sheets of copper are chemically etched to create the circuit.

Here, a realization and measurements of IAMS substrates are described and compared with that of conventional technology. The test structure design is introduced in Section II, and the experiments are depicted in Section III. The results along with a discussion are reported in Section IV. More than 7 °C reduction in LED junction temperature and 27% reduction in the total thermal resistance of the structure are reported, demonstrating the excellent performance of IAMS technology with thermal vias.

II. Test Structure Design

A. Test Substrates

Test structure consisted of four Luxeon Rebel high-power LEDs (LXML-PWC1-0100) with a typical drive current of 700 mA, forward voltage of 3.2 V and luminous flux of 180 lm [20] soldered onto circuit boards with an aluminum base plate and dimensions of 50 mm × 50 mm × 2 mm. The LED pitch was 20 mm. The test included 25 substrates in total: 10 IAMS substrates with a ceramic insulating layer and a ceramic solder mask (IAMS ceramic), 10 IAMS substrates with ceramic insulating layer and polymer solder mask (IAMS polymer), and 5 commercial MCPCBs as the reference. IAMS is an insulation system for aluminum metal substrates. Aluminum cannot handle temperature higher than 660 °C because this is its melting point. Standard thick-film products are ceramic based and must be fired at very high temperatures of 800 °C–900 °C. Because the IAMS pastes can be fired at less than 600 °C, the system is compatible with aluminum processing conditions. Most thick-film pastes have coefficient of thermal expansion (CTE) adjusted for use on ceramic substrates. However, with aluminum substrates, which have a very high CTE, a paste designed for ceramics will make the substrate bow due to the differences in CTE. The CTE of IAMS is designed to match the CTE of the aluminum, minimizing the bowing [19].

The test substrates are presented in Fig. 1. The Rebel LED has an electrically isolated thermal pad in the bottom of the component, and most of the heat is transferred through it. From Fig. 1(a) it can be seen that the IAMS substrate has a thermal via just below the LED. This via has the same size and shape as the thermal pad and it is filled with screen printed silver (type C8829B) for good heat conduction.

The test structures are shown in Fig. 2 and the materials are listed in Table I. The IAMS boards were manufactured by Heraeus. IAMS consists of three pastes: dielectric, conductor and solder mask. Thick-film pastes are dispersions of metal, ceramic, and glass powders in an organic printing medium often called a vehicle. The powders provide the desired functional properties (insulation, conduction, protection, etc.) after full processing. The vehicle is used only to give the material the screen printable qualities and is burned off during the thermal processing steps. The dielectric paste is a dispersion of proprietary, specially designed glass powder and other fillers that provide an insulating layer between the aluminum substrate and the circuit layer. The glass is designed to closely match the thermal expansion of aluminum (~20–25 ppm/°C) while sintering below

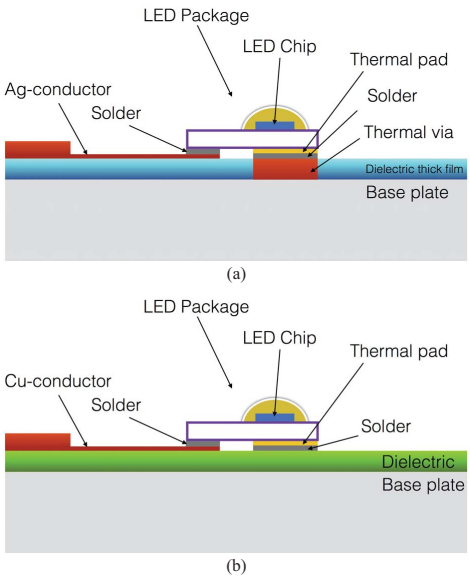

Fig. 1. (a) IAMS test substrate. (b) MCPCB test substrate.

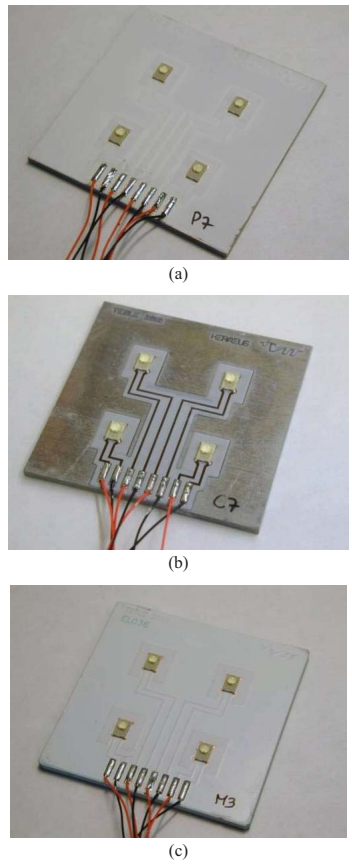

Fig. 2. (a) IAMS substrate with polymer overglaze. (b) IAMS substrate with ceramic overglaze. (c) MCPCB.

the melting point of the aluminum (∼660 °C). After thermal processing (firing between 550 °C–600 °C), the glass and other fillers form a dense, electrically insulating film that has excellent adhesion and compatibility with various grades of aluminum alloys (3000, 4000, 5000, and 6000 alloy grades). The conductor paste consists of silver powder (1–10 μm) with glass and oxide powders dispersed into a printing ink vehicle. The conductor paste is used both as the thermal via fill material and also to create the conductive circuit layer. The final paste in the system can be a polymer solder mask filled with white pigment.

The IAMS pastes were deposited through screen printing onto 2-mm-thick aluminum substrates. After printing, the inks were dried at 150 °C for 10–15 min in a box oven and then fired in a belt furnace at 550 °C–600 °C with a 30–40 min profile. Three layers of dielectric paste were printed and fired to build an insulating layer 40–50-μm thick. The thermal vias were filled with the silver conductor paste flush to the dielectric layers. Then the silver paste was used to create a circuit layer. Finally, either the dielectric layer was printed to create a solder dam (IAMS ceramic) or the white solder mask was printed to create a white top surface and to cover the dielectric/conductor layers (IAMS polymer). Thus both types of IAMS substrates used ceramic material as the insulating layer but differed by the overglaze material for the electrical leads: 10 substrates used polymer (IAMS polymer) and 10 used ceramic (IAMS ceramic). Also the MCPCB boards had a white overglaze to cover the green color of the T-preg layer.

B. Thermal Simulations

Steady-state thermal simulations were performed with 3-D computational fluid dynamics simulation software FloTHERM. Heat transfer mechanisms conduction, convection, and radiation were all included in the simulations. The goal of the simulations was to study the effect of thermal via on the thermal performance of the IAMS structure. The material properties used are listed in Table II. Thermal resistance of the LED was matched to measured 8 K/W. Ambient temperature, that is, the temperature of the surrounding air in the computational domain was 25 °C and the size of the domain was 11 cm × 12 cm × 8 cm (x, y, z). Mesh size varied from 7 μm to 3.5 mm in the computational domain which was at its tightest with the

TABLE I
MATERIALS OF THE TEST SUBSTRATES

Plate identifier	Base material	Dielectric material	Dielectric thickness, (μm)	Overglaze material
IAMS–polymer P0–P9	6061 Al	IP 6075	50–55	Polymer
IAMS–ceramic C0–C9	6061 Al	IP 6075	50–55	IP 6075
MCPCB M1–M5	EN AW1050	T-preg	150	Polymer

TABLE II
THERMAL SIMULATION PARAMETERS

Simulated structure		Material	Thermal conductivity (W/mK)	Surface emissivity	Layer thickness (μm)
IAMS	Core	Al 3003	162	0.06	2000
	Dielectric	IP 6075	2.05	0.9	60
	Conductors, thermal via	Ag C8829B	377	0.022	20, 60
	Solder	SnAgCu	60	0.2	50
MCPCB	Core	Al ENAW1050	229	0.06	2000
	Dielectric	T-preg	3.0	0.9	150
	Conductors, heat spreader layers	Cu	385	0.04	20
	Solder	SnAgCu	60	0.2	50

TABLE III
THERMAL SIMULATION RESULTS ($I_{LED} = 700$ mA)

	Via dimensions (mm)	ΔT (°C) = $T_{junction} - T_{ambient}$
IAMS without vias	–	28.6
IAMS with optimum via	1.77 × 2.8 × 0.06	20.2
IAMS with large via	3.0 × 4.0 × 0.06	20.1
IAMS with small via	1.0 × 1.0 × 0.06	23.2
MCPCB	–	26.2
MCPCB, no heat spreading layers	–	33.4

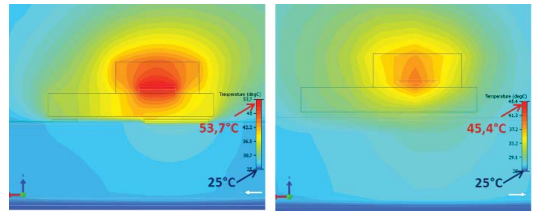

(a) (b)

Fig. 3. Simulated cross section of an LED on an IAMS substrate (a) without via and (b) with optimum via.

smallest structural details. The heating power, that is, the radiant power subtracted from the electrical power, was 1.97 W per LED ($I_{drive} = 700$ mA), which is the measured average for LEDs on IAMS boards. Substrates were placed on a 1-cm-thick aluminum plate with a 25 °C setting in the bottom imitating the cold plate temperature used in the measurements. Electric conductors are thin and narrow metallic layers and thus are not effective heat conductors. Consequently, they were omitted from the simulations when not located in the close vicinity of the LEDs.

Table III and Fig. 3 compare the simulated results of substrates with different configurations. The vias are located underneath the thermal pad of the LED. The optimum via size is 1.77 mm × 2.8 mm that coincides with the thermal pad size of the LED. Larger size thermal via would increase material costs, but would not improve thermal performance. Smaller size would degrade the performance. The MCPCB with and without a heat spreading layer is simulated as a reference. The results demonstrate a clear advantage of the IAMS substrate over the MCPCB technology. Without heat spreading layers typically used with MCPCB substrates, the advantage is even more prominent. The simulations indicate that the improvement of IAMS over MCPCB is mainly due to the thermal via. Without the via, the LED temperatures on IAMS and MCPCB with heat spreading layers are in the same range. Dielectric layer of the IAMS board is thinner, but has lower thermal conductivity compared with MCPCB.

C. Preparation of Samples

Four Luxeon Rebel LEDs were soldered on each substrate. The SAC305 solder with a composition of 96.5%Sn/3.0%Ag/0.5%Cu was used. The solder was screen printed using a 120-μm stencil, and the LEDs were set in place by hand. The soldering was done in a reflow oven. All the samples were X-ray inspected after soldering. In general, the soldering quality was equal between the IAMS and MCPCB substrates although some large voids were also detected, especially, with the IAMS polymer samples which suffered from a higher level of solder voiding than the IAMS ceramic and MCPCB. Fig. 4 illustrates an example of good soldering, bad soldering, and typical soldering of each board type.

III. MEASUREMENT PROCEDURE

A. Thermal Measurements

Temperature measurements were performed with a thermal transient tester (T3Ster, Mentor Graphics Corp.). T3Ster uses the temperature dependence of the LED forward voltage for thermal characterization of device packages [21].

The sensitivity coefficient for the particular LED was determined in a calibration measurement using a temperature-controlled thermostat chamber. The LED was driven with a

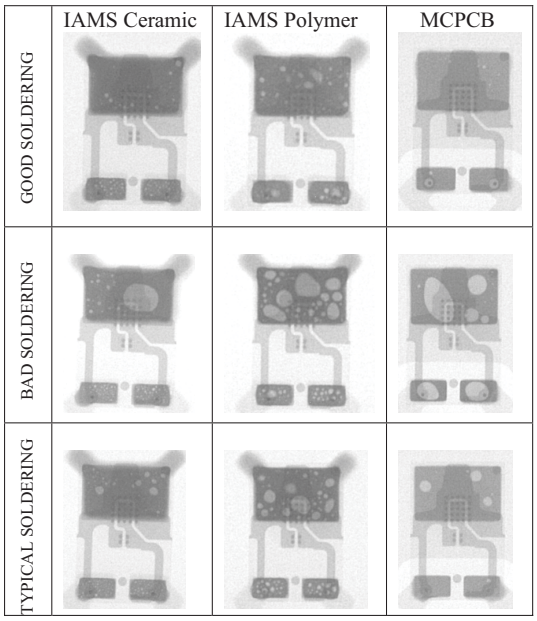

Fig. 4. X-ray image of good soldering, bad soldering, and typical soldering of each board type.

sensor current of 10 mA in order to generate only a negligible amount of heat. The voltage over the LED was recorded from 25 °C to 75 °C with 5 °C steps. A line was fitted to the measurement points using least square method. The slope of the line describes the dependence between the LED's voltage and temperature at the sensor current. The sensitivity coefficient was recorded for each LED.

After the calibration, the substrate was placed on a thermoelectric cooler that kept the bottom of the substrate at 25 °C. First, the LEDs were driven with 700 mA until the structure was thermally stabilized. Here, the stabilization time was 10 min. Then the current was suddenly switched to the sensor current (10 mA), and the voltages over the LEDs were recorded. From these voltage values, corresponding temperatures according to the individual sensitivity coefficients were calculated.

T3Ster measures the LED junction temperature as a function of time and calculates the thermal transient response of the structure describing the thermal resistance from the LED active junction to the 25 °C thermoelectric cooling plate. The differential structure function is defined as the derivative of the cumulative thermal capacitance with respect to the thermal resistance. Here, thermal resistance was recorded for each LED individually.

In addition to the measurements on a thermoelectric cooler, reference measurements were done with a passive heat sink to see how this would affect the overall shape of the structure function. Selected substrates were attached to a pinned heat sink with screws and thermal paste. The heat sink was set sideways to a small stand so it could be considered as floating in free air as illustrated in Fig. 5. Passive heat sink measurements were made using T3Ster operating at the same drive and sensor currents as above. The electrical connections were also identical. Heating and measuring times were considerably increased to 20 000 s.

B. Light Measurements

Luminous flux and radiant power of the test substrates were measured with an integrating sphere with diameter 0.5 m (type: UMBB-500, Gigahertz Optik). The sphere has openings for a detector and a light source, which make it less ideal. Measurement errors can also be present due to the geometry of the source and light absorbed by the source mounting [22]. A correction coefficient was calculated to take this absorption into account.

A substrate with four LEDs was placed in an opening of the sphere wall so that the light is guided into the sphere. The substrate was sitting on a thermoelectric cooler that kept the bottom of the substrate at a temperature of 25 °C. The measurement current was 700 mA and measuring time 900 s. The temperature of the LEDs and the luminous flux of the substrates were recorded simultaneously. During the measurement, all the LEDs were driven simultaneously, so the recorded luminous flux is a sum of the four LEDs. The radiant power was recorded in a separate measurement in a similar manner. Average of the measured radiant power of the LEDs on each substrate was subtracted from the electrical power to calculate the total heating power. Average radiant power of an LED was 0.51 W on IAMS ceramic, 0.55 W on IAMS polymer, and 0.53 W on MCPCB. Average electrical power was 2.50 ± 0.01 W for IAMS ceramic, 2.50 ± 0.02 W for IAMS polymer, and 2.38 ± 0.02 for MCPCB. A correction coefficient was calculated for each substrate before measurement.

IV. Results and Discussion

A. LED Temperature Coefficient

The sensitivity coefficient measurements showed that the temperature coefficient of the LED forward voltage ranged from –1.8 to –1.2 mV/K. The histogram presenting the distribution is shown in Fig. 6.

B. Thermal Measurements

One of the test substrates had a defect. Sample P0 had one LED with the electric contacts open so it did not light up. The results of thermal measurements are listed in Table IV, and a sample of structure functions giving thermal resistances is presented in Fig. 7. For structure function calculations the actual heating power, that is electrical power minus radiant power, is used.

Lower temperatures and thermal resistances were measured in thick-film manufactured IAMS substrates than in reference MCPCBs. The LED junction temperature can be calculated as the measured temperature change $\Delta T + T_{\text{ambient}}$ which was 25 °C here. The average LED junction temperature ($I_{\text{LED}} =$ 700 mA) on MCPCB was 53.1 °C whereas it was 45.0 °C on IAMS with ceramic overglaze and 46.2 °C on IAMS with

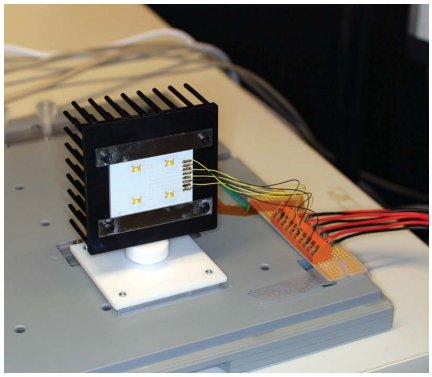

Fig. 5. Setup of passive heat sink measurements.

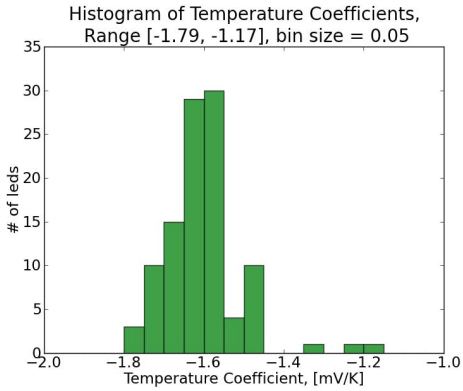

Fig. 6. Histogram of the distribution of temperature coefficients.

polymer overglaze. The mean value of total thermal resistance from the LED junction to the bottom of the substrate for MCPCB was 15.5 K/W with a standard deviation (σ) of 0.4 K/W. The mean total thermal resistances for polymer and ceramic overglazed IAMS substrates were 11.2 $\pm$ 0.6 and 10.4 $\pm$ 0.7 K/W, respectively. Thus among the polymer and ceramic overglazed IAMS substrates total thermal resistances from junction to ambient were on average 4.3 and 5.1 K/W lower than that of the MCPCBs, which is more than 27% reduction. When considering only the thermal resistance of the substrate, the advantage is even more significant. In Fig. 7, the thermal resistances of a sample of each substrate type are illustrated. Around 70% and 50% reductions in substrate thermal resistance were demonstrated when compared with MCPCB. However, these numbers are only indicative, because the accurate place of the LED package–board surface interface is hard to identify.

The measured and simulated LED temperatures differ only with 1 °C on IAMS boards and 2 °C on MCPCBs. Based on the simulations, the improvement of IAMS over MCPCB is mainly due to the thermal via. In addition, the dielectric layer of the IAMS board is thinner, but its lower thermal conductivity decreases this advantage.

TABLE IV
TOTAL TEMPERATURE CHANGES

Sample	ΔT [°C] LED 0	ΔT [°C] LED 1	ΔT [°C] LED 2	ΔT [°C] LED 3
P1	21.49	21.08	20.91	21.46
P2	21.64	22.51	21.97	21.83
P3	21.15	21.78	21.00	22.13
P4	22.50	20.81	19.75	18.63
P5	20.40	20.90	21.81	19.75
P6	21.03	21.47	22.02	21.22
P7	20.67	21.17	21.07	20.68
P8	21.70	21.96	21.38	21.42
P9	20.86	21.55	21.53	20.22
IAMS polymer group average 21.2 °C				
IAMS polymer group standard deviation 0.8 °C				
C0	21.21	20.45	20.90	20.88
C1	20.20	19.27	23.15	18.47
C2	18.68	23.67	19.55	18.48
C3	21.90	20.44	20.60	20.63
C4	18.47	22.13	19.21	17.86
C5	17.35	18.08	17.87	20.22
C6	19.81	19.05	20.76	22.91
C7	19.57	22.52	19.83	19.08
C8	20.45	17.36	18.37	19.80
C9	21.11	20.79	20.27	20.11
IAMS ceramic group average 20.0 °C				
IAMS ceramic group standard deviation 1.5 °C				
M1	26.53	27.17	27.26	27.38
M2	27.84	28.30	28.74	27.99
M3	27.77	30.16	30.52	27.69
M4	28.11	29.03	28.13	27.72
M5	27.04	28.78	28.27	28.14
MCPCB group average 28.1 °C				
MCPCB group standard deviation 1.0 °C				

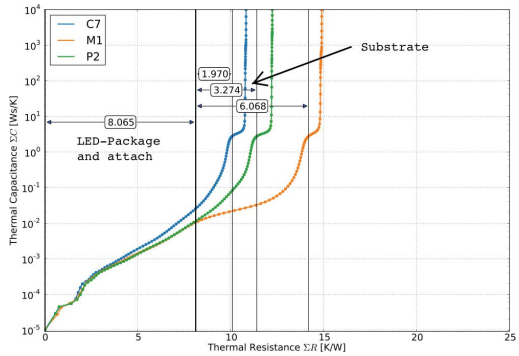

Fig. 7. Structure function of LED0 on MCPCB (orange), IAMS with polymer overglaze (green), and IAMS with ceramic overglaze (blue) substrates. Thermal resistance of the LED and substrates are illustrated.

Passive heat sink measurements were done for samples M1, M2, C1, C2, P1, and P2. In Fig. 8 passive cooling and active thermoelectric cooling measurements of samples M1 and P1 are shown. Passive cooling agrees with active cooling curves in resistance values below 8 K/W that is the region of the structure function corresponding to the LED package (see Fig. 7).

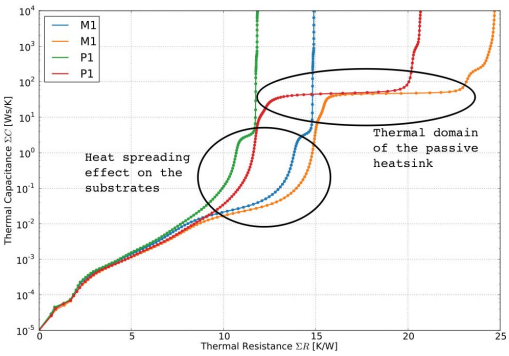

Fig. 8. Structure functions of the MCPCB sample M1 and IAMS sample P1 with active (IAMS green, MCPCB blue) and passive (IAMS red, MCPCB orange) cooling.

Some lengthening of the structure function curves of passive measurements on the substrate region can be seen. Also an increase of thermal resistance in the region of the heat sink is identified.

There was some variation in the soldering quality between the samples. All the test substrate types had samples with good soldering and samples with bad soldering with large voids. The soldering quality did not cause a large effect on the test results although a slight correlation between larger voids and increased LED temperatures was noticed for the IAMS polymer modules. The measurement procedure was proven and repeatable. Three test substrates (P7, C3, and M1) were measured twice and the maximum difference between two measurements of total thermal resistance and temperature changes were less than 0.5 K/W and less than 1.1 °C. The amount of thermal paste and pressure between the substrate and cooling can cause errors as the thermal paste was applied with a syringe, and the attachment was done with screws by hand. Thus, the amount of paste and pressure was not well controlled. However, this affects total thermal resistances only slightly.

One factor causing uncertainty on the measurements of the structure function is the multidimensionality of the heat flow. T3Ster system principle of measurement is based on the assumption of 1-D heat flow path. With active cooling the heat flow is essentially 1-D as the heat flows directly through the substrate. However with passive cooling the sideward heat spreading within the substrate, a 2-D effect, is stronger. This causes slight changes in the structure function in the substrate area of the curve as illustrated in Fig. 8. Also different measurement times in passive and active cooling cases might influence the structure function shapes.

Another factor is that convection and radiation are causing adjacent heat flow paths. In this paper, the temperatures were so low that the effect of convection and radiation is negligible. Simulations indicate that the radiation and convection losses at the substrate only amount to 1% of the total heat dissipation. To eliminate convection the measurement could be performed in vacuum as in [12].

C. Luminous Flux Measurements

The average luminous flux of the IAMS polymer and ceramic modules was 680 lm with a σ of 23 lm and 657 lm with a σ of 22 lm, respectively. As the LED temperatures are higher on the MCPCB boards there should be less light emitted than on the IAMS substrates because LED efficacy decreases as the junction temperature increases [23]. However, this was not discovered as the average luminous flux of the MCPCB modules was 681 lm with a σ of 29 lm. The results could be explained by the fact that as the LED temperatures were so low on both the IAMS and MCPCB substrates, the relatively small difference of 8.1 °C and 6.9 °C on average between the substrates is not visible in the luminous flux results. Horng *et al.* reported similar notion in their study [15]. Also, performance variations between LEDs are fairly large and could shadow the results. The range of the luminous flux of the LED bin used is around 30 lm at 700 mA [20]. In addition, it is believed that substrate color affects the luminous flux measurements performed in the integrating sphere, as the white substrates (IAMS polymer and MCPCB) outperformed the darker colored IAMS ceramic. The LED module with white substrate delivers more light than the module with darker substrate due to absorption losses.

V. Conclusion

This paper reported excellent thermal performance of IAMS substrates. More than 7 °C reduction in the LED junction temperature at 700 mA drive current and 27% reduction in the total thermal resistance from the LED junction to the bottom of the substrate were demonstrated for the IAMS technology when compared with MCPCB. When considering only the thermal resistance of the substrate, the advantage was even more prominent, and reductions of 70% and 50% were illustrated. The superior performance of the IAMS substrates is due to the use of thermal via underneath the LEDs. IAMS technology enables purely inorganic substrates. Consequently, there is a huge potential for the reliable packaging of LEDs as well as other high-power devices. In future, authors will concentrate on the development and characterization of the environmental reliability of the IAMS technology.

Acknowledgment

The authors would like to thank J. Ollila, A. Weissenfelt, R. Karjalainen, and M. Heikkinen, for all the help and valuable work they did for the preparation of the test structures.

References

[1] M.-H. Chang, D. Das, P. V. Varde, and M. Pecht, "Light emitting diodes reliability review," *Microelectron. Rel.*, vol. 52, no. 5, pp. 762–782, May 2012.

[2] X. Shao, Y. Cai, H. Li, and M. Wu, "Research of heat dissipation of RGB-LED backlighting system on LCD," in *Proc. 7th IEEE Int. Conf. Ind. Inf.*, Jun. 2009, pp. 807–812.

[3] M.-H. Lee, T. J. Lee, H. J. Lee, and Y.-J. Kim, "Design and fabrication of metal PCB based on the patterned anodizing for improving thermal dissipation of LED lighting," in *Proc. Microsyst. Packag. Conf.*, 2010, pp. 1–4.

[4] Y.-W. Kim, J.-P. Kim, J.-B. Kim, M.-S. Kim, J.-M. Sim, S.-B. Song, and N. Hwang, "Thermal analysis of a package substrate with filling via-holes for COB LED manufacturing," *J. Korean Phys. Soc.*, vol. 54. no. 5, pp. 1873–1878, May 2009.
[5] *Reliability and Lifetime of LEDs*, OSRAM, Wan Chai, Hong Kong, Jul. 2008.
[6] *Evaluating the Lifetime Behavior of LED Systems*, Philips Lumileds, San Jose, CA, 2010.
[7] *LED Reliability*, Cree, Durham, NC, 2007.
[8] X. Jordá, X. Perpiñá, M. Vellvehi, and J. Coleto, "Power-substrate static thermal characterization based on a test chip," *IEEE Trans. Device Mater. Rel.*, vol. 8, no. 4, pp. 671–679, Dec. 2008.
[9] S. Di Pascolia, P. E. Bagnolia, and C. Casarosab, "Thermal analysis of insulated metal substrates for automotive electronic assemblies," *Microelectron. J.*, vol. 30, no. 11, pp. 1129–1135, 1999.
[10] C. V. Godbold, V. A. Sankaran, and J. L. Hudgins, "Thermal analysis of high-power modules," *IEEE Trans. Power Electron.*, vol. 12, no. 1, pp. 3–11, Jan. 1997.
[11] J. D. Holmes, D. A. Stone, and M. P. Foster, "Effect of inter-layer interface quality on electrical and thermal characteristics of IMS," in *Proc. 5th IET Int. Conf. Power Electron., Mach. Drives*, 2010, pp. 1–4.
[12] G. Liu, Y. Shi, Y. Z. Tao, and S. Cao, "Measurement and significance of the effective thermal conductivity of the dielectric in an IMS," in *Proc. Microsyst. Packag. Assembly Circuits Technol. Conf.*, Taipei, Taiwan, Oct. 2010, p. 1–4.
[13] H. M. Cho and H. J. Kim, "Metal-core printed circuit board with alumina layer by aerosol deposition process," *IEEE Electron Device Lett.*, vol. 29, no. 9, pp. 991–993, Sep. 2008.
[14] S. Asai, M. Funaki, H. Sawa, and K. Kat, "Fabrication of an insulated metal substrate (IMS), having an insulating layer with a high dielectric constant," *IEEE Trans. Comp., Hybrids, Manuf. Technol.*, vol. 16, no. 5, pp. 499–504, Aug. 1993.
[15] R.-H. Horng, J.-S. Hong, Y.-L. Tsai, D.-S. Wuu, C.-M. Chen, and C.-J. Chen, "Optimized thermal management from a chip to a heat sink for high-power GaN-based light-emitting diodes," *IEEE Trans. Electron Devices*, vol. 57, no. 9, pp. 2203–2207, Sep. 2010.
[16] J. K. Park, Y. K. Lee, S. H. Choi, S. H. Shin, and M. S. Choi, "Formation of through aluminum via for noble metal PCB and packaging substrate," in *Proc. Electron. Comp. Technol. Conf.*, Jun. 2011, pp. 1787–1790.
[17] D. Mu and Y. Jin, "Study of anodized Al substrate for electronic packaging," *J. Mater. Sci., Mater. Electron.*, vol. 11, no. 3, pp. 239–242, 2000.
[18] L. Ha, G. Matijasevic, P. Gandhi, and C. Gallagher, "Thermal study of additive multilayer circuitry on polymer and metal substrates," in *Proc. 14th IEEE SEMI-THERMTM Symp.*, 1998, pp. 104–110.
[19] A. LaFond, "Thick-film technology with aluminum substrates optimizes LED assembly," *LEDs Mag.*, p. 55, Jul.–Aug. 2011.
[20] *LUXEON Rebel General Purpose Datasheet DS64*, Philips Lumileds, San Jose, CA, 2010.
[21] *T3Ster Thermal Transient Tester Technical Information*, Mentor Graphics Corporation, Wilsonville, OR, 2011.
[22] *Technical Guide: Integrating Sphere Radiometry and Photometry*, Labsphere Inc., North Sutton, NH, 2006.
[23] B. E. A. Saleh and M. C. Teich, *Fundamentals of Photonics* (Pure and Applied Optics). New York: Wiley, 1991.

Eveliina Juntunen received the M.Sc.(tech.) degree in electrical engineering from the University of Oulu, Oulu, Finland, in 2004.

Since 2004, she has been with the VTT Technical Research Centre of Finland, Oulu, where she is currently a Research Scientist with the Lighting and Integration Solutions Team. Since 2007, she has been involved in research on the topics listed below from an LED lighting point of view. Her current research interests include reliability of electronics packaging including thermal management and environmental testing.

Aila Sitomaniemi received the M.Sc. degree in physics from the University of Oulu, Oulu, Finland, in 2001.

Since 1998, she has been with the VTT Technical Research Centre of Finland, Oulu, where she has researched computer networks. Since 2006, she has been involved in research on optics-related electronic modules, at first concentrating on optical simulations on LED lighting. Her current research interests include thermal management in electronics, including thermal design, simulation, and characterization.

Olli Tapaninen received the B.Sc. degree in physics from the University of Oulu, Oulu, Finland, in 2010. He is currently pursuing the M.Sc. degree with the VTT Technical Research Centre of Finland, Oulu.

Since 2011, he has been with the VTT Technical Research Centre of Finland as a Research Trainee researching LED lighting. He was previously with Sodankylä Geophysical Observatory, Oulu, as a Research Assistant involved in research on space physics. His current research interests include thermal transient measurements and thermal analysis of high-power LED packages and systems.

Ryan Persons is a Technology Service Engineer with the Thick Film Division, Heraeus Materials Technology, LLC (Heraeus). He is the primary contact for the Insulated Aluminum Material System (IAMS) and involved in research on IAMS product development and testing. He has been with Heraeus since September 2009.

Mark Challingsworth is the Technology Manager with the Thick Film Division, Heraeus Materials Technology, LLC (Heraeus), where he has been since 2009. His group is involved in research on developing and providing the technical service for all the thick-film materials produced by Heraeus. His current research interests include development of materials for thermal management, RoHS compliant materials, and any use for thick-film technology in alternative technology areas.

Veli Heikkinen received the M.Sc.(tech.), Lic.es Sci., and D.Sc.(tech.) degrees in electrical engineering from the University of Oulu, Oulu, Finland, in 1986, 1999, and 2004.

He is a Senior Scientist with the VTT Technical Research Centre of Finland, Oulu. His current research interests include the optoelectronic module integration.

PUBLICATION IV

A smart LED luminaire for energy savings in pedestrian road lighting

In: Lighting Research and Technology,
7 November 2013, pp. 1–13.

Lighting Research and Technology
http://lrt.sagepub.com/

A smart LED luminaire for energy savings in pedestrian road lighting

E. Juntunen, E. Tetri, O. Tapaninen, S. Yrjänä, V. Kondratyev, A. Sitomaniemi, H. Siirtola, E.M. Sarjanoja, J. Aikio and V. Heikkinen

Lighting Research and Technology published online 7 November 2013
DOI: 10.1177/1477153513510015

The online version of this article can be found at:
http://lrt.sagepub.com/content/early/2013/11/06/1477153513510015

Published by:
SAGE
http://www.sagepublications.com

On behalf of:
The Society of Light and Lighting

Lighting Res. Technol. 2013; **0**: 1–13

A smart LED luminaire for energy savings in pedestrian road lighting

E Juntunen MSc[a], **E Tetri** DSc[b], **O Tapaninen** MSc[a], **S Yrjänä** MSc[a], **V Kondratyev** PhD[a], **A Sitomaniemi** MSc[a], **H Siirtola** MSc[a], **EM Sarjanoja** MSc[a], **J Aikio** PhD[a] and **V Heikkinen** DSc[a]
[a]VTT Technical Research Centre of Finland, Oulu, Finland
[b]Lighting Unit, Aalto University, Espoo, Finland

Received 2 July 2013; Revised 18 September 2013; Accepted 1 October 2013

In this paper, an energy efficient streetlight for pedestrian roads is introduced. Energy efficiency is achieved via up-to-date light-emitting diode (LED) technology and added intelligence utilising integrated sensors and wireless control. Thermal and electrical design of the luminaire contributed to good technical functionality. The performance of the luminaire was validated with testing. The luminaire was compared with commercial lamp and LED-based street lighting technology by technical values and user acceptance. Energy savings of 19–44% through improved luminous efficacy was demonstrated without added intelligence. With smart control further power saving potential of 40–60% was shown depending on the lighting environment and pedestrian presence. User feedback of a pilot installation comparing commercial luminaires with the newly developed streetlight revealed that on average the users preferred the developed streetlight over the commercial luminaires.

1. Introduction

Traditionally, light sources based on high pressure sodium (HPS), low pressure sodium (LPS) and metal halide (MH) lamps are used in street lighting due to their high luminous efficacy (80 lm/W–180 lm/W) and long lifetime even up to 60 000 hours for HPS with electronic ballasts. With HPS lamps the colour temperature and the colour rendering index (CRI) are low, but considerably higher with MH solutions.[1,2] Higher values are appreciated for the natural appearance of the environment whereas the yellow light of HPS lamps is favoured due to suitability for human circadian rhythms.[3,4] Still, due to the desire for greater energy savings in lighting and the rapid development of light-emitting diode (LED) technology, solid-state lighting (SSL) solutions are conquering the lighting world. Among other benefits, such as energy efficiency, long lifetime, small size and lack of low temperature start-up problems, easy control of the LEDs is appreciated, because it provides new features and energy saving possibilities via added intelligence.[5,6]

Currently energy savings in lighting are achieved via the switch from traditional light sources to more efficient ones such as LEDs.[7,8] Still, smart control is required to achieve the green targets set by many countries.[8,9] For example, up to 70% saving potential is predicted for advanced luminaires and control systems when compared with old technology. This is far more than the savings achieved by just changing light sources.[7,10] With smart control the savings potential is

Address for correspondence: E Juntunen, VTT Technical Research Centre of Finland, Kaitoväylä 1, 90571 Oulu, Finland.
E-mail: eveliina.juntunen@vtt.fi

10.1177/1477153513510015

significant as lighting covers about 19% worldwide, and 14% in the EU of all electricity consumption.[11,12]

In the past, most street lighting was controlled by a clock. Due to interest in energy savings, today, the most common control system is based on a photoelectric cell that detects the amount of daylight and adjusts the operating time according to natural light levels.[13] Still, the intelligence level of current street lighting is typically low because the daylight switches that control the street lighting schedule are not capable of controlling the light levels. In the past, active control was not feasible due to difficulty in dimming the light sources.[13] However, with the current LED revolution these features are becoming reality.

Advanced control with presence and light level sensing is more widespread in indoor applications with considerable energy savings of 40–65% having been demonstrated.[8,10,14] A review of 240 saving estimates from 88 papers and case studies in commercial buildings by Williams *et al.*[9] revealed that the average lighting energy saving potential was up to 38% with advanced control. Unfortunately smart solutions are sometimes disliked due to inadequate performance of the sensors.[8,10,15] For energy saving reasons the sensing techniques are under constant development and more and more sophisticated solutions are coming to the market with decreased costs.

The aim of this paper is to demonstrate energy savings in street lighting with advanced LED lighting technology without sacrificing end-user comfort. The target was set to use a pilot installation with commercial luminaires as a starting point to improve technical performance, as well as user acceptance. As a result, an energy efficient streetlight designed for pedestrian roads is introduced. The luminaire utilises smart control with integrated sensors and wireless communication for energy saving. The performance of the luminaire is validated with versatile testing. Technical values and end-user acceptance are compared with commercial street lighting technology of a reference pilot installation.

2. Background

The development of the streetlight was based on a pilot installation made with commercial luminaires on a pedestrian road in an outdoor recreation area in Helsinki in 2011. The pilot installation included HPS luminaires, MH luminaires and three different types of LED luminaires, indicated as LED1, LED2 and LED3. Four luminaires of each type were installed making 20 luminaires in total. Prior to installation the electrical and luminous characteristics of the luminaires were measured in the laboratory (Table 1). Also, the luminous intensity distribution curves were measured using a goniophotometer. The electrical powers of the luminaires were between 34 W and 66 W and the luminous efficacies were between 54 lm/W and 78 lm/W. The correlated colour temperature (CCT) varied from 1880 K to 4230 K. These luminaires represented the commercial technical status in 2011. At the installation site the illumination conditions including horizontal and semi-cylindrical illuminances were measured to find out the lighting conditions on the test road and the lighting was judged by the users. A user survey was carried out by 46 people using a questionnaire. People evaluated four statements ('There is enough light', 'The tone of the light is pleasant', 'The illumination is not glaring' and 'There is enough light on the verge of the road') with a five-point scale, where one means that the statement was totally disagreed and five that it was totally agreed. In addition, they gave an overall evaluation of the installation with a grade from 4 to 10, this rating being the same as school grade ratings in Finland.

The mean illuminances were between 10.5 lx and 17 lx and this was enough for

Table 1 Laboratory results of the pilot installation luminaires. The values in the table are calculated averages of four measured luminaires of each type. The luminaires represent the technical status in 2011, except for the Ath luminaire that was made in 2012

Luminaire	Power (W)	Power factor	Luminous flux (lm)	Efficacy (lm/W)	Colour temperature (K)	CRI (Ra)
LED1	38.4	0.92	2950	77	4220	68
LED2	38.5	0.92	2070	54	2960	84
LED3	33.8	0.94	2650	78	3980	69
HPS	66.4	0.93	3570	54	1880	23
MH	63.9	0.93	3770	59	3300	72
Ath	30.5	0.90	2940	96	4610	82

most of the respondents. The tone of the light was a somewhat controversial subject. Some people evaluated even the HPS with the highest grade, but the highest mean grade was given to the MH installation with its CCT being 3300 K. MH got the highest ratings also with the statement 'There is enough light on the verge of the road'. LED1 caused glare and got the lowest overall grade. The user evaluation is discussed more in detail by Paakkinen *et al.*[16] To conclude, the results showed that the spatial distribution of the luminous flux of the luminaire should be designed to give enough light on the verge of the road and to avoid glare. The design of the new luminaire adopted best practices learned from the user survey.

3. Smart streetlight design and performance

The smart luminaire for pedestrian roads developed for this study is illustrated in Figure 1. The luminaire consists of aluminium tubes modified to house the LEDs, optics and the control electronics. Four luminaires were installed on a pedestrian road in Helsinki where they were operated as normal streetlights. Integrated sensors and two-way wireless communication was utilised to deliver different lighting modes. The smart luminaire also recorded data of its functions. The recorded data included ambient temperature, LED board temperature, light reflected from the road, direct light from the LEDs, pedestrian presence sensor activations and most importantly energy consumption. These data were delivered to a web page also performing as a user interface for remote control of the pilot installation.

Figure 1 The smart LED luminaire for pedestrian road lighting (Ath)

Three different lighting modes were studied:

1) In the passive use mode, the smart luminaires were controlled as if they were

standard streetlights with no added intelligence. This mode was used as the reference point for technical performance and end-user acceptance relative to the original pilot installation constituting commercial street luminaires.

2) The light level sensing mode utilised light sensors to keep the light levels on the ground stable regardless of the changes in the ambient circumstances. Some energy savings was assumed during sunrise and sunset, but the main objective here was to study the difference between energy consumption in summer and winter, as the amount of reflected light is totally different due to snow in Finland.

3) The aim of the pedestrian sensing mode was to study the energy saving potential of dimming the street lighting levels at the quiet times of the night. The luminaires were dimmed down by reducing the current 50% and raised back to the state used in passive use mode when an approaching pedestrian was detected. In the passive use mode the power consumption was 30.5 W, and when dimmed it was reduced to 17.1 W.

All the luminaires were measured in the laboratory before assembling them on the pedestrian road. Four of each luminaire types were measured and the average values are listed in Table 1. The luminous efficacy of the commercial luminaires was 54 lm/W–78 lm/W while the luminaire developed in this study (Ath) achieved 96 lm/W. Thus, an energy saving of 19–44% through improved luminous efficacy was achieved in comparison with commercial luminaires. The commercial luminaires represent the technical status in 2011 while the developed streetlight was manufactured in 2012. Thus, in comparison with the LED luminaires, the streetlight has benefitted from the quick development of LED technology. The LED component used in the streetlight was a Cree XM-L[17] (240 lm @ 700 mA, Tjunction = 25°C) with a rather cool CCT (4600 K) but high CRI value (82). The CCT selected was based on the user survey made with the commercial luminaires. As only mild preference to warm CCTs was discovered,[16] a neutral CCT was chosen for the luminaire to reach higher energy efficiency.[17] In addition, this choice might have a positive effect on the feeling of safety because cooler CCTs appear brighter in dark environments.[13] Light pollution or photobiological issues related to blue-rich spectrum were not considered. The high CRI was selected to achieve the true colours of nature (grass, snow) for a pleasant and inviting scene at the pilot installation that took place in an outdoor recreation area.

3.1 Thermal management

The objective of the thermal management study was to guarantee acceptable LED temperatures for stable and efficient performance of the luminaire since with lower junction temperature the LEDs will perform longer, brighter and with higher efficacy.[17,18] Thermal structure of the luminaire was studied with a thermal transient tester (T3Ster®, Mentor Graphics Corp.). The T3Ster records the junction temperature of the LED as a function of time and calculates the thermal transient response of the structure.[19] From this response the cumulative structure function illustrated in Figure 2 is processed.[20,21] The structure function describes the thermal path from the LED junction through the luminaire chassis to the surrounding environment. The structure function can be used to identify physical parts of the luminaire and to compare the contribution of those parts by the overall thermal resistance.

The thermal performance of the luminaire was measured in an air-conditioned laboratory room where the ambient temperature was around 23°C. The luminaire was driven by a constant 720 mA drive current for 3.5 hours delivering 4000 lm. Once the structure

was thermally stable, the drive current was switched to a 20 mA sensor current and the voltage change of the LEDs was recorded for 3.5 hours while the luminaire cooled down back to ambient temperature. The measured maximum LED junction temperature was 40.4°C. As shown in Figure 2, the thermal resistance of the convection from the chassis to the environment is about 0.7 K/W which is larger than the total resistance of the other parts of the luminaire combined.

Steady-state thermal simulations were used to analyse the temperatures in the worst-case scenario that was still air and 35°C ambient temperature. Simulations were made with three-dimensional computational fluid dynamics software (FloTHERM®, Mentor Graphics Corp. Wilsonville, Oregon, USA) and conduction, convection and radiation heat transfers were included. An average LED temperature of 66°C (Figure 3) was found for the luminaire in the worst-case scenario ambient, which is well below the 135°C maximum temperature of the LED component.[17] Simulated temperatures are shown in Figure 3 illustrating a cross-section of the luminaire. The simulated model imitated the luminaire structure and was checked by comparing the results with measurements. Good agreement was found as the average simulated LED temperature in 23°C ambient was 39.6°C, that is, only 0.8°C different from the measured temperature. In conclusion, regardless of the ambient environment, the thermal management succeeded in maintaining LED temperatures low enough for high efficacy and reliable performance of the LED components.

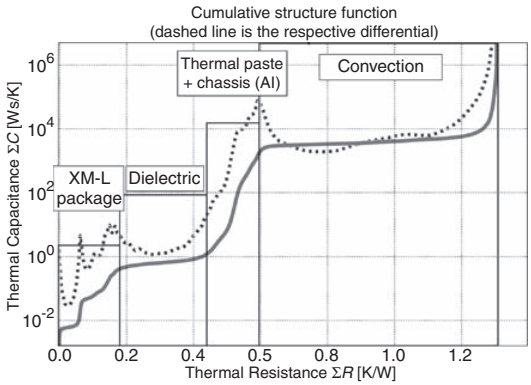

Figure 2 Cumulative (solid line) and differential (dashed line) structure function of the luminaire. Physical parts of the luminaire are identified in boxes

3.2 Optics

The luminaire consisted of 18 LEDs each fitted with a freeform optical lens. The LEDs

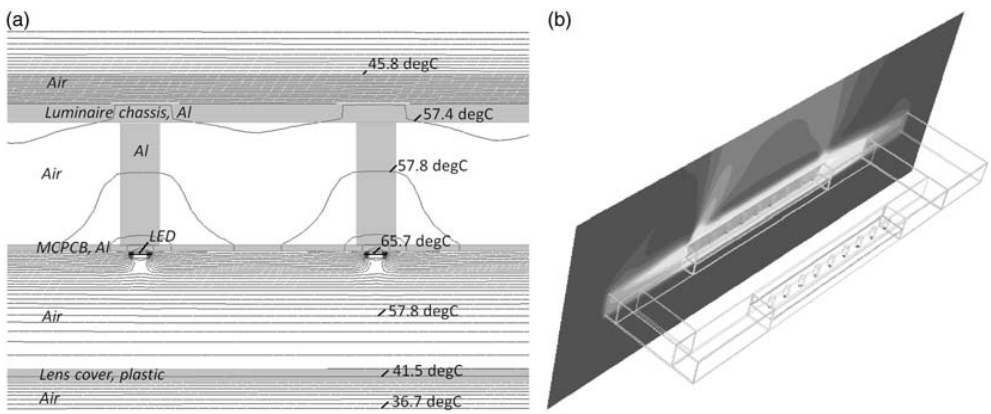

Figure 3 Simulated cross-section of the luminaire in still air in the 35°C worst-case scenario

were placed in two arrays, nine LEDs each, along the tube structure of the luminaire. The luminaires were installed into existing poles with 5 m height, 30 m apart and tilted by 20° to aim the maximum amount of luminous flux at the centre of the road. The illumination was designed according to S3 standard[22] requirements for Finnish pedestrian roads and the light distribution was based on gained experience from the pilot installation with commercial luminaires. Especially for user acceptance, the light distribution was spread over the verge of the road so that the neighbouring areas would be illuminated partly as well. To avoid glare the luminous flux was limited mostly to gamma angles less than 75°. Also the average illuminating area was large as the LEDs were spread along the tube structure with 60 mm pitch, creating the sensation of a large area emitter. The lens was manufactured by glass moulding and the resulting luminous intensity distribution is compared with the design in Figure 4. The small differences between the design and the realisation are due to larger thickness of the moulded lens.

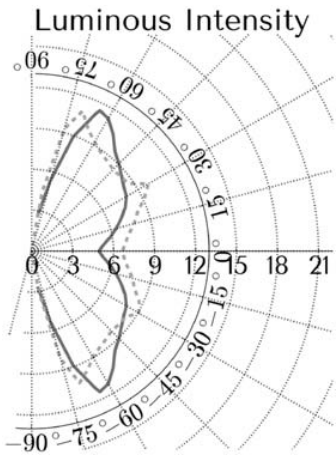

Figure 4 Simulated luminous intensity distribution curve of the lens design (solid line) compared with the measured luminous intensity distribution of the lens (dashed line)

3.3 Control and communication

A system of integrated sensors and low energy two-way wireless communication was utilised to enable intelligent control of the LED driving power electronics. The aim of the smart control development was to implement the functionality needed for the study. A robust field PC equipped with wireless communication capabilities was placed in range of the luminaires to record the sensor data and to control the luminaire functions. Communication between the luminaires and the field PC used 868/915 MHz frequencies and the range was measured to be over 100 m, which was enough for this study. To keep the system simple all communication ran through the PC and no luminaire to luminaire communication was implemented. Mostly the communication was initialised by the PC that asked for the sensor values periodically from the luminaires and gave control values to adjust their light output. Only when the presence of pedestrians was detected did the luminaire initialise communication. The field PC was connected to the internet through a wireless modem so that control and sensor data analysis could be done remotely. Typical state-of-art commercial smart road lighting systems follow a centralised architecture with a central terminal and a number of local branch nodes communicating with the luminaires. The central terminal is responsible for commanding the luminaires and monitoring the status of the system. Local branch nodes act as a link between the central terminal and the smart luminaires. Typically, there is a long-distance communication (GPRS, Internet) between the branch node and the server and shorter distance transmission (RF, ZigBee) from the local nodes to the luminaires.[23] The designed system resembles state-of-the-art road lighting systems described by Atici *et al.*[23] with the exception that the field PC was acting both as a local branch node and as the control terminal.

An evaluation board (Texas Instruments CC1110EMK868-915, Dallas, Texas, USA) with a microcontroller and an integrated low power RF-transceiver was chosen as the luminaire end controller. The controller was responsible for reading sensor values, adjusting LED current via a digital potentiometer and sending and receiving data to and from the field PC equipped with a USB radio module. Energy consumption measurement of the combined power and control parts was done with a Teridian Semiconductor Corporation evaluation board (78M6612-EVM-1, San Jose, CA, USA). A passive infrared (PIR) sensor (Panasonic AMN33111J, Kadoma, Osaka, Japan) was used to detect movement of the pedestrians under the 5 m high lighting pole. The sensor reacted to the sudden changes in temperature caused by a person passing by a given point in the field of view of the sensor. Because the PIR sensor was installed up in the lighting poles and aimed directly towards the road the distance of detection was around 5 m. Luminaire light output was monitored with two ambient light level sensors. A direct light sensor (Intersil, ISL29020, Milpitas, California, USA) was mounted on the LED PCB to monitor changes in luminaire light output and a reflected light sensor (Intersil, ISL29033, Milpitas, California, USA) was aimed at the illuminated area to detect reflected light from the ground. A temperature sensor (Texas Instruments, TMP100, Dallas, Texas, USA) mounted on the LED PCB monitored the changes in temperature.

All of the 18 LEDs in the luminaire were connected in series to guarantee identical LED currents and to maximise the efficiency of the LED driver. A dimmable LED driver (Philips Xitanium 75 W 0.70 A, Amsterdam, Netherlands) with high efficiency was chosen to utilise dimming of the luminaires for energy savings. The effect of dimming on the luminous efficacy of the luminaire was recorded and is illustrated in Figure 5. It can be seen that the luminaire can be dimmed to half of the maximum power without losing the ~95 lm/W luminous efficacy. The measured luminous efficacy is a product of changes in LED luminous efficacy and driver electronics efficiency. Rather constant LED efficacy can be expected because of the low (40.4°C) junction temperatures measured even in the full power conditions.[17] Only the minor drop in luminous

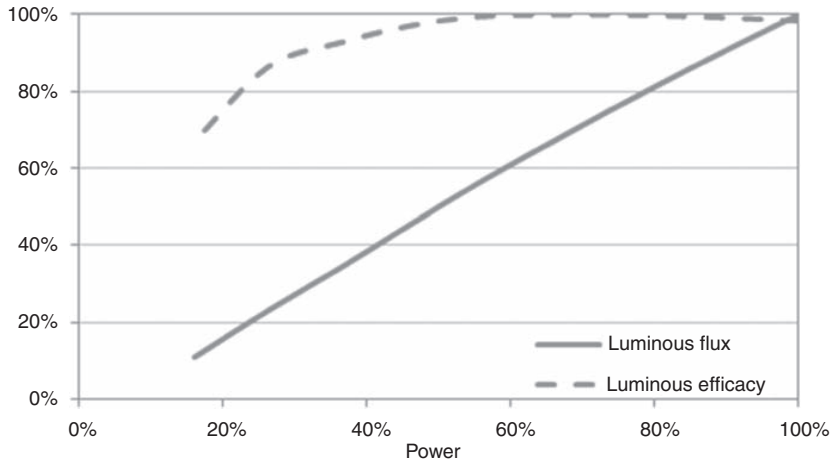

Figure 5 Dimming curve of the luminaire. The 100% luminous flux of the luminaire is 4000 lm with 93 lm/W luminous efficacy

efficacy at the end of the curve (Figure 5) is assumed to be caused by the LED efficacy. The efficiency of the driver decreases significantly when dimmed. This is the main cause for drop of luminous efficacy at low power levels.

4. User feedback

The developed luminaires were installed on the pilot installation site on a pedestrian road in Helsinki and the user survey was repeated with the same procedure described earlier. The survey took place in February 2013 in the evening time after the streetlights had been turned on. Pedestrians passing by were asked to walk along the road at the pilot installation site and evaluate the lighting by filling in a questionnaire of four statements and a question on the overall grade. They were asked to fill in the questionnaire, when they were between the second and third poles. After the test they were rewarded with a movie ticket worth about 8 euro. The survey received 23 answers. The proportions of different age groups among participants were <20 years, 4%; 21–30 years, 17%; 31–40 years, 48%; 41–50 years, 9% and 51–60 years, 17% and >60 years, 4%. Forty-eight per cent of participants were female and 52% male, 57% wore glasses and 43% did not. Luminaires were operated in the passive use mode as if they were standard streetlights with no added intelligence for reasonable comparison with the original pilot installation constituting commercial street luminaires.

In the second survey luminaires, LED1, LED3, MH and the developed luminaire (Ath) were included. Answers to the statements are given in Figure 6. The developed Ath installation got the best overall grade with the mean of 8.2. LED3 and MH received 8.0 and LED1 7.7. The Ath installation also got the highest mean for statements S1 ('There is enough light') and S4 ('There is enough light on the verge of the road'). In statement S3 ('The illumination is not glaring'), the Ath installation shared the highest mean with the LED3 installation. For the statement S2 ('The tone of the light is

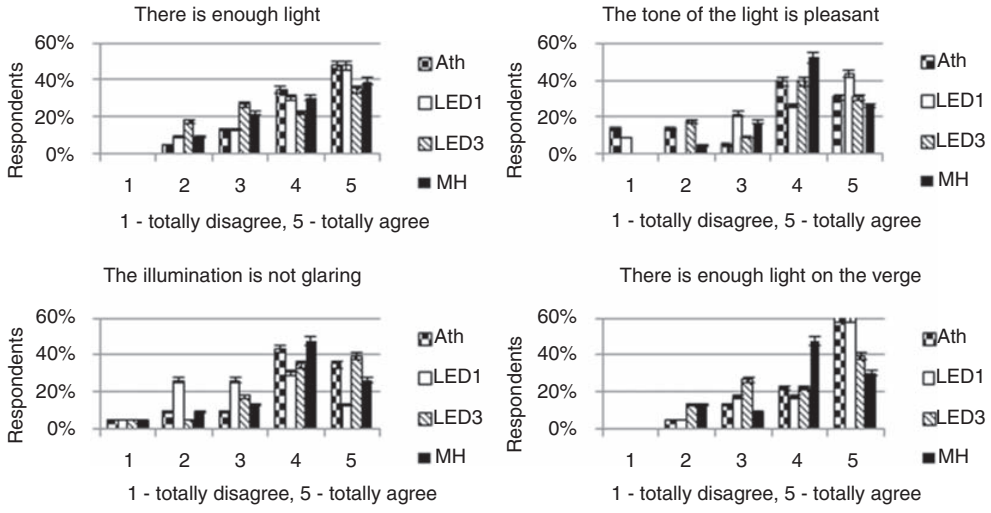

Figure 6 Distributions of the ratings given for the statements with 95% confidence intervals

pleasant'), users gave the lowest rating to the Ath installation. The CIE CCTs for the Ath, LED1, LED3 and MH luminaires were 4610 K, 4220 K, 3980 K and 3300 K, respectively. If we consider ratings 4 and 5 as positive, the proportion of positive ratings for the Ath luminaire was 83% for statement S1, 70% for S2, 78% for S3 and 83% for S4. Even if the people evaluating the statement considered the colour of the light lower for the Ath luminaire than for the other luminaires, still the majority (70%) had a positive attitude to the colour of its light.

Based on the original pilot installation with commercial luminaires it was concluded that when designing a streetlight that will be well accepted by pedestrians the spatial distribution of the luminous flux should give enough light on the verge of the road and avoid glare. This strategy was proven successful as the developed luminaire gained the highest overall score in the second user feedback survey even though the cool tone of the light was not appreciated. Regarding the statement 'The tone of the light is pleasant', in both surveys users gave the lowest rating for the luminaire with the highest CCT. However, there were big differences in the luminaires and consequently many variables affecting the opinions of the respondents. In future, different properties can be examined separately so that user acceptance is more limited to certain properties, such as the tone of the light.

5. Energy savings with added intelligence

5.1 Light level sensing

Reflected light from the ground was recorded to study the possibility to utilise changes in luminance of the surroundings for energy savings in street lighting. This is of particular interest in Nordic countries where wintertime is long and dark but snowy. The light level sensing mode was realised by equipping a light sensor with the same optics as the LEDs. Thus, the monitored area coincided with the illuminated area. The data were recorded with fresh snow (March), inter-season (April) and with no snow (May). Major changes in the lighting environment were discovered as the reflected light sensor value of 6.5 in the winter decreased to around 1 with the melting snow as shown in Figure 7.

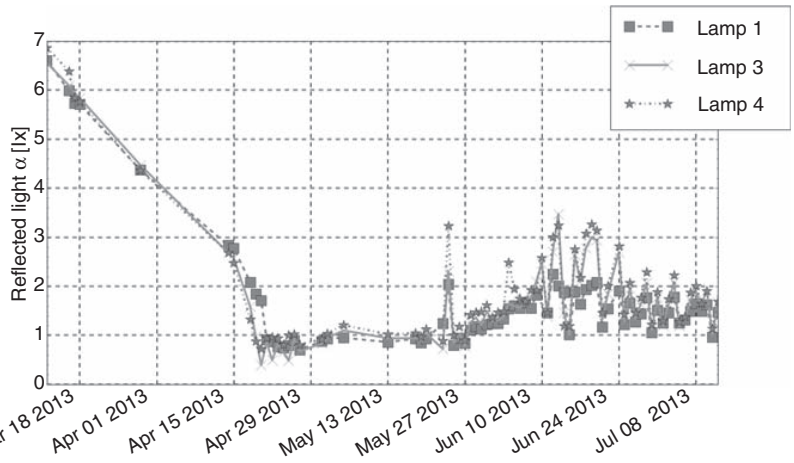

Figure 7 Daily median reflected light during melting of the snow. Luminaires were operated in the passive use mode

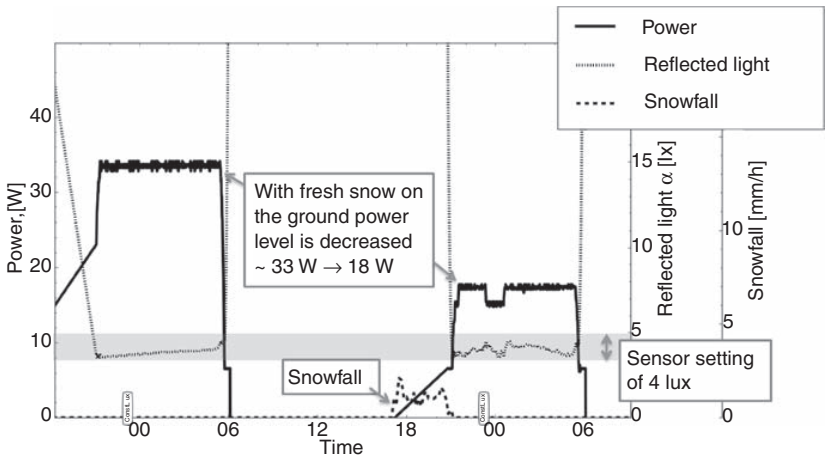

Figure 8 Power demand of the luminaire decreased after snowfall when reflectivity of the surroundings was enhanced

As illustrated in Figure 8, approximately 45% less power could be used with fresh snow when compared with no snow on the road while maintaining the same reflected light value. In Helsinki, Finland the average snow season (1981–2010) was approximately 3 months while in Sodankylä, Lapland the snow stayed for 7.5 months.[24] This could mean significant energy savings in street lighting. For example, the City of Helsinki has 85 000 streetlights that consume 54,000 MWh energy annually. The example shown in Figure 8 would realise estimated annual savings of 7,900 MWh and 0.8 M€ without losing the required light levels if the light sensing were to be generally utilised.

Figure 9 demonstrates the energy saving potential of light level sensing at sunrise and sunset. The light level sensor detects the increase in natural light and the system controls the luminaire to lower the power until the specified minimum level is reached. Finally, the luminaire is turned off by the central control in Helsinki area. Figure 9 shows that due to sunrise the electrical power is gradually decreased to 37% for about 30 minutes before it is turned off. If compared with passive use, the median energy savings

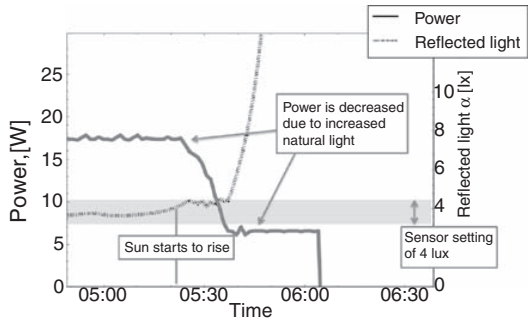

Figure 9 Power can be decreased in the morning during the natural light increase

for 16 days was 28 Wh/day/luminaire when light level sensing was utilised at different sensor settings. These results suggest that instead of the widely used central control more sophisticated solutions could generate major energy savings worldwide.

5.2 Pedestrian sensing

The energy saving potential of dimming the streetlight levels at the quiet times of the night was studied by operating luminaires in the pedestrian sensing mode. For comfort and safety reasons the lighting cannot be totally

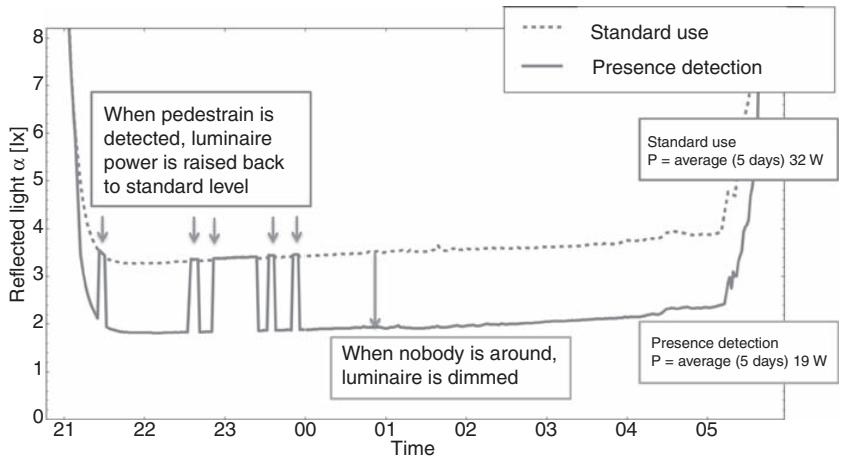

Figure 10 Detected light level and average electrical power of luminaires with pedestrian sensing mode in comparison with passive use mode

turned off although that would pose the biggest energy savings. Here, the luminaires were dimmed down to 50% drive current and raised back to passive use mode when an approaching pedestrian was detected. The set-up utilised PIR sensors integrated into the luminaires. Via wireless communication other luminaires were informed in the case of detection. The system was constituted so that the pedestrian would not notice a change in light level of the luminaire closest to him. Instead the light level increased to the normal light level ahead of the pedestrian and dimmed down 5 minutes after the last PIR detection. The same kind of scenario was found pleasant by Haans and de Kort.[25] and Viliûnas *et al.*[26] according to which pedestrians prefer having light in their immediate surroundings while light levels further away are less important. An example showing the pedestrian sensing function is illustrated in Figure 10 where the pedestrian sensing mode is compared with the passive use mode. These results were recorded in March 2013 when the lighting was turned on after 9 p.m. Consequently, only a few pedestrians appeared and all of them prior to midnight. During a five-day test period of pedestrian sensing, the luminaries operated on average at 40% lower power than in the passive use mode.

The saving potential depends on the time delay used for dimming.[10,15] A shorter delay would contribute to energy savings but might cause negative user experience due to quicker changes in light level.[8,15] Saving potential is also dependent on the degree of utilisation of the road; the fewer pedestrians, the more energy savings. To conclude, there are always some quiet hours on pedestrian roads that could provide for energy savings by smart street lighting (Figure 10). However, this method should be considered carefully as changes in light levels might affect user experience negatively and could also cause problems with vandalism for instance. Therefore, investigating dimming scenarios and luminance distributions around pedestrians is essential for smart lighting system development and the authors would like to concentrate on that topic in the future.

6. Conclusions

In this paper, an energy efficient streetlight for pedestrian roads is introduced. Energy efficiency is achieved via up-to-date LED technology and added intelligence utilising integrated sensors and wireless control. Thermal, electrical and optical design of the luminaire contributed to good technical functionality. Smart control utilisation of lighting conditions in snowy circumstances demonstrated a 45% electrical power decrease when compared with power consumption when there was no snow on the road while having the same luminance (measured reflected illuminance from the road). This poses major energy saving potential, especially, in Nordic countries with long winters and short daylight times. Energy can also be saved when the streetlight is dimmed adapting its light level to the changing natural light during sunrise and sunset. An example of a 63% power decrease for about 30 minutes during sunrise is shown in this paper.

Adaptive lighting set to respond to the presence of pedestrians was studied and on average an electrical power reduction of 40% was observed. This was achieved by dimming the luminaire down to 50% after 5 minutes delay from the last detection and by raising the light level back when an approaching pedestrian was detected. Although definite saving potential with adaptive lighting was demonstrated, more research is still required as changes in light levels might affect user experience negatively and increase vandalism.

User feedback of the pilot installation comparing commercial luminaires with the developed streetlight revealed that on average the users preferred the developed streetlight over the commercial luminaires. From the results of the original pilot study with the commercial installation the goals were set for the spatial distribution of the luminous flux to give enough light on the verge of the road and to avoid glare. These goals were achieved since 83% of the respondent gave positive feedback to the statement 'There is enough light on the verge of the road' and 78% to statement 'The illumination is not glaring'. The overall grade was also highest with the developed street lighting luminaire.

Funding

This work was supported in part by Tekes, Finnish Funding Agency for Technology and Innovation, and the Infotech Oulu Doctoral Program.

Acknowledgements

The authors would like to thank the entire AthLEDics (1205/31/2010) project group and the following organisations: Alppilux, the City of Helsinki, the City of Jyväskylä, Enerpoint, Ensto Finland, Hella Lighting Finland, Helvar, Herrmans, LumiChip, MTG-Meltron, Oplatek, Sabik, Senate Properties, Valopaa and YIT for their co-operation in the project.

References

1 Fotios S. LRT Digest 1: Maintaining brightness while saving energy in residential roads. *Lighting Research and Technology* 2013; 45: 7–21.
2 Gil-de-Castro A, Moreno-Munoz A, Larsson A, de la Rosa JJG, Bollen MHJ. LED street lighting: a power quality comparison among street light technologies. *Lighting Research and Technology* 2012; 44: 1–19. DOI: 10.1177/1477153512450866.
3 Falchi F, Cinzano P, Elvidge CD, Keith DM, Haim A. Limiting the impact of light pollution on human health, environment and stellar visibility. *Journal of Environmental Management* 2011; 92: 2714–2722.
4 Žukauskas A, Vaicekauskas R, Vitta P. Optimization of solid-state lamps for photobiologically friendly mesopic lighting. *Applied Optics* 2012; 51: 8423–8432.

5 Haitz R, Tsao JY. Solid-state lighting: the case 10 years after and future prospects. *Physica Status Solidi* 2011; 208: 17–29.
6 DiLaura DL, Houser KW, Mistrick RW, Steffy GR. *The Lighting Handbook*, 10th Edition. New York: Illuminating Engineering Society of North America, 2011.
7 Second Strategic Research Agenda of the European Technology Platform. *Lighting the Way Ahead*. Photonics21, 2010: 30. Düsseldorf, Germany: European Technology Platform Photonics21.
8 Dubois MC, Blomsterberg Å. Energy saving potential and strategies for electric lighting in future North European, low energy office buildings: a literature review. *Energy and Buildings* 2011; 43: 2572–2582.
9 Williams A, Atkinson B, Garbesi K, Page E, Rubinstein F. Lighting controls in commercial buildings. *Leukos* 2012; 8: 161–180.
10 Galasiu AD, Newsham GR, Suvagau C, Sander DM. Energy saving lighting control systems for open-plan offices: a field study. *Leukos* 2001; 4: 7–29.
11 International Energy Agency. *Light's Labour's Lost*. OECD Publishing, 2006.
12 European Commission. *Lighting the Future, Accelerating the Deployment of Innovative Lighting Technologies, COM(2011) 889 final*. Retrieved August 21 2012, from http://ec.europa.eu/information_society/digital-agenda/actions/ssl-consultation/docs/com_2011_0889_ssl_green_paper_en.pdf.
13 Boyce PR, Fotios S, Richards M. Road lighting and energy saving. *Lighting Research and Technology* 2009; 41: 245–260.
14 Chiogna M, Mahdavi A. Energy efficiency of alternative lighting control systems. *Lighting Research and Technology* 2012; 44: 397–415.
15 Pigg S, Eilers M, Reed J. *Behavioral aspects of lighting and occupancy sensors in private offices: a case study of a university office building: Proceedings Paper of ACEEE Summer Study*, Panel 8, Paper 18, Asilomar Conference Center Pacific Grove, CA, USA, August 25–31: 1996: 8161–8170.
16 Paakkinen M, Tetri E, Halonen L. User evaluation of pedestrian way lighting. *Light and Engineering*. (in press).
17 Cree® XLamp® XM-L LEDs, Product Family Data Sheet, CLD-DS33 Rev 9A, 2010–2013. Retrieved 25 September 2013, from http://www.cree.com/products/pdf/xlampxm-l.pdf
18 Cree® XLamp® Long-Term Lumen Maintenance, Application Note CLD-AP28 Rev 2, 2008–2013. Retrieved 25 September 2013, from http://www.cree.com/xlamp_app_notes/XRE_lumen_maintenance
19 T3Ster Thermal Transient Tester Technical Information, Mentor Graphics Corporation (2011). Retrieved 25 September 2013, from http://s3.mentor.com/public_documents/datasheet/products/mechanical/products/t3ster-technical-info.pdf.
20 JEDEC Solid State Technology Association. *Implementation of the Electrical Test Method for the Measurement of Real Thermal Resistance and Impedance of Light-Emitting Diodes with Exposed Cooling, JESD51-51. Arlington, VA*, USA: JEDEC Solid State Technology Association, 2012.
21 Szekely V, Van Bien T. Fine structure of heat flow path in semiconductor devices: a measurement and identification method. *Solid-State Electronics* 1988; 31: 1363–1368.
22 European Standard EN 13201-2:2003. Road Lighting – Part 2: Performance Requirements.
23 Atici C, Özcelebi T, Lukkien JJ. Exploring user-centered intelligent road lighting design: a road map and future research directions. *IEEE Transactions on Consumer Electronics* 2011; 57: 788–793.
24 Finish Meteorological Institute web site. Retrieved 2 July 2013, from http://ilmatieteenlaitos.fi/lumitilastot
25 Haans A, de Kort YAW. Light distribution in dynamic street lighting: two experimental studies on its effects on perceived safety, prospect, concealment, and escape. *Journal of Environmental Psychology* 2012; 32: 342–352.
26 Viliûnas V, Vaitkevicius H, Stanikunas R, Vitta P, Bliumas R, Auskalnyte A, Tuzikas A, Petrulis A, Dabasinskas L, Zukauskas A. Subjective evaluation of luminance distribution for intelligent outdoor lighting. *Lighting Research and Technology*. Epub ahead of print 21 June 2013. DOI: 10.1177/1477153513491760.

Series title and number

VTT Science 64

Title	**From LED die to a lighting system** Performance improvement in LED lighting by means of thermal management and smart control
Author(s)	Eveliina Juntunen
Abstract	Light-emitting diodes (LEDs) are solid-state light sources increasingly used in general illumination. Advanced properties, such as energy efficiency and long lifetime, are promoting LED replacement over traditional lamp-based solutions. Features like small size and ease of control are also appreciated among the lighting community. Smart lighting with advanced control has attracted particular attention recently due to the increased energy savings via added intelligence. Besides the environmental reasons, the economic impact of LED lighting technology development is significant, with solid growth predicted for the energy-efficient lighting market. This thesis addresses high-power LED lighting technology development at four different levels. At the component, module and luminaire levels, the research concentrates on thermal management, which is considered one of the main factors for reliability and performance. The research focus is on reducing the thermal resistance of the high-power LED structure. This is achieved with thermal vias through the insulation layer of the substrate under the heat source. As a result, a total thermal resistance reduction of 10–55% is shown in comparison with commercial substrate technologies. Energy efficiency is considered the measure of the achievements at the luminaire and system levels. The topic is studied with a pedestrian street lighting installation in a real use environment. Case examples of dimming the street lighting according to natural light levels and pedestrian presence revealed power savings of more than 40% with smart control.
ISBN, ISSN	ISBN 978-951-38-8152-8 (Soft back ed.) ISBN 978-951-38-8153-5 (URL: http://www.vtt.fi/publications/index.jsp) ISSN-L 2242-119X ISSN 2242-119X (Print) ISSN 2242-1203 (Online)
Date	October 2014
Language	English, Finnish abstract
Pages	82 p. + app. 46 p.
Name of the project	
Commissioned by	
Keywords	LED lighting, street lighting, thermal resistance, thermal via, smart control, energy savings
Publisher	VTT Technical Research Centre of Finland P.O. Box 1000, FI-02044 VTT, Finland, Tel. 020 722 111

Julkaisun sarja ja numero

VTT Science 64

Nimeke	**LED-sirulta valaistusjärjestelmään** LED-valaisuratkaisujen suorituskyvyn parantaminen lämmönhallinnan ja älykkään ohjauksen keinoin
Tekijä(t)	Eveliina Juntunen
Tiivistelmä	LEDien (light emitting diodes) käyttö valaistuksessa yleistyy kiihtyvällä tahdilla. Kehityksen taustalla ovat LEDien edistykselliset ominaisuudet erityisesti energiatehokkuuden ja luotettavuuden kannalta. Lisäksi komponenttien pieni koko ja helppo ohjattavuus ovat laajentaneet LED-valaistuksen mahdollisuuksia. Energiansäästösyistä erityisesti älykästä ohjausta hyödyntävä valaistus onkin kasvattanut suosiotaan voimakkaasti viime vuosina. Ympäristösyiden ohella LED-valaistuksen yleistyminen on merkittävää myös taloudellisesti, sillä alalle on ennustettu jatkuvaa liiketoiminnan kasvua. Tässä väitöskirjassa tarkastellaan LED-valaistusratkaisujen suorituskyvyn parantamista neljällä eri tasolla. Komponentti-, moduuli- ja valaisintasolla tutkimus keskittyy LED-ratkaisujen lämmönhallintaan, sillä käytännössä kaikki LEDin keskeiset ominaisuudet, kuten valontuotto, hyötysuhde ja elinikä, ovat suoraan riippuvaisia komponentin toimintalämpötilasta. Väitöskirja keskittyy kokonaislämpöresistanssin alentamiseen kehitettyjen piirilevyratkaisujen avulla. Tutkimus suoritetaan toteuttamalla ja vertailemalla erilaisia LED-moduuli- ja valaisinrakenteita. Tulokset osoittavat, että kehitetyt alustaratkaisut alentavat rakenteen kokonaislämpöresistanssia 10–55 % verrattuna yleisesti käytettyihin teknologioihin. Valaisin- ja järjestelmätasolla tutkimus kohdistuu energiankulutuksen pienentämiseen älykkään ohjauksen keinoin. Sovelluskohteena on kevyen liikenteen väylän valaistus, ja tutkimuksessa hyödynnetään koeasennusta todellisissa käyttöolosuhteissa. Ohjaamalla valaistusta ympäristön valaistusolosuhteiden tai jalankulkijoiden läsnäolon perusteella demonstroidaan yli 40 % alenema valaistuksen tehonkulutuksessa.
ISBN, ISSN	ISBN 978-951-38-8152-8 (nid.) ISBN 978-951-38-8153-5 (URL: http://www.vtt.fi/publications/index.jsp) ISSN-L 2242-119X ISSN 2242-119X (Painettu) ISSN 2242-1203 (Verkkojulkaisu)
Julkaisuaika	Lokakuu 2014
Kieli	Englanti, suomenkielinen tiivistelmä
Sivumäärä	82 s. + liitt. 46 s.
Projektin nimi	
Rahoittajat	
Avainsanat	LED lighting, street lighting, thermal resistance, thermal via, smart control, energy savings
Julkaisija	VTT PL 1000, 02044 VTT, puh. 020 722 111

From LED die to a lighting system

Performance improvement in LED lighting by means of thermal management and smart control

Light-emitting diodes (LEDs) are solid-state light sources increasingly used in general illumination. Advanced properties, such as energy efficiency and long lifetime, are promoting LED replacement over traditional lamp-based solutions. Features like small size and ease of control are also appreciated among the lighting community. Smart lighting with advanced control has attracted particular attention recently due to the increased energy savings via added intelligence. Besides the environmental reasons, the economic impact of LED lighting technology development is significant, with solid growth predicted for the energy-efficient lighting market.

This thesis addresses high-power LED lighting technology development at four different levels. At the component, module and luminaire levels, the research concentrates on thermal management, which is considered one of the main factors for reliability and performance. The research focus is on reducing the thermal resistance of the high-power LED structure. This is achieved with thermal vias through the insulation layer of the substrate under the heat source. As a result, a total thermal resistance reduction of 10–55% is shown in comparison with commercial substrate technologies.

Energy efficiency is considered the measure of the achievements at the luminaire and system levels. The topic is studied with a pedestrian street lighting installation in a real use environment. Case examples of dimming the street lighting according to natural light levels and pedestrian presence revealed power savings of more than 40% with smart control.

ISBN 978-951-38-8152-8 (Soft back ed.)
ISBN 978-951-38-8153-5 (URL: http://www.vtt.fi/publications/index.jsp)
ISSN-L 2242-119X
ISSN 2242-119X (Print)
ISSN 2242-1203 (Online)